AD-A068 548 ILLINOIS UNIV AT URBANA-CHAMPAIGN ELECTROMAGNETICS LAB F/G 20/14
ANALYSIS OF ARBITRARILY SHAPED WIRE ANTENNAS RADIATING OVER A L--ETC(U)
MAR 79 P PARHAMI, R MITTRA DAAG29-77-G-0111
UNCLASSIFIED UIEM79-6 ARO-14686.4-EL NL

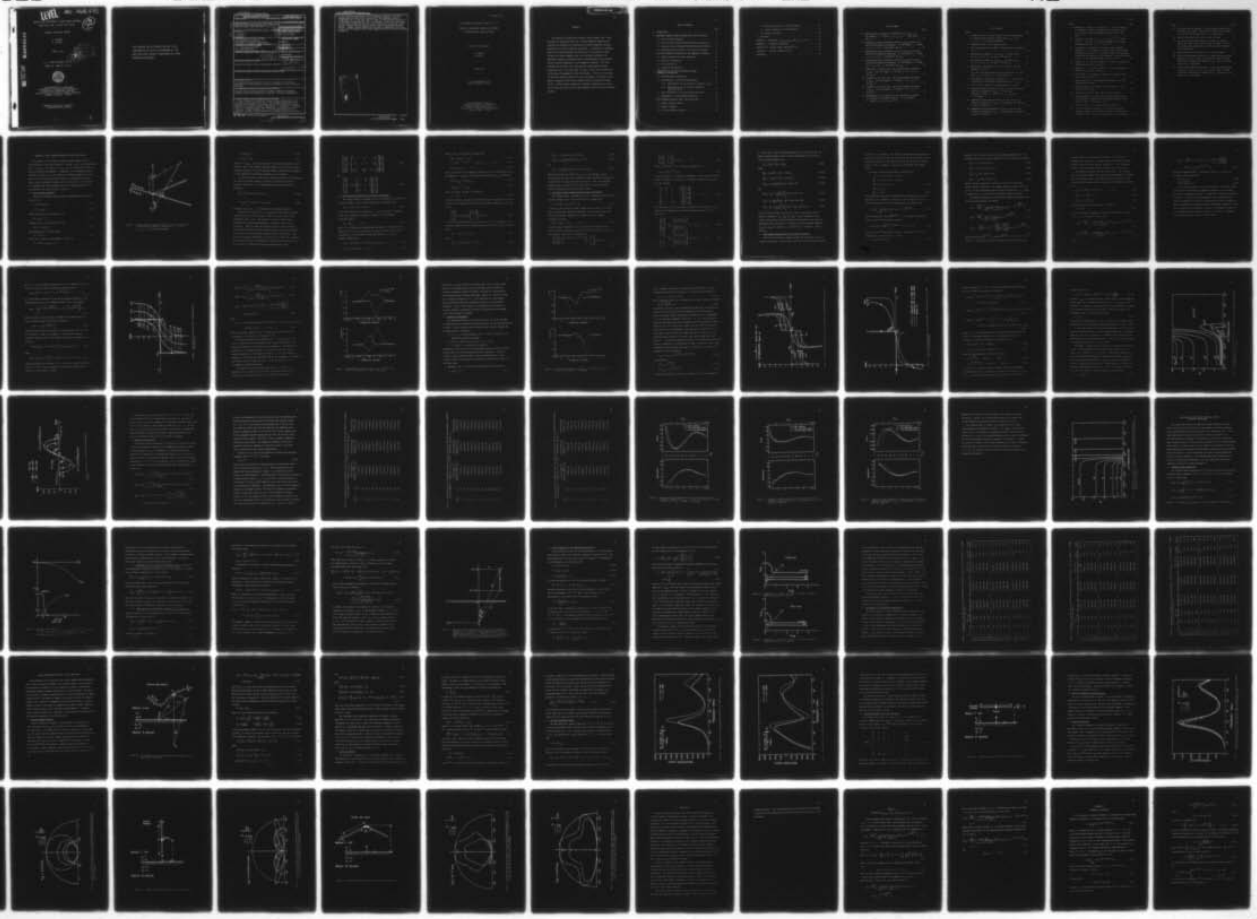

ARO 14686.4-EC

ANALYSIS OF ARBITRARILY SHAPED WIRE ANTENNAS RADIATING OVER A LOSSY HALF-SPACE

(12) NW

INTERIM TECHNICAL REPORT

P. PARHAMI
R. MITTRA

MARCH 1979

U. S. ARMY RESEARCH OFFICE
GRANT NO. DAAG29-77-G0111

ELECTROMAGNETICS LABORATORY
DEPARTMENT OF ELECTRICAL ENGINEERING
ENGINEERING EXPERIMENT STATION
UNIVERSITY OF ILLINOIS AT URBANA-CHAMPAIGN
URBANA, ILLINOIS 61801

THE FINDINGS IN THIS REPORT ARE NOT TO BE CONSTRUED AS AN OFFICIAL DEPARTMENT OF THE ARMY POSITION, UNLESS SO DESIGNATED BY OTHER AUTHORIZED DOCUMENTS.

UNCLASSIFIED

SECURITY CLASSIFICATION OF THIS PAGE (When Data Entered)

REPORT DOCUMENTATION PAGE

READ INSTRUCTIONS BEFORE COMPLETING FORM

1. REPORT NUMBER

2. GOVT ACCESSION NO.

3. RECIPIENT'S CATALOG NUMBER

4. TITLE (and Subtitle)

ANALYSIS OF ARBITRARILY SHAPED WIRE ANTENNAS RADIATING OVER A LOSSY HALF-SPACE

5. TYPE OF REPORT & PERIOD COVERED

Interim Technical Report

6. PERFORMING ORG. REPORT NUMBER

EM79-6, UILU-ENG-79-2546

7. AUTHOR(s)

P. Parhami
R. Mittra

8. CONTRACT OR GRANT NUMBER(s)

DAAG29-77-G-0111

9. PERFORMING ORGANIZATION NAME AND ADDRESS

Electromagnetics Laboratory
Department of Electrical Engineering
University of Illinois, Urbana, Illinois

10. PROGRAM ELEMENT, PROJECT, TASK AREA & WORK UNIT NUMBERS

P-14686-EL

11. CONTROLLING OFFICE NAME AND ADDRESS

U. S. Army Research Office
Post Office Box 12211
Research Triangle Park, NC 27709

12. REPORT DATE

March, 1979

13. NUMBER OF PAGES

135

14. MONITORING AGENCY NAME & ADDRESS (if different from Controlling Office)

137 p.

15. SECURITY CLASS. (of this report)

UNCLASSIFIED

15a. DECLASSIFICATION/DOWNGRADING SCHEDULE

NA

16. DISTRIBUTION STATEMENT (of this Report)

Approved for public release; distribution unlimited.

ARO

14686.4-EL

17. DISTRIBUTION STATEMENT (of the abstract entered in Block 20, if different from Report)

18. SUPPLEMENTARY NOTES

The findings in this report are not to be construed as an official Department of the Army position, unless so designated by other authorized documents.

19. KEY WORDS (Continue on reverse side if necessary and identify by block number)

antennas over lossy ground; method of moments; Sommerfeld integrals; steepest descent path integration; reflection coefficient approximation.

20. ABSTRACT (Continue on reverse side if necessary and identify by block number)

The problem of an arbitrarily oriented current element over a lossy half-space is analyzed in this work. Various numerical approaches are developed and discussed for evaluating the infinite Sommerfeld integrals appearing in the vector potential expressions. In particular, a technique based on the steepest descent path integration is introduced for exact evaluation of these integrals, and, as an efficient alternative, an additional technique is developed based on approximating the well-behaved (cont.)

DD FORM 1 JAN 73 1473 EDITION OF 1 NOV 65 IS OBSOLETE

UNCLASSIFIED

SECURITY CLASSIFICATION OF THIS PAGE (When Data Entered)

408 102

Fourier transform expressions of the Sommerfeld integrals. The latter technique has the merit of not requiring any time-consuming infinite integrations and, at the same time, is shown to yield accurate results for a wide range of parameters of practical interest. Finally, in this paper, the thin-wire antenna problem over a lossy half-space is analyzed via the method of moments and the current element solution techniques discussed earlier. Several antenna examples are included to demonstrate the effect of the lossy half-space on their input impedance and the far-field radiation patterns.

UILU-ENG-79-2546

Electromagnetics Laboratory Report No. 79-6

ANALYSIS OF ARBITRARILY SHAPED WIRE ANTENNAS RADIATING OVER A LOSSY HALF-SPACE

Interim Technical Report

P. Parhami

R. Mittra

March 1979

U. S. Army Research Office
Grant No. DAAG29-77-G-0111

Electromagnetics Laboratory
Department of Electrical Engineering
Engineering Experiment Station
University of Illinois at Urbana-Champaign
Urbana, Illinois 61801

ABSTRACT

The problem of an arbitrarily oriented current element over a lossy half-space is analyzed in this work. Various numerical approaches are developed and discussed for evaluating the infinite Sommerfeld integrals appearing in the vector potential expressions. In particular, a technique based on the steepest descent path integration is introduced for exact evaluation of these integrals, and, as an efficient alternative, an additional technique is developed based on approximating the well-behaved Fourier transform expressions of the Sommerfeld integrals. The latter technique has the merit of not requiring any time-consuming infinite integrations and, at the same time, is shown to yield accurate results for a wide range of parameters of practical interest. Finally, in this paper, the thin-wire antenna problem over a lossy half-space is analyzed via the method of moments and the current element solution techniques discussed earlier. Several antenna examples are included to demonstrate the effect of the lossy half-space on their input impedance and the far-field radiation patterns.

TABLE OF CONTENTS

LIST OF TABLES

LIST OF FIGURES

Figure Page

Figure Page

1. INTRODUCTION

The conventional approach to analyzing antenna structures radiating in the presence of a lossy half-space involves repeated evaluation of the Sommerfeld integrals, which were originally introduced by Sommerfeld about 70 years ago [1] and appeared in the expressions for the vector potentials [2]. Since these infinite integrals are generally highly oscillatory and difficult to evaluate numerically, much attention has been focused in recent years on developing techniques for efficiently evaluating the Sommerfeld integrals without unduly sacrificing the accuracy [3] - [14]. Even though the latest reported procedures [7] - [12] require an order of magnitude less computing time than the earlier "brute-force" numerical integration techniques [3] - [5], the overall computing time severely limits the physical dimensions of the antenna structures being numerically analyzed. Brittingham et al. [10] have used an interpolation scheme on a precalculated grid of Sommerfeld integral values in order to analyze larger structures. However, this technique is only useful for fixed frequency and ground parameters, since a new grid is required each time any of these parameters are changed.

Considerable computing time is saved if one uses the first term in the asymptotic expansion of the Sommerfeld integrals, better known as the Fresnel's Reflection Coefficient Method (RCM). These approximations, which are expressed in a simple closed form, are valid only when the antenna structures and the observation points are sufficiently high above the ground. As expected, the RCM expressions have only been employed for analyzing antenna structures at the high end of the frequency spectrum [10], [12], [13].

An important contribution of this paper is the development of a novel technique which is computationally comparable to the RCM approximation, yet valid for a much wider range of parameters.

In Chapter 2, the complex vector potential expressions for an arbitrarily oriented electric-current element source over a lossy half-space are derived demonstrating that three of the vector potential components contain the troublesome Sommerfeld integrals. An efficient numerical technique, based on the Steepest Descent Path (SDP) integration, is presented in Chapter 3 for evaluating the exact Sommerfeld integral expressions, and the results are compared with the one- and two-term asymptotic expansions of these integrals. In Chapter 4, a unique procedure is developed in which the well-behaved Fourier transform representations of the Sommerfeld integrals are approximated such that the inverse transform is performed via a set of known exact identities. These approximate expressions are shown not only to closely follow the SDP integration results for a wide range of parameters of practical interest, but to be in a convenient form for numerical evaluation. Finally, in Chapter 5, several examples, which are solved via the method of moments in conjunction with the approximate expressions derived in Chapter 4, are presented of various antenna structures radiating over a lossy half-space.

2. ARBITRARY CURRENT ELEMENT RADIATING OVER LOSSY HALF-SPACE

The geometry of an arbitrarily oriented current element P_1 over a lossy half-space is depicted in Figure 1. Regions 1 and 2 are characterized by $(\varepsilon_1 = \varepsilon_{1r}\varepsilon_0, \mu_1 = \mu_0)$ and $(\varepsilon_2 = \varepsilon_{2r}\varepsilon_0, \mu_2 = \mu_0)$, respectively, where ε_0 and μ_0 are free-space parameters. In addition to the standard Cartesian coordinate system (x, y, z), two spherical coordinate systems (r, θ_1, ϕ_1) and (r_2, θ_2, ϕ_2) are also defined in Figure 1 centered about the source point P_1 and its geometrical image point P_2, respectively. Our objective is to determine the field radiated by P_1 at the observation point O, in the presence of the lossy half-space (region 2).

2.1 Vector Potential Approach

Starting with Maxwell's equation and the suppressed time convention $\exp(j\omega t)$, viz.,

$$\nabla \times \vec{H} = j\omega\varepsilon_0\varepsilon_r\vec{E} + \vec{J} \tag{2.1a}$$

$$\nabla \times \vec{E} = -j\omega\mu_0\vec{H} \quad , \tag{2.1b}$$

one may define the vector potential $\vec{\Pi}$ as

$$\vec{H} = j\omega\varepsilon_0\varepsilon_r\nabla \times \vec{\Pi} \quad . \tag{2.2}$$

Introduction of a scalar potential Φ from

$$\nabla\Phi = \vec{E} - \omega^2\mu_0\varepsilon_0\varepsilon_r\vec{\Pi} \tag{2.3}$$

and application of the Lorentz gauge

$$\nabla \cdot \vec{\Pi} - \Phi = 0 \quad , \tag{2.4}$$

allows one to finally express Maxwell's equation as

$$(\nabla^2 + k^2)\vec{\Pi} = -(j\omega\varepsilon_0\varepsilon_r)^{-1}\vec{J} \quad , \tag{2.5}$$

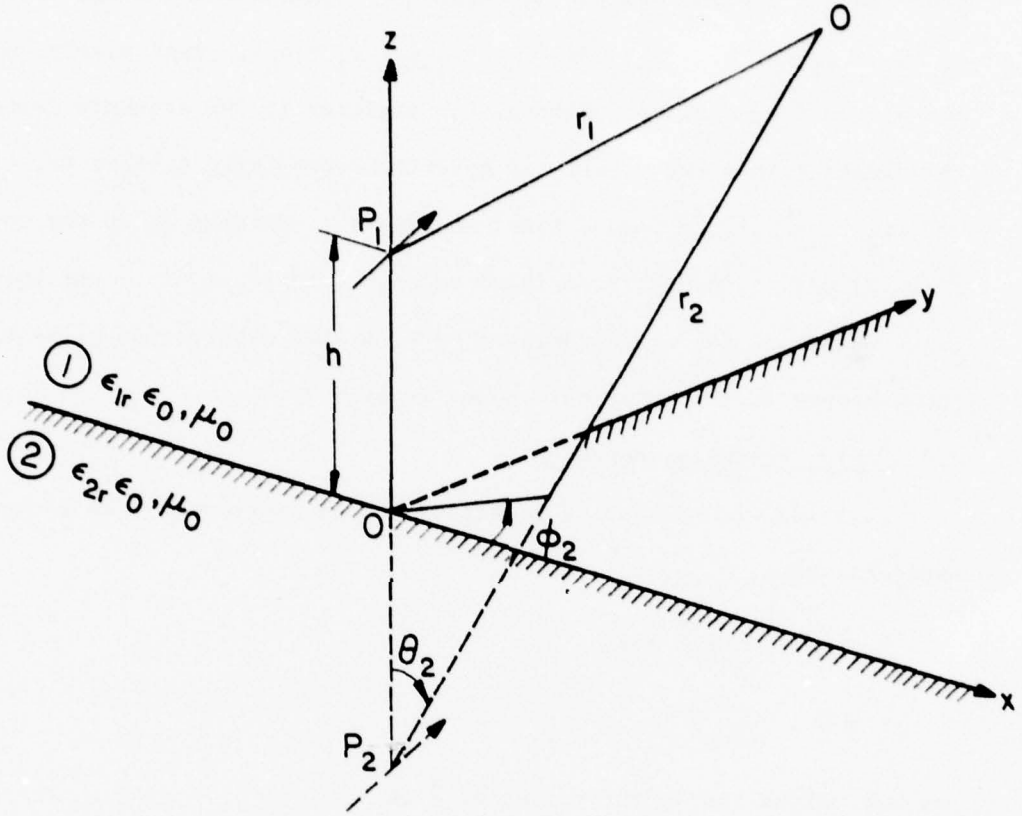

Figure 1. Geometry and the coordinate systems for the current element P_1 radiating over imperfect ground, where $\varepsilon_{1r} = 1$ and $\varepsilon_{2r} = \varepsilon_g - j\sigma/(\omega\varepsilon_0)$ have been assumed.

$$\vec{H} = j\omega\varepsilon_0\varepsilon_r \nabla \times \vec{\Pi} \tag{2.6}$$

$$\vec{E} = (\nabla\nabla\cdot + k^2)\vec{\Pi} \tag{2.7}$$

where $k^2 = \omega^2\mu_0\varepsilon_0\varepsilon_r$. The preceding results are general and valid for both regions 1 and 2. The boundary conditions needed to solve the vector differential Equation (2.5) can be obtained simply by enforcing the continuity of the tangential $\vec{E}$- and $\vec{H}$-field components at the interface.

As in most infinite-interface-type problems reported in the literature, the Fourier transform technique is employed for deriving the vector potential expressions. The two-dimensional Fourier transform pair is defined as

$$\tilde{\vec{\Pi}} = \int_{-\infty}^{\infty}\int \vec{\Pi} \exp[-j(\alpha x + \beta y)]\, dx\, dy \tag{2.8a}$$

$$\vec{\Pi} = \frac{1}{4\pi^2}\int_{-\infty}^{\infty}\int \tilde{\vec{\Pi}} \exp[j(\alpha x + \beta y)]\, d\alpha\, d\beta \quad . \tag{2.8b}$$

Throughout this paper, ~ on top denotes the transformed quantity.

Without loss of generality, the problem of an arbitrarily oriented current source over lossy half-space (Figure 1) can be treated as two independent cases: first, the problem of a vertical current source oriented in the z-direction and, second, a horizontal source in the x-direction. These two cases are analyzed in detail in the following sections with subscripts v and h denoting the field quantities belonging to the vertical and the horizontal current sources, respectively. Once the vector potential expressions are derived, the $\vec{E}$- and $\vec{H}$-field components are directly obtained by transforming the general vector equations given in (2.6) and (2.7) into the following convenient matrix forms:

$$\begin{bmatrix} \tilde{E}_x \\ \tilde{E}_y \\ \tilde{E}_z \end{bmatrix} = \begin{bmatrix} k^2 - \alpha^2 & -\alpha\beta & j\alpha \frac{\partial}{\partial z} \\ -\alpha\beta & k^2 - \beta^2 & j\beta\frac{\partial}{\partial z} \\ j\alpha \frac{\partial}{\partial z} & j\beta\frac{\partial}{\partial z} & (k^2 + \frac{\partial^2}{\partial z^2}) \end{bmatrix} \begin{bmatrix} \tilde{\Pi}_x \\ \tilde{\Pi}_y \\ \tilde{\Pi}_z \end{bmatrix} \tag{2.9}$$

and

$$\begin{bmatrix} \tilde{H}_x \\ \tilde{H}_y \\ \tilde{H}_z \end{bmatrix} = j\omega\varepsilon_0\varepsilon_r \begin{bmatrix} 0 & -\frac{\partial}{\partial z} & j\beta \\ \frac{\partial}{\partial z} & 0 & -j\alpha \\ -j\beta & j\alpha & 0 \end{bmatrix} \begin{bmatrix} \tilde{\Pi}_x \\ \tilde{\Pi}_y \\ \tilde{\Pi}_z \end{bmatrix} . \tag{2.10}$$

2.2 Vertical Current Element-Transform Domain Expressions

The current element is assumed to be in the z-direction (see Figure 1), located at height h over the lossy ground, and with a moment $I_v dz'$:

$$\vec{J}_v = \hat{z}\, I_v\, dz'\, \delta(x)\, \delta(y)\, \delta(z) \quad . \tag{2.11}$$

As has been verified in the literature [2], only the vertical component of the vector potential is needed to satisfy all of the boundary conditions, namely

$$\vec{\Pi}_{vi} = \hat{z}\Pi_{viz} \quad ; \quad i = 1,2 \tag{2.12}$$

where i = 1,2 indicates the region under consideration. Using the source condition in (2.11), one can express the general solution for the vector potential $\tilde{\Pi}_{viz}$ by satisfying both the wave Equation (2.5) and the radiation conditions as

$$\tilde{\Pi}_{v1z} = I_{v0} \exp[-j\gamma_1|z - h|]/2j\gamma_1 + A_1 \exp(-j\gamma_1 z) \quad ; \quad z \geq 0 \tag{2.13a}$$

$$\tilde{\Pi}_{v2z} = A_2 \exp(j\gamma_2 z) \quad ; \quad z \leq 0 \tag{2.13b}$$

where A_1 and A_2 are arbitrary constants and

$$I_{v0} = (j\omega\varepsilon_0\varepsilon_{1r})^{-1} I_v \, dz' \tag{2.14}$$

$$\gamma_i = [k_i^2 - \alpha^2 - \beta^2]^{1/2} \quad ; \quad I_m(\gamma_i) \leq 0 \quad ; \quad i = 1,2 \tag{2.15}$$

$$k_i^2 = \omega^2\mu_0\varepsilon_{1r}\varepsilon_0 \quad ; \quad i = 1,2 \quad . \tag{2.16}$$

If the continuity of the tangential components of the E- and H-fields across the boundary is enforced, the following constraints on $\tilde{\Pi}_{viz}$ are obtained

$$\frac{\partial}{\partial z} \tilde{\Pi}_{v1z}\Big|_{z=0} = \frac{\partial}{\partial z} \tilde{\Pi}_{v2z}\Big|_{z=0} \tag{2.17a}$$

$$\tilde{\Pi}_{v1z}\Big|_{z=0} = \kappa \, \tilde{\Pi}_{v2z}\Big|_{z=0} \tag{2.17b}$$

where the complex constant κ is defined as

$$\kappa = \varepsilon_{2r}/\varepsilon_{1r} \quad . \tag{2.18}$$

Constants A_1 and A_2, present in the vector potential expressions (2.13a) and (2.13b) can be determined by satisfying the boundary conditions (2.17a) and (2.17b):

$$\begin{bmatrix} A_1 \\ A_2 \end{bmatrix} = I_{v0} \frac{1}{j(\kappa\gamma_1 + \gamma_2)} \begin{bmatrix} \frac{\kappa\gamma_1 - \gamma_2}{2\gamma_1} \\ 1 \end{bmatrix} \exp(-j\gamma_1 h) \quad . \tag{2.19}$$

If (2.19) is substituted back into (2.13a) and (2.13b), the complete vector potential expression in the transform domain can be written in the following form:

$$\tilde{\Pi}_{v1z} = \tilde{\Pi}^i_{v1z} + \tilde{\Pi}^r_{v1z} + {}_0\tilde{\Pi}_{v1z} \tag{2.20}$$

where

$$\tilde{\Pi}^i_{v1z} = I_{v0} \exp[-j\gamma_1|z - h|]/2j\gamma_1 \tag{2.21a}$$

$$\tilde{\Pi}^{r}_{v1z} = - I_{v0} \exp[-j\gamma_1(z + h)]/2j\gamma_1 \qquad (2.21b)$$

$$_0\tilde{\Pi}_{v1z} = I_{v0} \frac{\kappa}{j(\kappa\gamma_1 + \gamma_2)} \exp[-j\gamma_1(z + h)] \qquad (2.21c)$$

and

$$\tilde{\Pi}_{v2z} = I_{v0} \frac{1}{j(\kappa\gamma_1 + \gamma_2)} \exp(-j\gamma_1 h) \exp(j\gamma_2 z) \quad . \qquad (2.22)$$

Note that the first two terms of $\tilde{\Pi}_{v1z}$, viz., $\tilde{\Pi}^{i}_{v1z}$ and $\tilde{\Pi}^{r}_{v1z}$, can be interpreted as the direct and the perfect ground reflection contributions to the fields for observation points in region 1. Thus, the remaining component $_0\tilde{\Pi}_{v1z}$ is simply the correction term to the perfect ground solution in the general lossy half-space problem.

2.3 Horizontal Current Element-Transform Domain Expressions

The current element is assumed to be in the x-direction (see Figure 1), located at height h over lossy ground and with a moment $I_h dx'$:

$$\vec{J}_h = \hat{x}\, I_h dx'\, \delta(x)\, \delta(y)\, \delta(z - h) \quad . \qquad (2.23)$$

As expected, the horizontal current element solution above a lossy half-space is indeed more complicated than that for the vertical case, and two vector potential components are needed to obtain a complete solution [2], namely,

$$\vec{\Pi}_{hi} = \hat{x}\, \Pi_{hix} + \hat{z}\, \Pi_{hiz} \quad ; \quad i = 1,2 \quad . \qquad (2.24)$$

Using the source condition in (2.23), the general solutions for the vector potential components satisfying both the wave Equation (2.5) and the radiation condition can be expressed as

$$\begin{bmatrix} \tilde{\Pi}_{h1x} \\ \tilde{\Pi}_{h1z} \end{bmatrix} = \begin{bmatrix} I_{h0} \exp[-j\gamma_1|z - h|]/2j\gamma_1 \\ 0 \end{bmatrix} + \begin{bmatrix} B_{1x} \\ B_{1z} \end{bmatrix} \exp(-j\gamma_1 z) \quad ; \quad z \geq 0 \qquad (2.25)$$

$$\begin{bmatrix} \tilde{\Pi}_{h2x} \\ \tilde{\Pi}_{h2z} \end{bmatrix} = \begin{bmatrix} B_{2x} \\ B_{2z} \end{bmatrix} \exp(j\gamma_2 z) \quad ; \quad z \leq 0 \tag{2.26}$$

where γ_i is defined in (2.15) and I_{h0} is assumed to be

$$I_{h0} = (j\omega\varepsilon_0\varepsilon_{1r})^{-1} I_h \, dx' \quad . \tag{2.27}$$

If the continuity of the tangential components of the E- and the H-fields across the boundary is enforced, the following constraints on $\tilde{\Pi}_{hix}$ and $\tilde{\Pi}_{hiz}$ are obtained:

$$\begin{bmatrix} j\alpha & \frac{\partial}{\partial z} & -j\alpha & -\frac{\partial}{\partial z} \\ 1 & 0 & -\kappa & 0 \\ 0 & 1 & 0 & -\kappa \\ \frac{\partial}{\partial z} & 0 & -\kappa\frac{\partial}{\partial z} & 0 \end{bmatrix} \begin{bmatrix} \tilde{\Pi}_{h1x} \\ \tilde{\Pi}_{h1z} \\ \tilde{\Pi}_{h2x} \\ \tilde{\Pi}_{h2z} \end{bmatrix} = 0 \quad ; \quad z = 0 \quad . \tag{2.28}$$

The conditions in (2.28) are used to determine the constants B_{ix} and B_{iz} present in the general vector potential expressions given in (2.25) and (2.26):

$$\begin{bmatrix} B_{1x} \\ B_{1z} \end{bmatrix} = I_{h0} \begin{bmatrix} \frac{\gamma_1 - \gamma_2}{2j\gamma_1(\gamma_1 + \gamma_2)} \\ \frac{j\alpha(\gamma_1 - \gamma_2)}{k_1^2(\kappa\gamma_1 + \gamma_2)} \end{bmatrix} \exp(-j\gamma_1 h) \quad ; \quad z \geq 0 \tag{2.29a}$$

$$\begin{bmatrix} B_{2x} \\ B_{2z} \end{bmatrix} = I_{h0} \begin{bmatrix} \frac{1}{j\kappa(\gamma_1 + \gamma_2)} \\ \frac{j\alpha(\gamma_1 - \gamma_2)}{k_1^2\kappa(\kappa\gamma_1 + \gamma_2)} \end{bmatrix} \exp(-j\gamma_1 h) \quad ; \quad z \leq 0 \tag{2.29b}$$

If (2.29a) and (2.29b) are substituted back into (2.25) and (2.26), the complete transform domain vector potential expressions can be put into the following convenient form:

$$\tilde{\Pi}_{h1x} = \tilde{\Pi}^{i}_{h1x} + \tilde{\Pi}^{r}_{h1x} + {}_{0}\tilde{\Pi}_{h1x} \tag{2.30}$$

where

$$\tilde{\Pi}^{i}_{h1x} = I_{h0} \exp\left[-j\gamma_1|z - h|\right]/2j\gamma_1 \tag{2.31a}$$

$$\tilde{\Pi}^{r}_{h1x} = - I_{h0} \exp\left[-j\gamma_1(z + h)\right]/2j\gamma_1 \tag{2.31b}$$

$${}_{0}\tilde{\Pi}_{h1x} = I_{h0} \frac{1}{j(\gamma_1 + \gamma_2)} \exp\left[-j\gamma_1(z + h)\right] \tag{2.31c}$$

and

$${}_{0}\tilde{\Pi}_{h1z} = I_{h0}\, j\alpha \frac{\gamma_1 - \gamma_2}{k_1^2(\kappa\gamma_1 + \gamma_2)} \exp\left[-j\gamma_1(z + h)\right] \tag{2.32}$$

$$\tilde{\Pi}_{h2x} = I_{h0} \frac{1}{j\kappa(\gamma_1 + \gamma_2)} \exp\left(-j\gamma_1 h\right) \exp\left(j\gamma_2 z\right) \tag{2.33}$$

$$\tilde{\Pi}_{h2z} = I_{h0}\, j\alpha \frac{\gamma_1 - \gamma_2}{k_1^2\kappa(\kappa\gamma_1 + \gamma_2)} \exp\left(-j\gamma_1 h\right) \exp\left(j\gamma_2 z\right) \quad . \tag{2.34}$$

As in the vertical case, the first two terms of the dominant vector potential component, viz., $\tilde{\Pi}^{i}_{h1x}$ and $\tilde{\Pi}^{r}_{h1x}$, can be interpreted as the direct and the perfect ground reflection contributions to the fields for observation points in region 1. Therefore, the two remaining components ${}_{0}\tilde{\Pi}_{h1x}$ and ${}_{0}\tilde{\Pi}_{h1z}$ are simply the correction terms to the perfect ground solution.

2.4 Space-Domain Representation of the Vector Potentials

Since for most practical antenna problems the observation points are located above ground, in this section, only the vector potential components

in region 1 are considered. The complete transform domain expressions for these vector potentials, both for the vertical and the horizontal current elements, are derived in the previous sections, and the inverse transform relation (2.8b) is employed to obtain the corresponding space-domain results.

By using a spherical-type change of variables, viz.,

$$\begin{cases} x = r_2 \sin\theta_2 \cos\phi_2 = \rho_2 \cos\phi_2 \\ y = r_2 \sin\theta_2 \sin\phi_2 = \rho_2 \sin\phi_2 \\ z + h = r_2 \cos\theta_2 = z_2 \end{cases} \tag{2.35}$$

$$\begin{cases} \alpha = -\lambda \cos\zeta \\ \beta = -\lambda \sin\zeta \quad , \end{cases} \tag{2.36}$$

the incident and the perfect ground-reflection components of the vector potentials, viz., Equations (2.21a),(2.21b) and (2.31a),(2.31b) can be inverse transformed into the following general space-domain form:

$$W = \frac{I_0}{4\pi j} \int_0^\infty \frac{\lambda}{\sqrt{k_1^2 - \lambda^2}} J_0(\rho_2\lambda) \exp\left[-j|z|\sqrt{k_1^2 - \lambda^2}\right] d\lambda \tag{2.37}$$

with the requirement that $\mathrm{Im}\sqrt{k_1^2 - \lambda^2} \leq 0$. In deriving the preceding equation, the following identity was used

$$\cos(n\tau)J_n(z) = \frac{(-j)^{-n}}{2\pi} \int_{-\pi}^{\pi} e^{-jz\cos(\tau'-\tau)} \cos(n\tau')\, d\tau' \tag{2.38}$$

where J_n is the n^{th}-order Bessel function. Expression (2.37) can be integrated in a closed form [15] to yield:

$$W = I_0 \exp(-jk_1 r)/4\pi r \quad . \tag{2.39}$$

Equation (2.39) is used to write the space-domain expressions for the aforementioned vector potential components in the following closed forms:

$$\Pi^{i}_{v1z} = I_{v0} \exp(-jk_1 r_1)/4\pi r_1 \tag{2.40a}$$

$$\Pi^{r}_{v1z} = -I_{v0} \exp(-jk_1 r_2)/4\pi r_2 \tag{2.40b}$$

$$\Pi^{i}_{h1x} = I_{h0} \exp(-jk_1 r_1)/4\pi r_1 \tag{2.41a}$$

$$\Pi^{r}_{h1x} = -I_{h0} \exp(-jk_1 r_2)/4\pi r_2 \quad . \tag{2.41b}$$

One may recognize Equations (2.40a) and (2.41a) as the free-space Green's function solution for the current element P_1, while (2.40b) and (2.41b) are the corresponding perfect ground contributions, i.e., source at image point P_2, to the fields at observation points in region 1.

Inverting the remaining vector potential components in region 1 and after some manipulations, one obtains:

$$0\Pi_{v1z} = \frac{2I_{v0}\kappa}{4\pi j} \int_0^\infty \frac{\lambda}{\kappa\sqrt{k_1^2 - \lambda^2} + \sqrt{\kappa k_1^2 - \lambda^2}} J_0(\rho_2\lambda) \quad e^{-jz_2\sqrt{k_1^2-\lambda^2}} \, d\lambda \tag{2.42}$$

$$0\Pi_{h1x} = \frac{2I_{h0}}{4\pi j} \int_0^\infty \frac{\lambda}{\sqrt{k_1^2-\lambda^2} + \sqrt{\kappa k_1^2-\lambda^2}} J_0(\rho_2\lambda) e^{-jz_2\sqrt{k_1^2-\lambda^2}} \, d\lambda \tag{2.43}$$

$$0\Pi_{h1z} = -\frac{2I_{h0}}{4\pi k_1^2} \cos\phi_2 \int_0^\infty \lambda^2 \frac{\sqrt{k_1^2-\lambda^2} - \sqrt{\kappa k_1^2-\lambda^2}}{\kappa\sqrt{k_1^2-\lambda^2} + \sqrt{\kappa k_1^2-\lambda^2}} J_1(\rho_2\lambda) e^{-jz_2\sqrt{k_1^2-\lambda^2}} \, d\lambda \tag{2.44}$$

where relations $\mathrm{Im}\sqrt{k_1^2 - \lambda^2} \leq 0$ and $\mathrm{Im}\sqrt{\kappa k_1^2 - \lambda^2} \leq 0$ in (2.42) - (2.44) must hold. The infinite integrals present in the above equations are

popularly known as the Sommerfeld integrals [1] and cannot be expressed in a closed form. Efficient numerical evaluation of these integrals, which have been recently verified [3] - [14], represents the major task in analyzing antenna structures over lossy ground.

The Sommerfeld integral can take several forms. For this work, the forms containing Hankel functions in their integrands are preferred, since the integrals appear to be numerically more tractable. Incorporating the well-known identities between Bessel and Hankel functions, viz.,

$$J_i(x) = \frac{1}{2}\left[H_i^{(1)}(x) + H_i^{(2)}(x)\right] \quad ; \quad i = 0,1 \tag{2.45a}$$

$$H_0^{(1)}(x) = -H_0^{(2)}(-x) \tag{2.45b}$$

$$H_1^{(1)}(x) = H_1^{(2)}(-x) \quad , \tag{2.45c}$$

and introducing the following change of variable

$$\lambda = k_1 \sin\xi \quad , \tag{2.46}$$

the vector potential components containing the Sommerfeld integrals (2.42) - (2.44) take the following form

$$\Pi_{v1z}^{0} = \frac{I_{v0}k_1\kappa}{4\pi j}\int_{\Gamma} \frac{\sin\xi\cos\xi}{\kappa\cos\xi + \sqrt{\kappa-\sin^2\xi}} H_0^{(2)}(k_1\rho_2\sin\xi)e^{-jk_1z_2\cos\xi}\,d\xi \tag{2.47}$$

$$\Pi_{h1x}^{0} = \frac{I_{h0}k_1}{4\pi j}\int_{\Gamma} \frac{\sin\xi\cos\xi}{\cos\xi + \sqrt{\kappa-\sin^2\xi}} H_0^{(2)}(k_1\rho_2\sin\xi)\; e^{-jk_1z_2\cos\xi}\,d\xi \tag{2.48}$$

and

$$0\Pi_{h1z} = -\frac{I_{h0}k_1}{4\pi}\cos\phi_2 \int_\Gamma \sin^2\xi\cos\xi\,\frac{\cos\xi - \sqrt{\kappa-\sin^2\xi}}{\kappa\cos\xi + \sqrt{\kappa-\sin^2\xi}}$$

$$\cdot H_1^{(2)}(k_1\rho_2\sin\xi)e^{-jk_1z_2\cos\xi}\,d\xi \qquad (2.49)$$

where the integration path Γ is depicted in Figure 2, on which the following conditions must hold

$$\mathrm{Im}(\cos\xi) \leq 0 \qquad (2.50a)$$

$$\mathrm{Im}(\sqrt{\kappa - \sin^2\xi}) \leq 0 \quad . \qquad (2.50b)$$

In the following chapter, an efficient numerical integration scheme is discussed for evaluating the Sommerfeld integrals via the steepest descent path integration technique. An additional approach is introduced in Chapter 4 in which the transform domain of the troublesome vector potential components are initially approximated such that the Sommerfeld infinite integrals do not appear in their space-domain expressions. These two techniques plus the asymptotic solution to the Sommerfeld integrals are compared, and several numerical results are included to demonstrate the efficiency and the accuracy of each procedure.

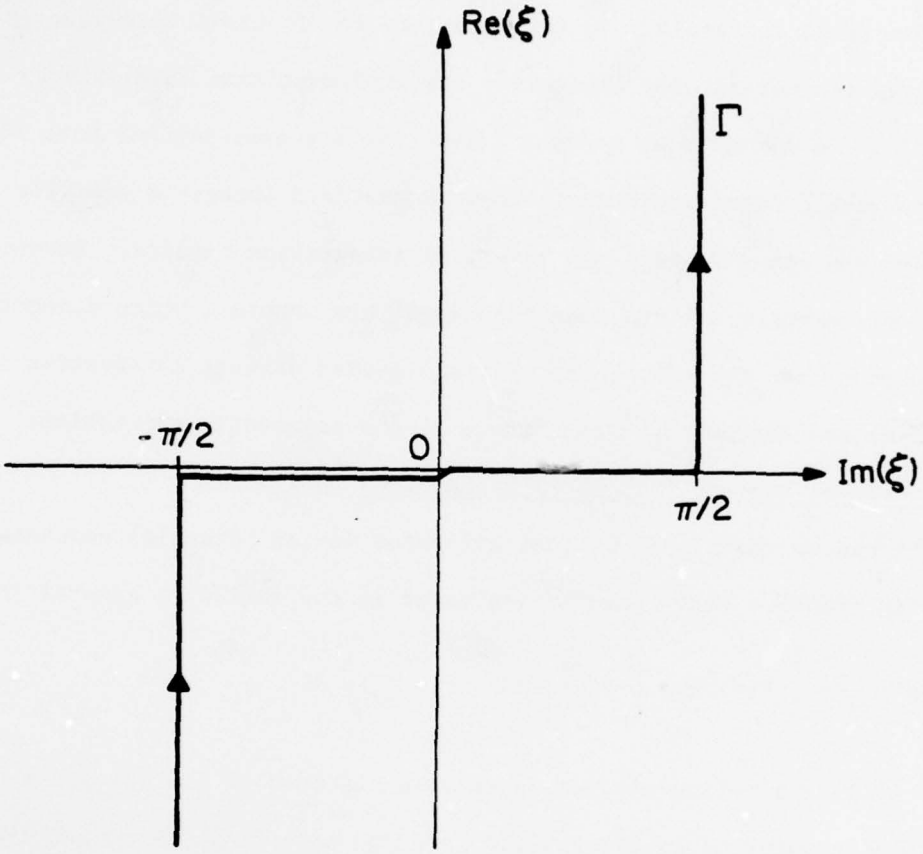

Figure 2. Integration path Γ in the complex ξ-plane.

3. EXACT AND ASYMPTOTIC EVALUATION OF THE SOMMERFELD INTEGRALS

The three correction vector potential components derived in the previous chapter, viz., Equations (2.47)-(2.49), cannot be expressed in a closed form and contain a certain class of infinite integrals known as the Sommerfeld integrals. In this chapter, an efficient technique is presented for numerically evaluating the aforementioned integrals by deforming the integration contour Γ into the steepest descent path (SDP). The asymptotic approximations to these Sommerfeld integrals are also obtained and compared with the numerical integration results. Several numerical examples are included throughout the chapter, which demonstrate the accuracy and the efficiency of the steepest descent integration technique and define the useful range of the asymptotic expressions.

3.1 Steepest Descent Path (SDP) Integration

It can be readily shown that all three vector potential components given in (2.47) - (2.49) can be expressed in the following general form:

$$u = \frac{1}{4\pi j} \int_{\Gamma} P(\xi) \exp\left[-jk_1 r_2 \cos(\xi - \theta_2)\right] d\xi \tag{3.1}$$

where $P(\xi)$ is a relatively slowly varying function of ξ. The point $\xi = \theta_2$ is a saddle point of Equation (3.1), and the path Γ can be deformed to a steepest descent path (SDP) by enforcing the condition $\mathrm{Re}[\cos(\xi - \theta_2)] = 1$. (At this point it is assumed that no poles or branch points of $P(\xi)$ are intercepted.) On SDP, the following convenient change of variable is introduced:

$$\cos(\xi - \theta_2) = 1 - jt^2 \tag{3.2}$$

where t is a real parameter ranging from $-\infty$ to $+\infty$. Equation (3.2) can be used to explicitly define the steepest descent path as:

$$\xi_{SDP} = \pm\left[\pi/2 + j \text{ Ln } (t^2 + j + |t| \sqrt{t^2 + 2j})\right] + \theta_2 \quad ; \quad t \gtrless 0 \ , \tag{3.3}$$

or if one needs to separate the real and the imaginary behaviors of the steepest descent path, the following equivalent form can be derived

$$\xi_{SDP} = \pm \begin{cases} \cos^{-1}\left[\dfrac{-t^2 + \sqrt{t^4+4}}{2}\right] + j \ \cosh^{-1}\left[\dfrac{t^2 + \sqrt{t^4+4}}{2}\right] \end{cases} + \theta_2 \ , \quad t \gtrless 0 \tag{3.4}$$

where the inverse cosine function is assumed to be between 0 and $\pi/2$ and the inverse hyperbolic function is defined as

$$\cosh^{-1} \Psi = \text{Ln}\left[\Psi + \sqrt{\Psi^2 - 1}\right] \ . \tag{3.5}$$

The SDP can be traced in the ξ-plane, by using Equations (3.3) or (3.4) as a function of t and θ_2 (see Figure 3). Applying the change of variable in Equation (3.2) to the integral expression in Equation (3.1), we obtain

$$u = \exp(-jk_1 r_2 - j\pi/4)/(2\sqrt{2}\,\pi) \int_{-\infty}^{\infty} Q(t) \exp(-k_1 r_2 t^2)\, dt \tag{3.6}$$

where

$$Q(t) = \left[P(\xi) \sec \frac{\xi - \theta_2}{2}\right]_t = \sqrt{2}\, e^{j\pi/4} (t^2 + 2j)^{-1/2} P(\xi)\Big|_t \ . \tag{3.7}$$

Using the general form obtained in (3.6), the vector potential expressions in (2-47) - (2.49) can be formulated on the steepest descent path as a function of real variable t, namely,

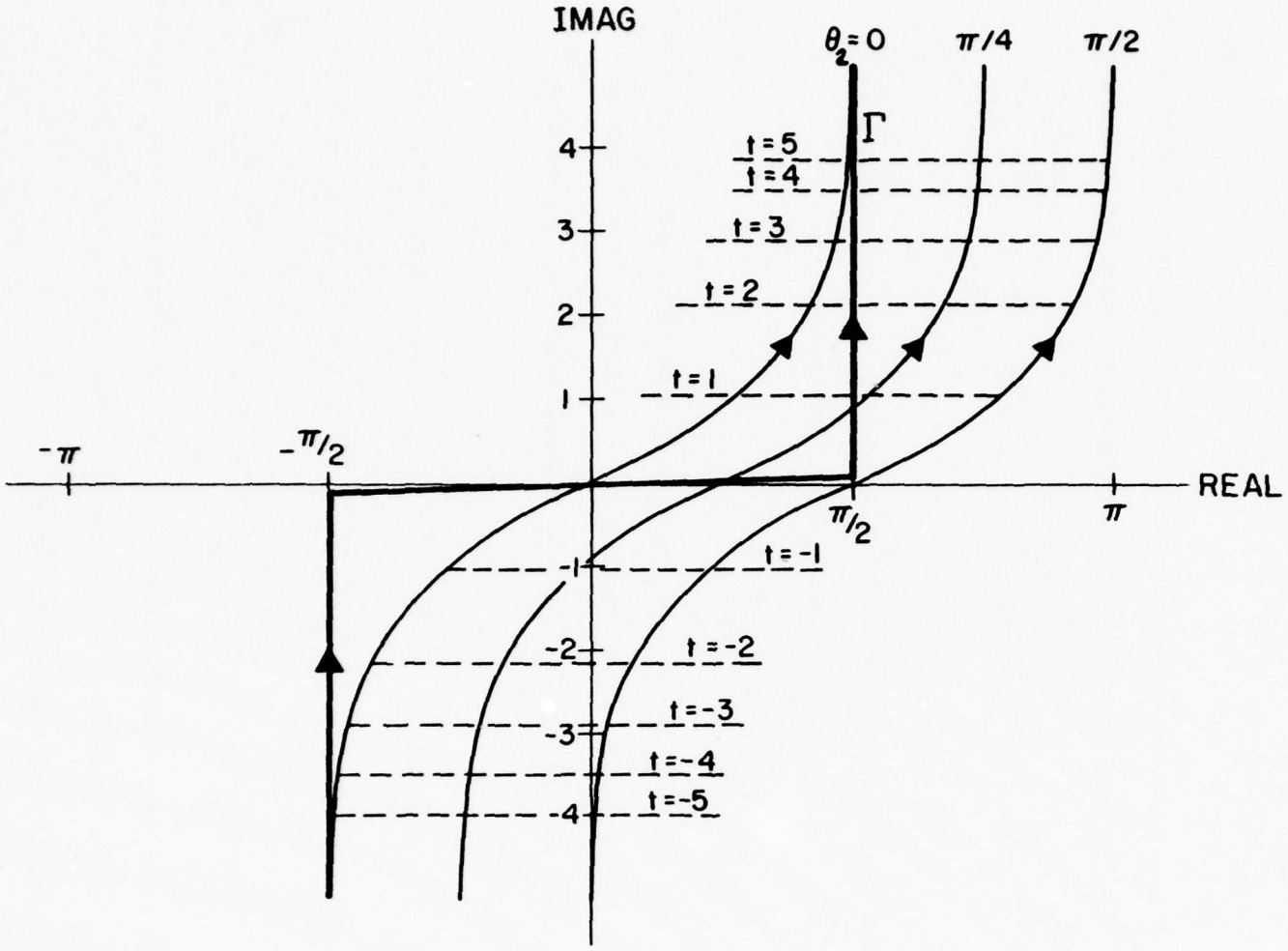

Figure 3. The steepest descent path (SDP) of integration as a function of θ_2.

$$0^{\Pi}_{v1z} = I_{v0} \int_{-\infty}^{\infty} \frac{\kappa R_0(t)}{\left[\kappa \cos \xi + \sqrt{\kappa - \sin^2 \xi}\right]_t} \exp\left(-k_1 r_2 t^2\right) dt \qquad (3.8)$$

$$0^{\Pi}_{h1x} = I_{h0} \int_{\infty}^{\infty} \frac{R_0(t)}{\left[\cos \xi + \sqrt{\kappa - \sin^2 \xi}\right]_t} \exp\left(-k_1 r_2 t^2\right) dt \qquad (3.9)$$

$$0^{\Pi}_{h1z} = -jI_{h0} \cos \phi_2 \int_{-\infty}^{\infty} R_1(t) \left[\sin \xi \frac{\cos \xi - \sqrt{\kappa - \sin^2 \xi}}{\kappa \cos \xi + \sqrt{\kappa - \sin^2 \xi}}\right]_t$$

$$\cdot \exp\left(-k_1 r_2 t^2\right) dt \qquad (3.10)$$

where

$$R_i(t) = (2\pi)^{-1} k_1 \exp(-jk_1 r_2)(t^2 + 2j)^{-1/2} [\sin \xi \cos \xi \exp(jk_1 \rho_2 \sin \xi)]_t$$

$$\cdot H_i^{(2)}(k_1 \rho_2 \sin \xi)\Big|_t \quad ; \quad i = 0,1 \quad , \qquad (3.11)$$

$H_i^{(2)}$ is the Hankel function of the i^{th} order and of second kind, and ξ is expressed as a function of t in Equation (3.3).

The relations expressed in Equations (3.8) - (3.10) are exact if no poles or branch points are intercepted under the path deformation. The detailed discussions of the possible pole and branch-cut contributions are presented in the following sections. It should also be noted that the apparent singularity of the Hankel functions at $\theta_2 = 0$ in the Sommerfeld integrals is overcome by the remaining terms in the integrands. In Appendix I, equivalent versions of Equations (3.8) - (3.10) are derived for $\theta_2 = 0$ for numerical integration purposes.

By observing the integral expressions in (3.8) - (3.10), it is apparent that for large $k_1 r_2$ the effective integration interval will be quite small and contain relatively few oscillations (see Figure 4).

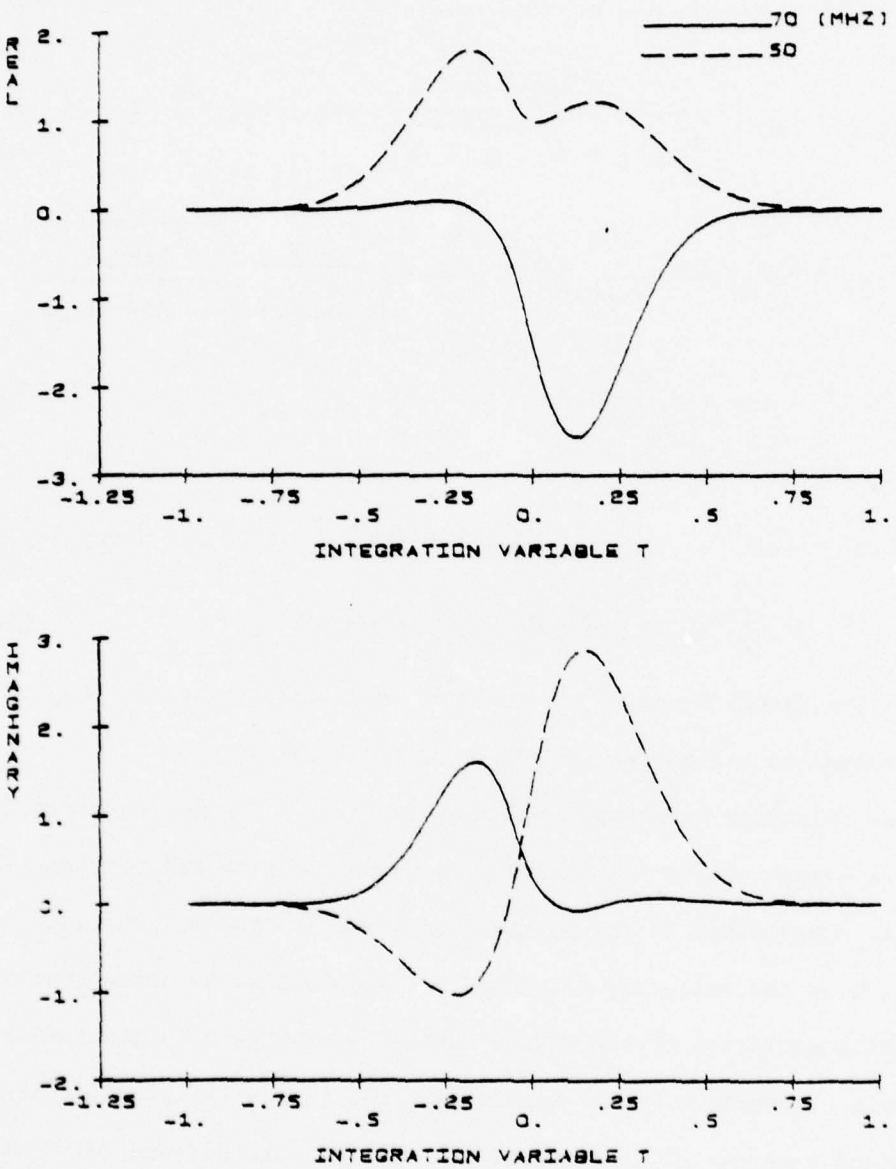

Figure 4. High-frequency examples of the Π_{0hlx}. For these cases, $\theta_2 = 5°$, h = 5m, $\varepsilon_g = 10$, and $\sigma = .01$ mhos/m.

Fortunately, at lower frequencies (smaller $k_1 r_2$), the oscillatory terms present in the integrands are scaled accordingly and, even though the effective integration interval increases, the number of oscillations in the integrand does not increase appreciably (Figure 5). This fact allows one to integrate Equations (3.8) - (3.10) numerically by employing an efficient Gaussian quadrature integration routine for a wide range of parameters. Later in this chapter, the efficiency and the accuracy of the above numerical integration procedure are demonstrated and compared to the other available techniques.

3.2 Branch-Cut Contribution

The expressions derived in the previous section are valid only when no singularities are intercepted during the steepest descent path deformation. In order to locate the poles and the branch points, one must consider the following physical constraints:

a) $0 \leq \theta_2 < \pi/2$, since Equations (3.8) - (3.10) are valid only for observation points above ground;

b) $\mathrm{Re}(\kappa) \geq 1$ and $\mathrm{Im}(\kappa) \leq 0$, since $\kappa = \varepsilon_g - j\sigma/(\omega\varepsilon_0)$;

c) $-\frac{\pi}{2} < \mathrm{Re}(\xi) < \pi$ on the SDP (see Figure 3).

Furthermore, since $\cos(\xi)$ is a single-valued function, condition (2.50a) does not have to be satisfied during the path deformation. Condition (2.50b) is used to define an upper- and a lower-Riemann sheet in the ξ-plane in which this condition is satisfied in the upper and violated in the lower sheet.

Equations (3.8) - (3.10) have the same branch points satisfying

$$\kappa - \sin^2 \xi_b = 0 \quad . \tag{3.12}$$

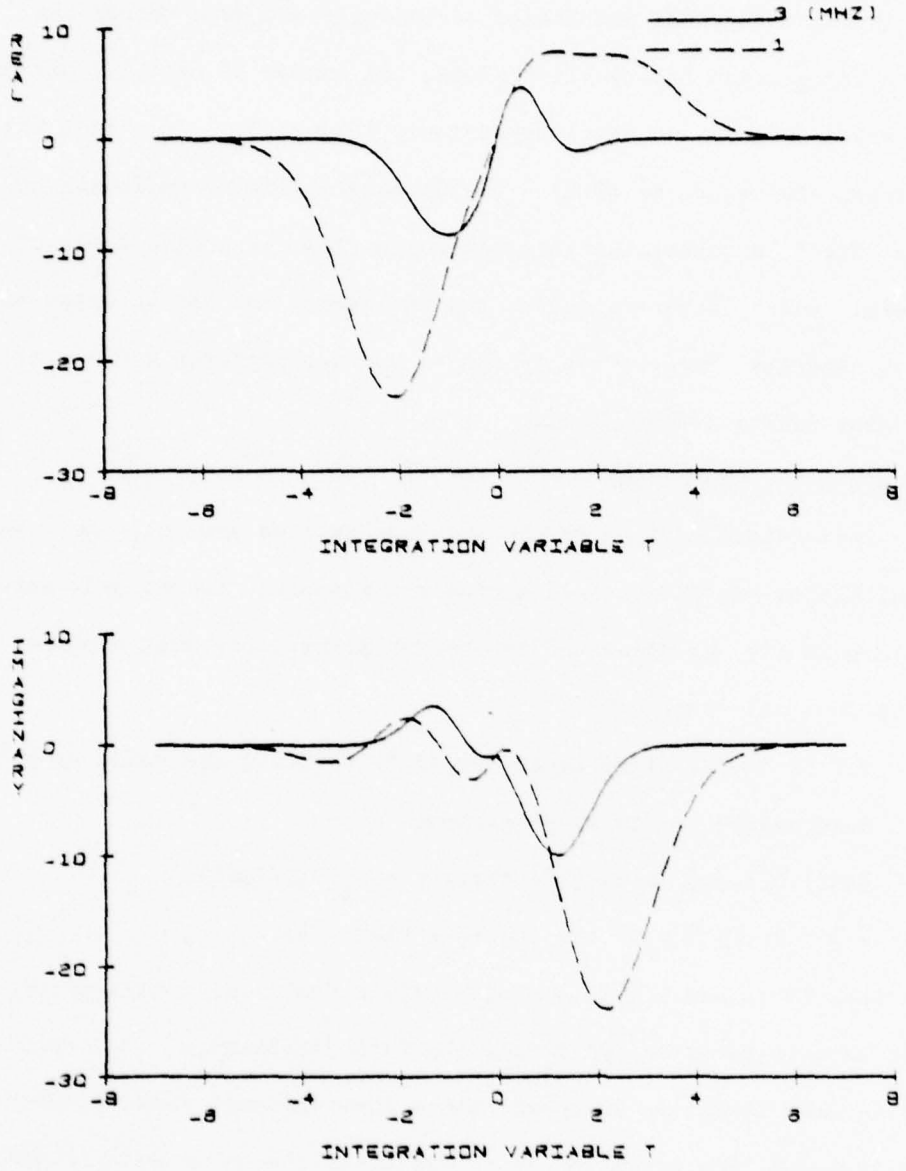

Figure 5. Low-frequency examples of the Π_{h1x}. For these cases, $\theta_2 = 5°$, h = 5m, $\varepsilon_g = 10$, and $\sigma = .01$ mhos/m.

If one considers the physical constraints discussed earlier, only the following two branch point solutions are of importance (see Figure 6):

$$\xi_b = \pi/2 \pm j \text{ Ln } (\sqrt{\kappa} + \sqrt{\kappa - 1}) \quad . \tag{3.13}$$

The corresponding branch cuts of Equation (3.13) which satisfy the relation

$$\text{Im } (\sqrt{\kappa - \sin^2 \xi}) = 0 \quad , \tag{3.14}$$

as depicted in Figure 6, are the boundaries through which the integration path will travel to and from the two Riemann sheets defined earlier. Since the steepest descent path defined in Equation (3.3) is independent of κ, one can easily demonstrate that for $0 \leq \theta_2 < 90°$ only the branch point with the upper sign can be captured by the SDP deformation (Figure 7). Therefore, one can allow the SDP to enter the lower sheet only when the lower branch cut, corresponding to the lower sign of Equation (3.13), is intercepted, since the path will always intercept the lower cut at an additional point forcing it to return to the upper Riemann sheet (see Figure 7). A branch-cut integration, however, is performed around the upper branch cut whenever it is intercepted in order to remain the proper sheet. The branch cut in the upper-half plane as a function of a positive real parameter β can be expressed as

$$\xi_{bc} = \pi/2 + j \text{ Ln } (\sqrt{\kappa - \beta^2} + \sqrt{\kappa - 1 - \beta^2}) \quad , \tag{3.15a}$$

or, equivalently,

$$\sin \xi_{bc} = \sqrt{\kappa - \beta^2} \tag{3.15b}$$

$$\cos \xi_{bc} = -j \sqrt{\kappa - 1 - \beta^2} \quad . \tag{3.15c}$$

By applying the change of variable in Equation (3.15) to the Sommerfeld

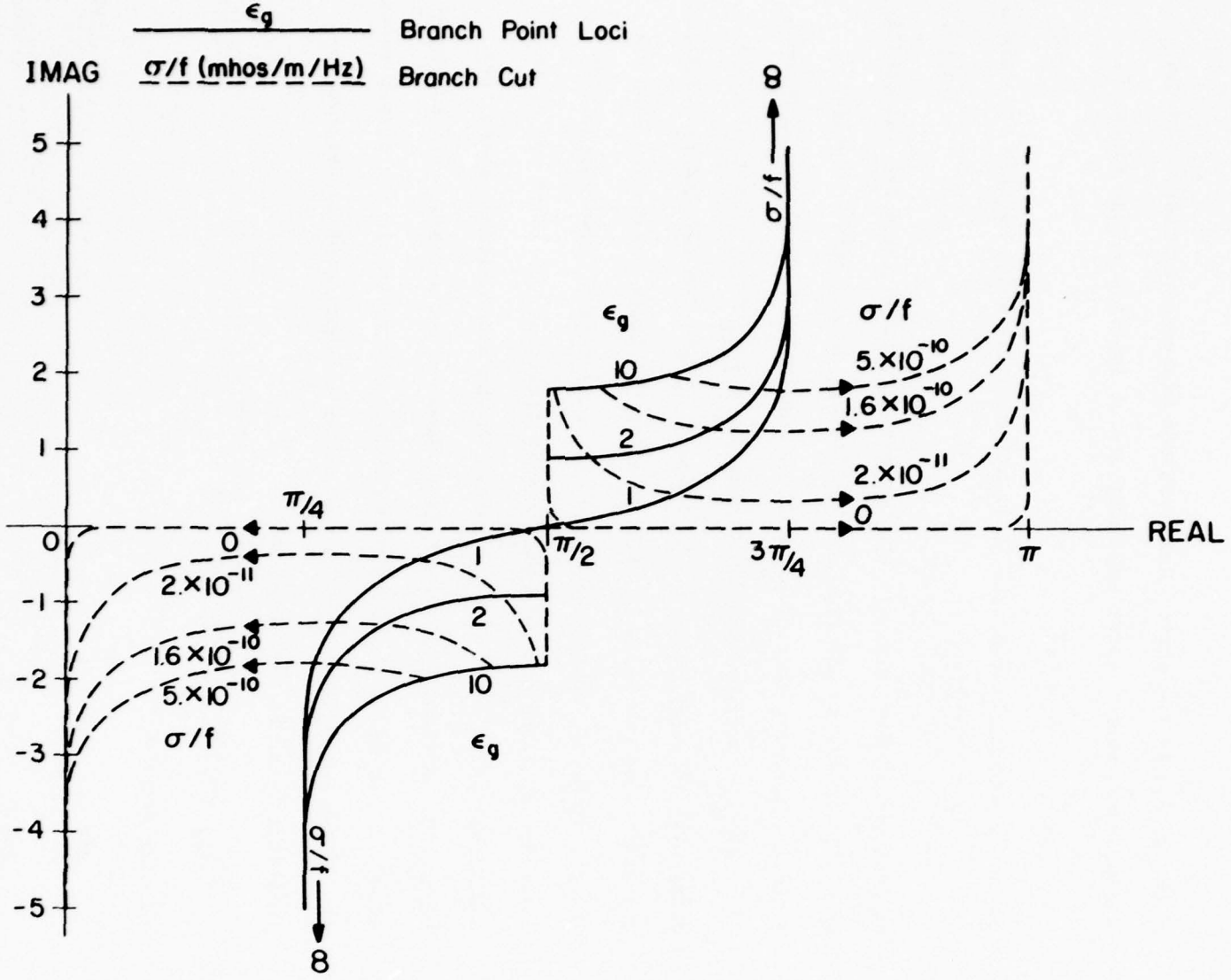

Figure 6. Branch-point and branch-cut loci as a function of ground parameters ϵ_g and σ/f.

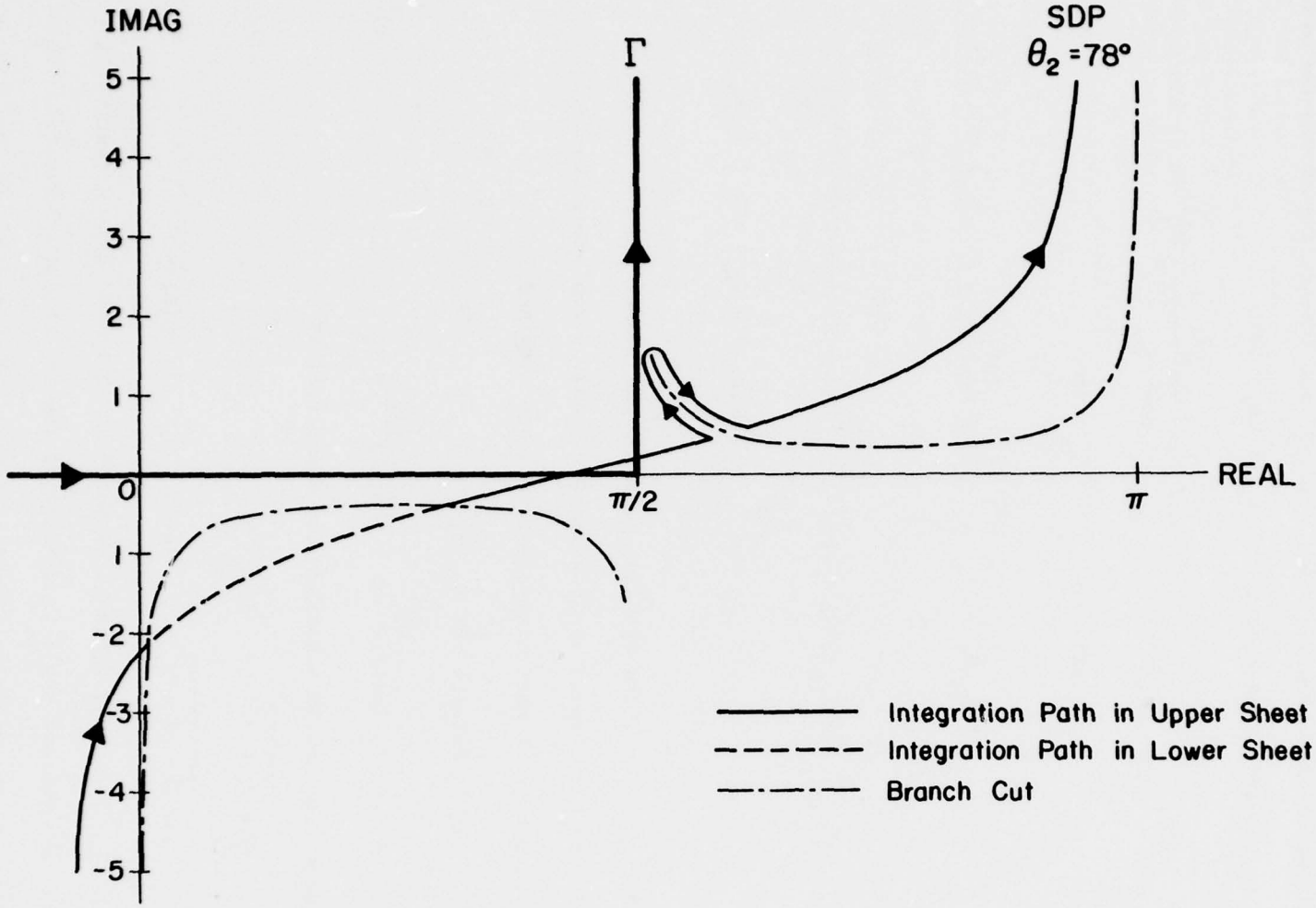

Figure 7. The correct SDP when branch cuts are intercepted. For this case, $\varepsilon_g = 10$, and $\sigma/f = 2 \times 10^{-11}$ mhos/m/Hz.

integrals expressed in (2.47) - (2.49) and integrating around the branch cut, the following contributions are obtained:

$$ {}_0\Pi_{v1z}\Big|_{bc} = I_{v0} k_1 \kappa (2\pi j)^{-1} \int_0^{\beta_1} \frac{\beta^2}{\kappa^2 \cos^2 \xi_{bc} - \beta^2} H_0^{(2)}(k_1 \rho_2 \sin \xi_{bc}) $$

$$ \cdot \exp(-jk_1 z_2 \cos \xi_{bc})\, d\beta \qquad (3.16) $$

$$ {}_0\Pi_{h1x}\Big|_{bc} = I_{h0} k_1 (2\pi j)^{-1} \int_0^{\beta_1} \frac{\beta^2}{\kappa - 1} H_0^{(2)}(k_1 \rho_2 \sin \xi_{bc}) \exp(-jk_1 z_2 \cos \xi_{bc}) d\beta \qquad (3.17) $$

$$ {}_0\Pi_{h1z}\Big|_{bc} = I_{h0} k_1 (2\pi)^{-1} \cos \phi_2 \int_0^{\beta_1} (1 + \kappa) \frac{\beta^2}{\kappa^2 \cos^2 \xi_{bc} - \beta^2} $$

$$ \cdot \sin \xi_{bc} \cos \xi_{bc} H_1^{(2)}(k_1 \rho_2 \sin \xi_{bc}) \exp(-jk_1 z_2 \cos \xi_{bc}) d\beta, \qquad (3.18) $$

where $\beta = \beta_1$ is the crossing point of the branch cut and the SDP in the ξ-place. By expanding Equation (3.2) and by employing the (3.15) relations, the following conditions are obtained for β_1

$$ \sin \theta_2 \, \mathrm{Re}(A) + \cos \theta_2 \, \mathrm{Im}(B) = 1 \qquad (3.19a) $$

$$ [-\sin \theta_2 \, \mathrm{Im}(A) + \cos \theta_2 \, \mathrm{Re}(B)]^{1/2} = t_1 \qquad (3.19b) $$

where the complex numbers A and B are defined as

$$ A = \sqrt{\kappa - \beta_1^2} \quad ; \quad \mathrm{Re}(A) \geq 0 \quad , \quad \mathrm{Im}(A) \leq 0 \qquad (3.20a) $$

$$ B = \sqrt{\kappa - 1 - \beta_1^2} \quad ; \quad \mathrm{Re}(B) \geq 0 \quad , \quad \mathrm{Im}(B) \leq 0 \quad . \qquad (3.20b) $$

In (3.19), $t = t_1$ defines the point at which the SDP, corresponding to the observation angle θ_2, intercepts the branch cut of Equation (3.15) at $\beta = \beta_1$. After some algebraic manipulations, Equation (3.19a) can be

further simplified to

$$\theta_2 = \sin^{-1}\left([\mathrm{Re}^2(A) + \mathrm{Im}^2(B)]^{-1/2}\right) - \tan^{-1}\left(\frac{\mathrm{Im}(B)}{\mathrm{Re}(A)}\right) \tag{3.21}$$

from which θ_{min}, the observation angle at which SDP will pass through the branch point, can be computed by setting $\beta_1 = 0$. Since θ_{min} is only a function of κ, Figure 8 is constructed to show its variations as a function of the ground parameters and the frequency. Therefore, whenever the observation angle θ_2 satisfies the condition

$$\theta_2 > \theta_{min} \quad , \tag{3.22}$$

the branch-cut contributions in (3.16) - (3.18) are to be added to their respective SDP vector potential formulations expressed in (3.8) - (3.10).

It should be pointed out that once the condition (3.22) is met, the branch-cut integration limit β_1 can be computed numerically by iterating on Equation (3.21). Also, because of the branch-cut interception, the SDP integrand will be discontinuous at point $t = t_1$, which is readily computed by substituting the value of β_1 into (3.19b).

Fortunately, in many cases, the branch-cut contributions are several orders of magnitude smaller than the SDP integral value and can be ignored [16]. Therefore, it is necessary to introduce a condition for which one can ignore the branch-cut integration and thereby compute the vector potentials more efficiently. This task can be accomplished by initially considering the $\exp(-k_1 r_2 t^2)$ term present in all three vector potential integrands shown in (3.8) - (3.10). If no poles are present on or near the contour, a finite integration in the interval

$$|t| \leq \left(\frac{9}{k_1 r_2}\right)^{1/2} \tag{3.23}$$

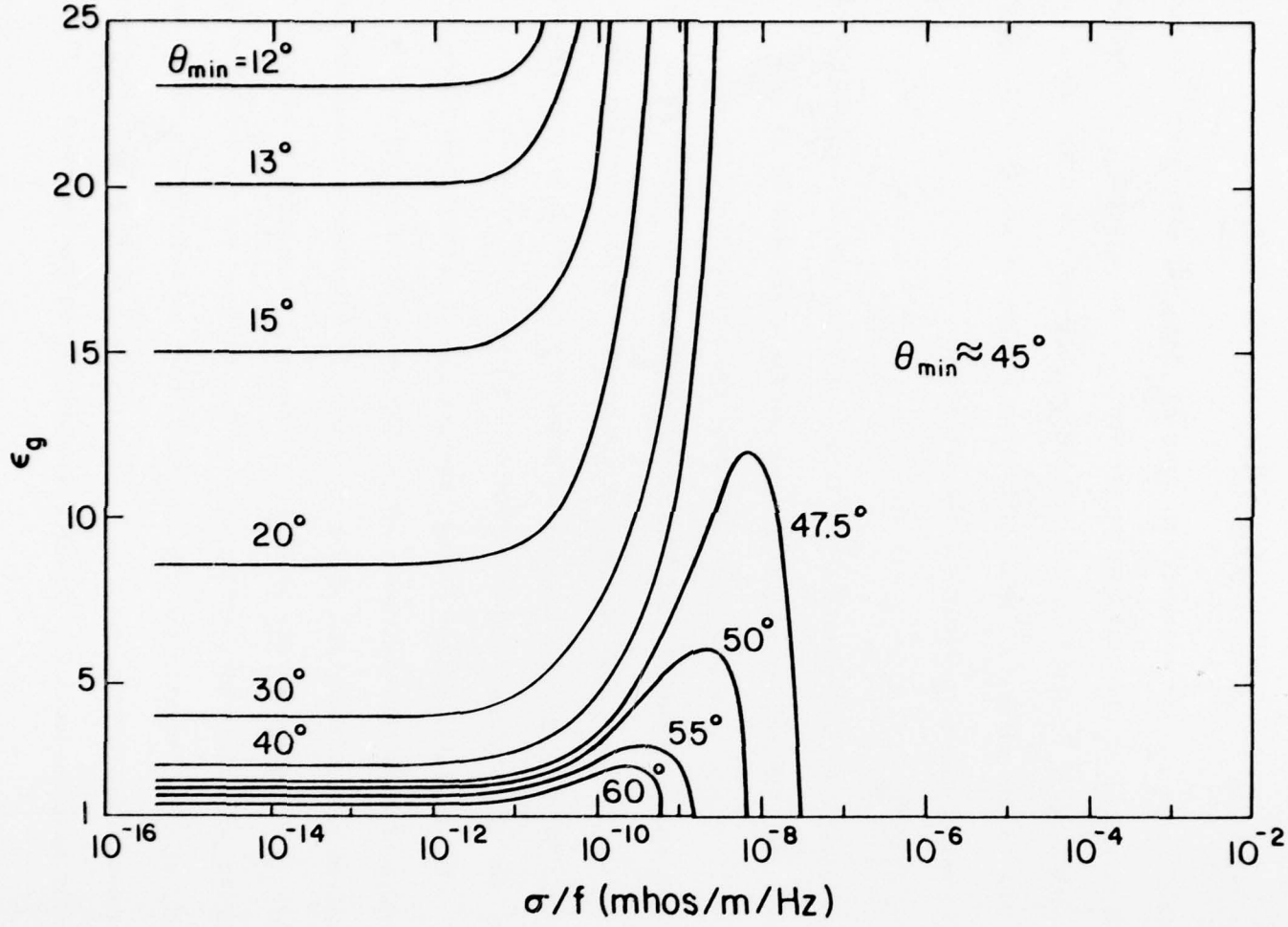

Figure 8. The minimum θ_2 contours as a function of κ. A branch point is captured by the SDP path deformation when $\theta_2 > \theta_{min}$.

will result in an error on the order of 0.01% as compared to the full infinite integration. By examining the branch-cut loci (Figure 6) and the SDP behavior (Figure 3) in the ξ-plane, an assumption can be made which states that if the branch cut intercepts the SDP inside the finite integration interval defined in (3.23), then the branch-cut contribution is not negligible. Or equivalently, the branch-cut contribution requires an additional condition, namely,

$$t_1 \leq t_{max} = 3(k_1 r_2)^{-1/2} \tag{3.24}$$

where $t = t_1$ is the SDP and branch-cut intercept defined earlier.

In summary, condition (3.22) signals the capture of the branch point during the path deformation. If captured, condition (3.24) is used to decide whether the branch-cut integration can be ignored or not. Table 3.1 is constructed to verify the validity of the assumptions which led to Equation (3.24) by comparing the branch-cut values with the SDP integration results for a wide range of parameters.

3.3 Pole Contribution

Unlike the branch points, which exist in all three of the correction vector potential components, the poles only exist in the vertical components of the vector potentials, viz., ${}_0\Pi_{hlz}$ and ${}_0\Pi_{vlz}$, and satisfy the relation

$$\kappa \cos \xi_p + \sqrt{\kappa - \sin^2 \xi_p} = 0 \tag{3.25}$$

Again, by considering the physical constraints discussed at the start of the previous section, only the following two poles need to be considered (see Figure 9):

$$\xi_p = \pi/2 \pm j \left[\mathrm{Ln}\left(\sqrt{\kappa} - j\right) - \mathrm{Ln}\left(\sqrt{\kappa + 1}\right)\right] \tag{3.26}$$

Table 3.1 Demonstrating the branch-cut contribution for $_0\Pi_{v1z}$. In this example: $f = 30$ MHz, $\phi_2 = 0$, $\varepsilon_g = 10$, $\sigma = .001$ mhos/m, and $I_{v0} = 1$.

r_2(meters)	θ_2	t_{max}	t_1	β_1	SDP integration result $\times 10^4$	Branch-cut contribution $\times 10^4$	Total value $\times 10^4$
20.	0.	.85	---	---	55.2-j2.07	---	55.2-j2.07
20.	30.	.85	---	---	53.2-j2.47	---	53.2-j2.46
20.	60.	.85	.81	1.8	44.6-j4.74	$-7.3 \times 10^{-4}+j1.3 \times 10^{-3}$	44.6-j4.74
20.	90.	.85	.55	2.0	14.5-j20.9	-.223+j.308	14.3-j20.6
10.	0.	1.2	---	---	111.6-j6.02	---	111.1-j6.02
10.	30.	1.2	---	---	107.6-j7.38	---	107.6-j7.38
10.	60.	1.2	.81	1.8	93.0-j14.4	-.128+j.204	92.9-j14.2
10.	90.	1.2	.55	2.0	50.2-j47.1	-3.85+j2.45	46.3-j44.7
5.	0.	1.7	---	---	-226.5+j17.5	---	-226.5+j17.5
5.	30.	1.7	---	---	-221.3+j21.3	---	-221.3+j21.3
5.	60.	1.7	.81	1.8	-199.1+j36.0	3.17-j3.61	-195.9+j32.4
5.	90.	1.7	.55	2.0	-140.3+j86.6	16.5-j22.7	-123.8+j63.9

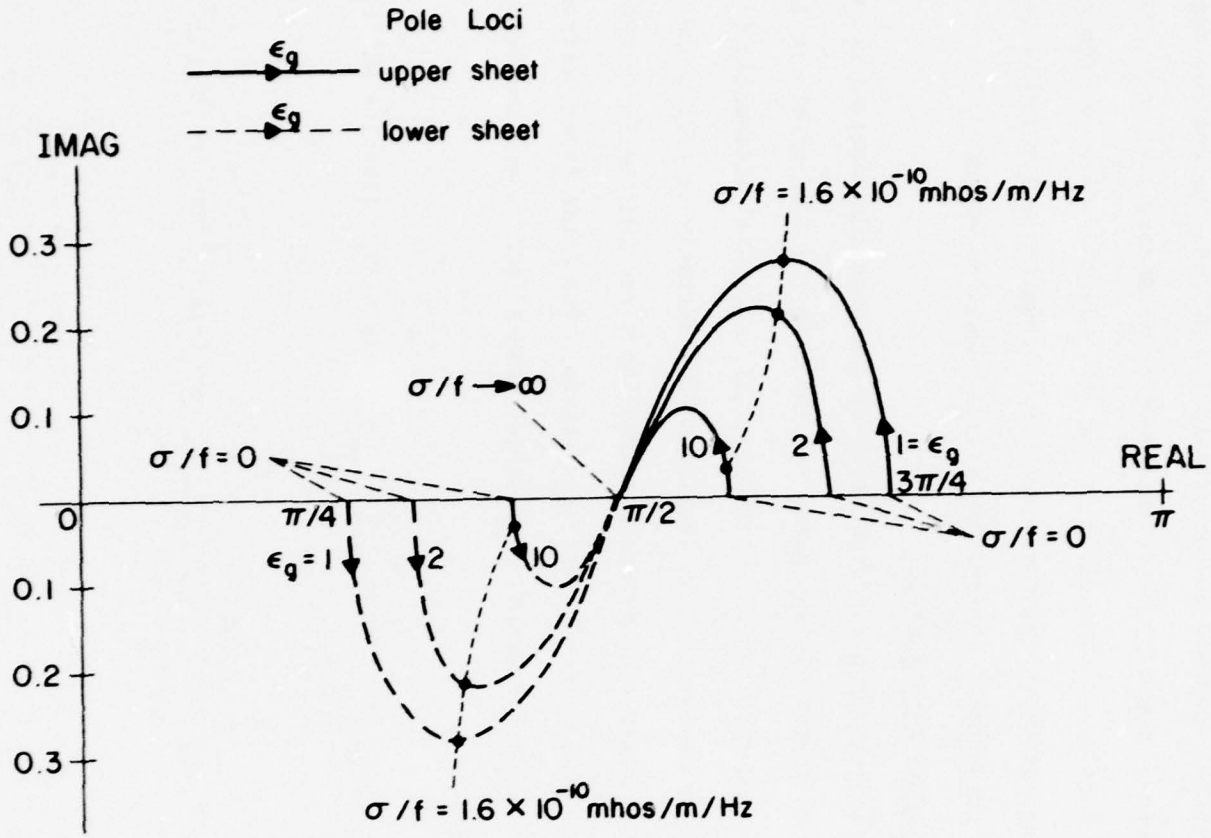

Figure 9. Pole loci as a function of ground parameters ϵ_g and σ/f.

Fortunately, one can verify that for $0 \leq \sigma/f < \infty$, $0 \leq \theta_2 < 90°$, and by considering the correct Riemann sheets (see Figure 7), the poles in Equation (3.26) will not be captured by the SDP and the residue contribution is not needed. However, under extreme circumstances, i.e., $\theta_2 \simeq 90°$ and small ε_g, a pole can come close to the SDP. In this case, a higher-order Gaussian quadrature integration routine is required and possibly the effective integration interval in (3.23) should be expanded.

3.4 Asymptotic Approximation

The steepest descent formulation of the previous sections can be used to derive an asymptotic expansion for the Sommerfeld integrals in terms of inverse powers of $k_1 r_2$. In Appendix II, a general discussion is presented for asymptotically evaluating the integral in (3.1), and as an example, the first two asymptotic expansion terms for the vector potential expressions in (2.47) - (2.49) are derived. The first terms, better known as the Fresnel's reflection coefficient method (RCM) approximations, are shown to be:

$$0^{\Pi}_{v1z} = I_{v0} \frac{2\kappa \cos\theta_2}{\kappa \cos\theta_2 + \sqrt{\kappa - \sin^2\theta_2}} \exp(-jk_1 r_2)/4\pi r_2 + O(k_1 r_2)^{-2} \tag{3.27}$$

$$0^{\Pi}_{h1x} = I_{h0} \frac{2 \cos\theta_2}{\cos\theta_2 + \sqrt{\kappa - \sin^2\theta_2}} \exp(-jk_1 r_2)/4\pi r_2 + O(k_1 r_2)^{-2} \tag{3.28}$$

$$0^{\Pi}_{h1z} = I_{h0}\, 2 \cos\phi_2 \sin\theta_2 \cos\theta_2 \frac{\cos\theta_2 - \sqrt{\kappa - \sin^2\theta_2}}{\kappa \cos\theta_2 + \sqrt{\kappa - \sin^2\theta_2}}$$

$$\cdot \exp(-jk_1 r_2)/4\pi r_2 + O(k_1 r_2)^{-2} \quad . \tag{3.29}$$

The above RCM expressions have been extensively used for high-frequency antenna applications ($k_1 r_2$ large) with surprisingly accurate results, e.g., [13], [14]. This success has been mainly due to the fact that for observation points away from the interface, the remaining vector potential components present in (2.20) and (2.30) tend to dominate over the RCM components thereby reducing the net error in the total vector potential values computed. Therefore, little is gained by adding the complicated second terms in the asymptotic expansion of the vector potentials, derived in Appendix II, since the accuracy of the total vector potential will not be affected appreciably.

An error of 5% or less can be expected in the RCM vector potential components shown in (3.27) - (3.29) when

$$k_1 r_2 \geq 10 \quad , \tag{3.30}$$

and as long as the branch-cut conditions given in the previous section are not violated (see Tables 3.2 - 3.4). These conditions are more general than the one proposed by Sarkar [7] in defining the useful range of the RCM expressions. The second terms in the asymptotic expansion, as demonstrated in Tables 3.2 - 3.4, only offer a slight improvement in the accuracy of the $\overset{\Pi}{0}_{h1x}$ RCM expression in the region where the branch-cut contribution is negligible. The remaining vector potential components, however, do not benefit from the 2^{nd} term in the asymptotic expansions, possibly because they contain a pole in their Sommerfeld integrals. Figures 10 - 12 also compare the RCM, two-term asymptotic expansion and the exact integration values of the correction vector potential components for a typical half-space as a function of $k_1 r_2$. Finally, in order to

Table 3.2 Comparing the exact integration values for $_0\Pi_{v1z}$ with its one- and two-term asymptotic expansions. In this example, f = 30 MHz, $\phi_2 = 0$, $\varepsilon_g = 10$, $\sigma = .001$ mhos/m, and $I_{v0} = 1$.

$k_1 r_2$	θ_2	1-term asymptotic expansion (RCM) $\times 10^3$	2-term asymptotic expansion $\times 10^3$	SDP integration result $\times 10^3$
1.	20.	35.7-j58.0	57.3-j51.8	34.6-j68.2
4.	20.	-10.9+j13.1	-12.2+j12.5	-10.4+j14.1
8.	20.	-1.40-j8.40	-1.08-j8.55	-1.69-j8.41
12.	20.	4.85+j2.96	4.80+j3.11	4.93+j2.85
1.	60.	28.6-j46.8	64.4-j55.2	29.1-j59.0
4.	60.	-8.73+j10.6	-11.0+j10.8	-7.97+j1.31
8.	60.	-1.15-j6.76	-.813-j7.23	-2.02-j6.96
12.	60.	3.91+j2.37	3.97+j2.62	4.23+j2.08
1.	80.	15.5-j26.0	-192.9-j169.2	19.8-j48.6
4.	80.	-4.76+j5.87	6.87+j16.6	-4.54+j11.5
8.	80.	-.668-j3.72	-4.59-j3.27	-2.82-j4.69
12.	80.	2.17+j1.28	3.16-j.168	3.24+j.619

Table 3.3 Comparing the exact integration values for $_0\Pi_{h1x}$ with its one- and two-term asymptotic expansions. In this example, f = 30 MHz, $\phi_2 = 0$, $\varepsilon_g = 10$, $\sigma = .001$ mhos/m, and $I_{h0} = 1$.

$k_1 r_2$	θ_2	1-term asymptotic expansion (RCM) $\times 10^3$	2-term asymptotic expansion $\times 10^3$	SDP integration result $\times 10^3$
1.	20.	17.1-j24.3	17.2-j34.3	14.1-j36.0
4.	20.	-5.10+j5.42	-4.24+j6.17	-4.48+j6.32
8.	20.	-.383-j3.70	-.667-j3.66	-.665-j3.70
12.	20.	2.03+j1.42	2.10+j1.31	2.11+j1.32
1.	60.	11.4-j15.8	-10.0-j31.7	7.76-j36.9
4.	60.	-3.38+j3.50	-2.19+j4.67	-2.26+j4.84
8.	60.	-.217-j2.42	-.634-j2.40	-.635-j2.41
12.	60.	1.32+j.946	1.43+j.796	1.43+j.799
1.	80.	4.72-j6.36	-17.0-j24.2	.329-j39.8
4.	80.	-1.39+j1.41	-.208+j2.71	.405+j2.31
8.	80.	-.077-j.987	-.516-j.975	-.537-j.953
12.	80.	.532+j.391	.655+j.240	.651+j.236

Table 3.4 Comparing the exact integration values for ${}_0\Pi_{h1z}$ with its one- and two-term asymptotic expansions. In this example, f = 30 MHz, $\phi_2 = 0$, $\varepsilon_g = 10$, $\sigma = .001$ mhos/m, and $I_{h0} = 1$.

$k_1 r_2$	θ_2	1-term asymptotic expansion (RCM) $\times 10^3$	2-term asymptotic expansion $\times 10^3$	SDP integration result $\times 10^3$
1.	20.	-3.18+j5.00	-7.88+j3.04	-3.84+j6.20
4.	20.	.963-j1.13	1.24-j.963	.895-j1.33
8.	20.	.112+j.733	.036+j.758	.172+j.739
12.	20.	-.418-j.263	-.405-j.296	-.437-j.242
1.	60.	-8.08+j12.5	-17.7+j16.5	-12.9+j21.9
4.	60.	2.44-j2.80	3.07-j2.97	1.97-j4.50
8.	60.	.261+j1.84	.190+j1.98	.739+j1.93
12.	60.	3.91+j2.37	3.97+j2.62	4.23+j2.08
1.	80.	-5.96+j9.14	84.9+j79.0	-20.6+j34.1
4.	80.	1.80-j2.05	-3.21-j7.17	.419-j6.80
8.	80.	.189+j1.35	1.98+j1.24	1.48+j1.84
12.	80.	-.764-j.493	-1.25+j.140	-1.32-j.111

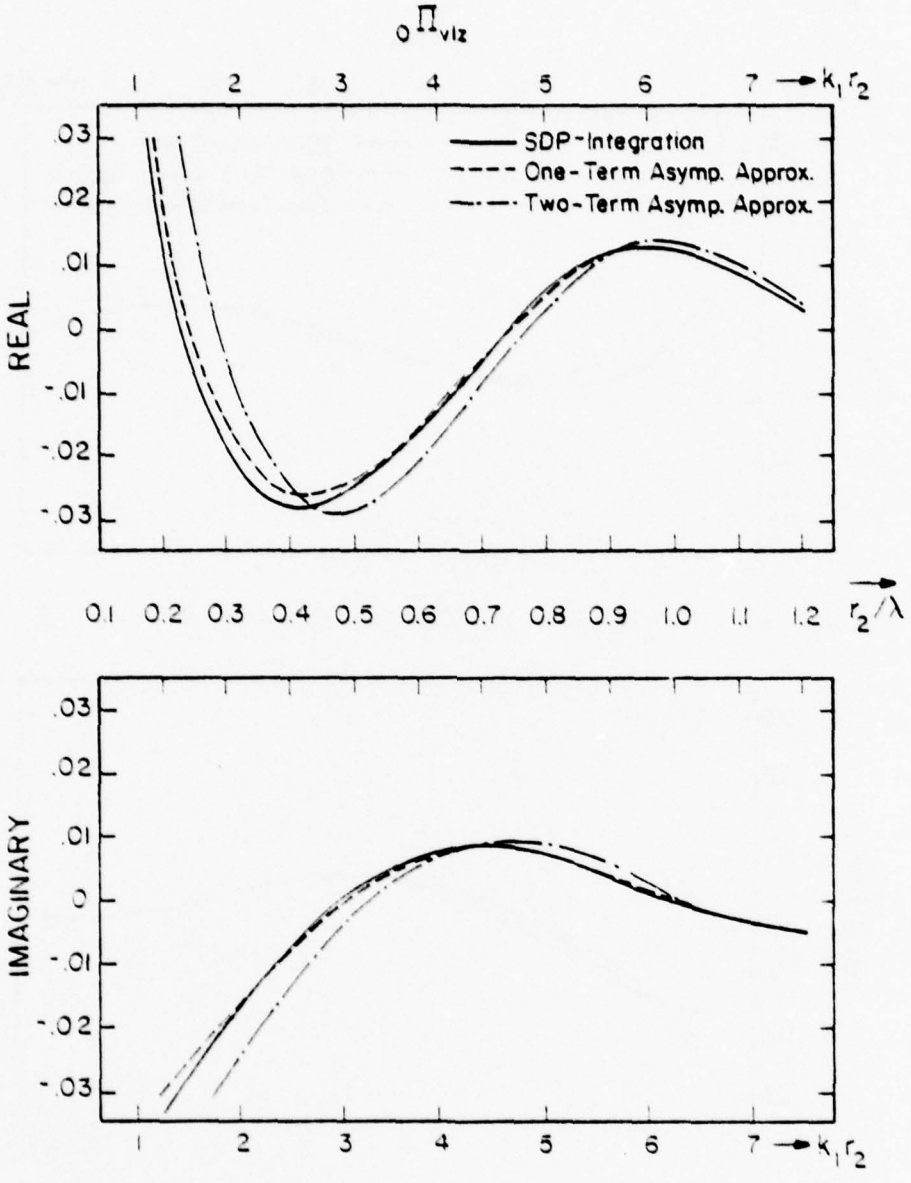

Figure 10. Comparing the SDP integration with the one- and the two-term asymptotic expansions of $_0\Pi_{v1z}$. For this case, frequency = 30 MHz $\theta_2 = 10°$, $\phi_2 = 0$, $\varepsilon_g = 10$, and $\sigma = .01$ mhos/m.

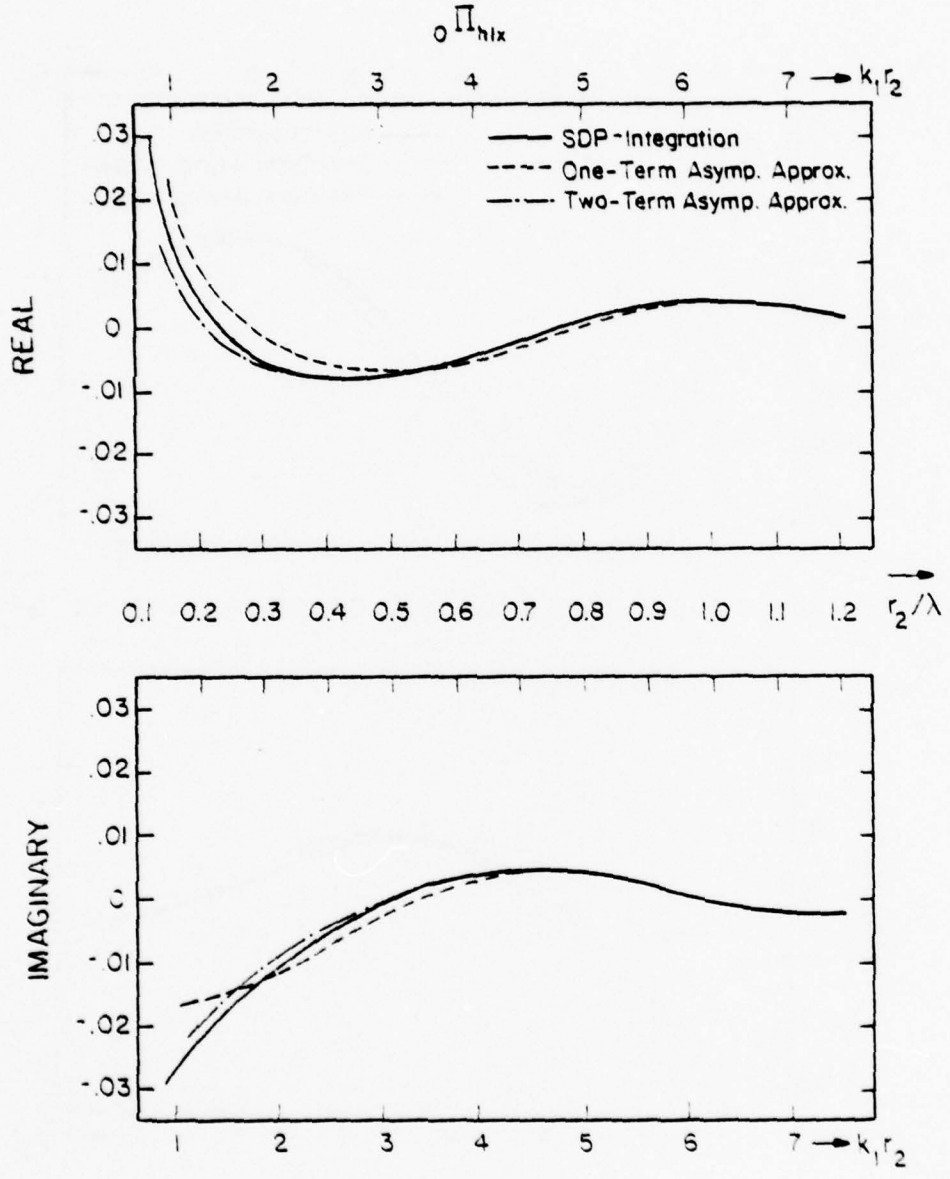

Figure 11. Comparing the SDP integration with the one- and two-term asymptotic expansions of $_0\Pi_{h1x}$. The parameters are identical to those in Figure 10.

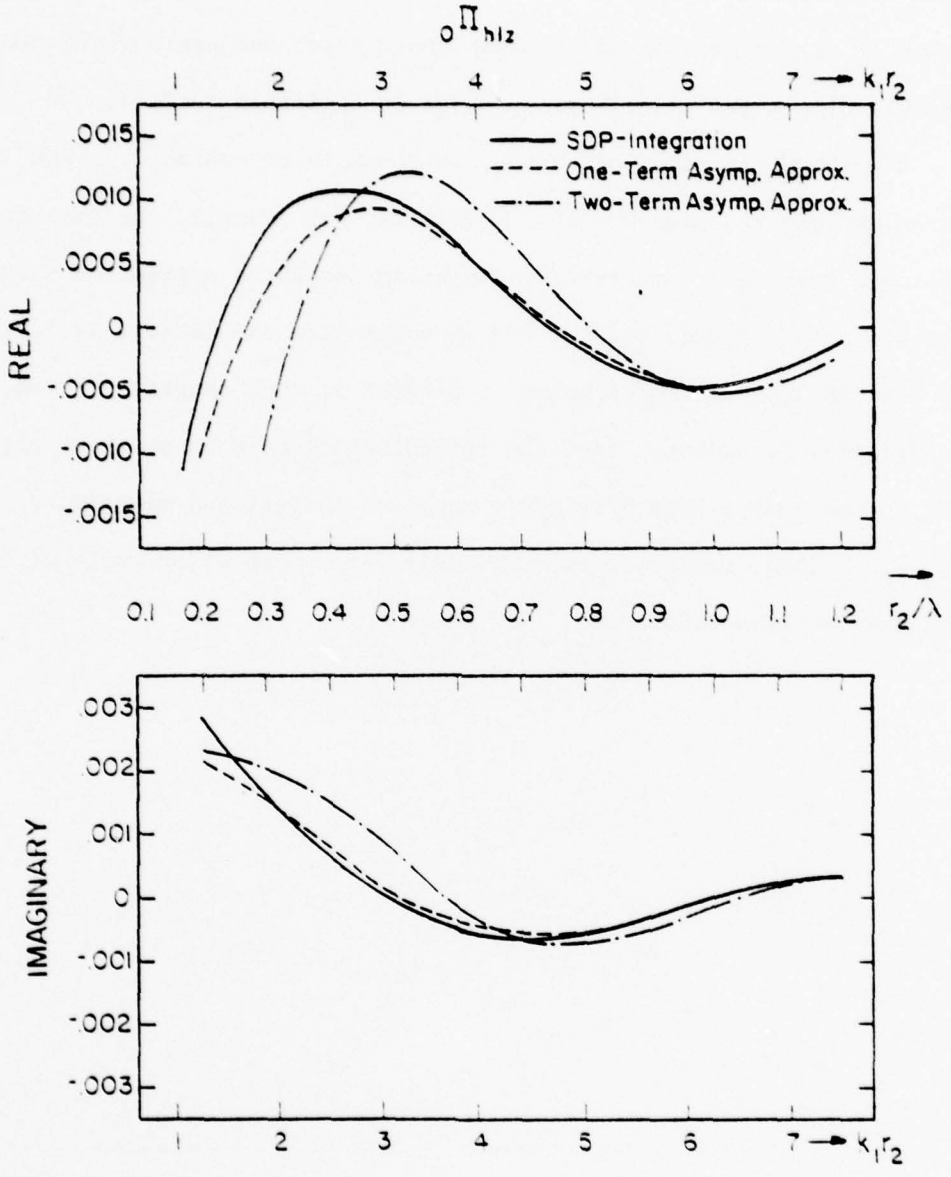

Figure 12. Comparing the SDP integration with the one- and the two-term asymptotic expansions of $_0\Pi_{h1z}$. The parameters are identical to those in Figure 10.

demonstrate the branch-cut effect, Figure 13 is included to show the minimum $k_1 r_2$ contours in the κ-plane above which one can neglect the possible branch-cut contribution (based on condition (3.24)).

The computing time, of course, is the main reason why the RCM approximations are used whenever possible. For example, the execution time on a Cyber 175 computer for computing the three correction vector potentials is $\approx$ 1 msec for the RCM approximation and as high as 50-100 msec for the SDP integration technique presented in this chapter. It should be pointed out, however, that the SDP integration is an order of magnitude faster than many of the previously reported integration techniques [3] - [9], [12], making it more suitable for a much wider range of low-frequency applications.

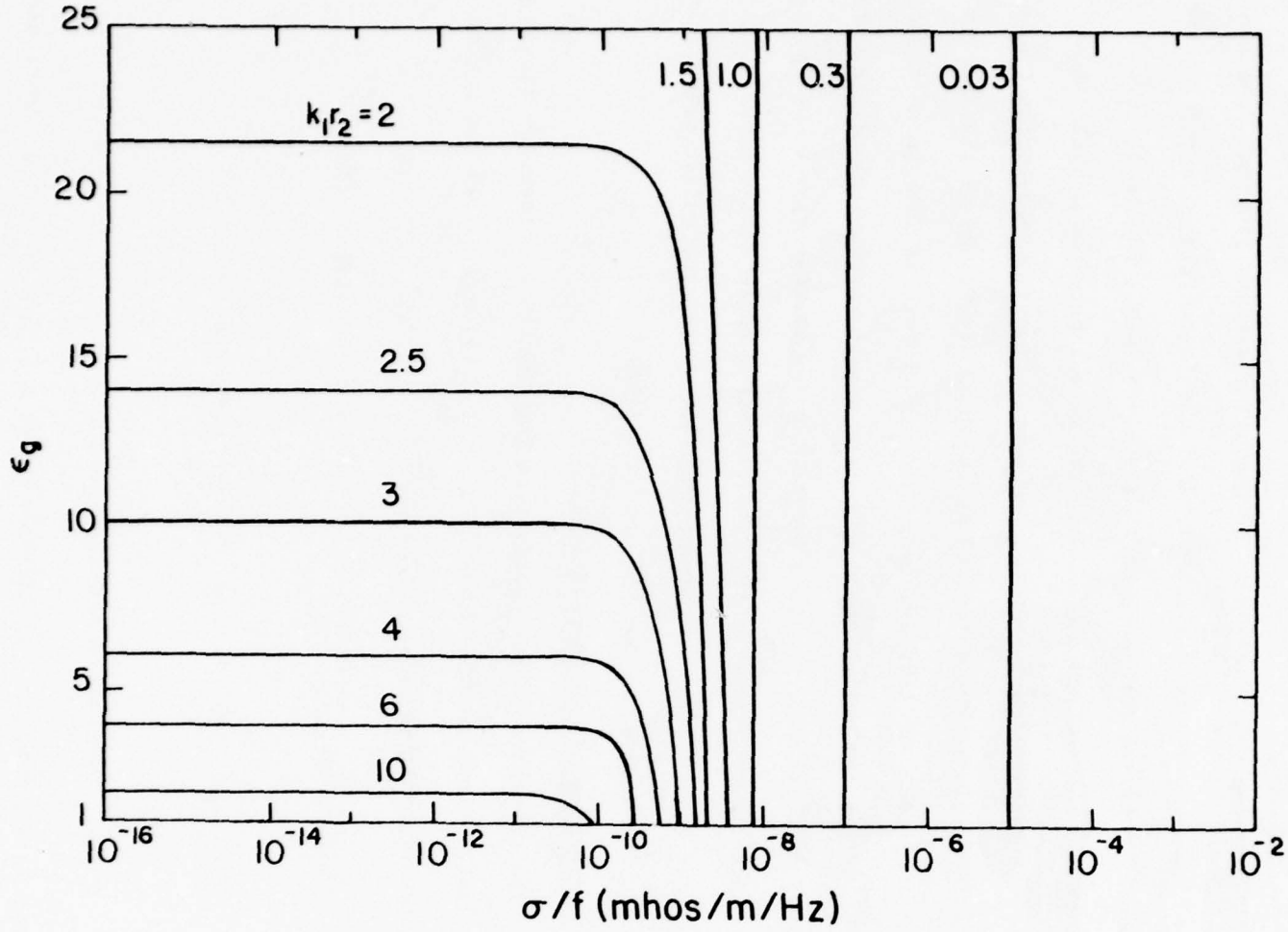

Figure 13. Minimum $k_1 r_2$ contours as a function of ϵ. Once a branch point is captured, a branch-cut integration is negligible if the $k_1 r_2$ is greater than the minimum values depicted in this graph.

4. COMPUTATIONS OF THE VECTOR POTENTIALS WITHOUT SOMMERFELD INTEGRATION

The conventional approach for analyzing antenna problems over lossy ground involves repeated evaluations of the Sommerfeld integrals appearing in the expressions for the vector potentials, viz., Equations (3.8) - (3.10). Even though the SDP procedure discussed in the previous chapter is an efficient integration technique, the computation time needed for evaluating these integrals severely limits the physical dimensions of the antenna problems being analyzed. In this chapter, a novel approach is introduced by initially approximating the well-behaved transform domain expressions of these integrals, derived in Chapter 2, and then performing the inverse transform operations via a set of exact identities. The resulting space domain expressions are valid for a wide range of parameters, with their computation times being comparable to those of the RCM approximation.

4.1 Transform Domain Expressions

The transform domain expressions for the three correction vector potential components shown in Equations (2.21c), (2.31c), and (2.32) can be rewritten in the following forms:

$$\tilde{\Pi}_{0hlx} = I_{h0} \frac{1}{jk_1^2(1-\kappa)} (\gamma_1 - \gamma_2) \exp(-j\gamma_1 z_2) \tag{4.1}$$

$$\tilde{\Pi}_{0hlz} = I_{h0} \frac{j\alpha}{k_1^2 \kappa} \left[1 - (\kappa + 1) \frac{\gamma_2}{\kappa\gamma_1 + \gamma_2}\right] \exp(-j\gamma_1 z_2) \tag{4.2}$$

$$\tilde{\Pi}_{0vlz} = I_{v0} \frac{\kappa}{j(\kappa\gamma_1 + \gamma_2)} \exp(-j\gamma_1 z_2) \tag{4.3}$$

where $z_2 = z + h$, and $\gamma_{1,2}$, defined in (2.15), are explicitly expressed as

$$\gamma_1 = (k_1^2 - \alpha^2 - \beta^2)^{1/2} \quad ; \quad \mathrm{Im}(\gamma_1) \leq 0 \tag{4.4a}$$

$$\gamma_2 = (\kappa k_1^2 - \alpha^2 - \beta^2)^{1/2} \quad ; \quad \mathrm{Im}(\gamma_2) \leq 0 \quad . \tag{4.4b}$$

In addition, the free-space Green's function g can also be expressed in the transform domain (see Equations (2.41b) and (2.31b)) yielding the following transform pair:

$$\tilde{g}(\alpha, \beta, z_2) = \frac{1}{2j\gamma_1} \exp(-j\gamma_1 z_2) \tag{4.5a}$$

$$g(x, y, z_2) = \exp(-jk_1 r_2)/4\pi r_2 \quad ; \quad r_2 = [x^2 + y^2 + z_2^2]^{1/2} \quad . \tag{4.5b}$$

By applying a successive $\partial/\partial z$ operator to (4.5), an infinite set of transform pairs is obtained, viz.,

$$\tilde{Q}_n = \gamma_1^{n-1} \exp(-j\gamma_1 z_2) \tag{4.6a}$$

$$Q_n = 2(j)^{n+1} \frac{\partial^n}{\partial z^n} g(x, y, z_2) \quad ; \quad n = 0,1,2,\ldots \tag{4.6b}$$

where Q is expressed in a closed form for all n and can be numerically evaluated quite rapidly (see Appendix III).

An examination of the Fourier transformed vector potentials in (4.1) - (4.3) and the $\tilde{Q}_n$ in (4.6a) reveals two important and useful properties. First, all of the expressions have an identical z-variation term that corresponds to a space-domain solution emanating at the image point P_2. Second, it is apparent that all of the equations are well-behaved in the Fourier domain and decay exponentially to zero outside the circle $\alpha^2 + \beta^2 = k_1^2$. These properties give rise to the possibility of performing the inverse transform operation on Equations (4.1) - (4.3) via the use of the (4.6) identities. The major obstacle to such a procedure is the existence

of γ_2 in these expressions which is overcome in the following section by an appropriate approximation.

4.2 Approximating γ_2 and Space-Domain Results

All three Fourier transform domain expressions in (4.1) - (4.3) can be put into the following general form

$$\tilde{\Pi}_0 = f(\gamma_1, \gamma_2) \exp(-j\gamma_1 z_2) \quad . \tag{4.7}$$

As mentioned in the previous section, an important property of Equation (4.7) is the exponential term which rapidly decays to zero outside the circle $\alpha^2 + \beta^2 = k_1^2$ (also see Figure 14). This fact enables one to replace γ_2, defined in (4.4b), by the first term of its Taylor's series expansion $\bar{\gamma}_2$, that is,

$$\gamma_2 = k_1\sqrt{\kappa}\left[1 - \frac{\alpha^2+\beta^2}{2k_1^2\kappa} - \frac{1}{8}\left(\frac{\alpha^2+\beta^2}{k_1^2\kappa}\right)^2 - \ldots\right] \quad ; \quad \alpha^2+\beta^2 \leq k_1^2|\kappa| \tag{4.8a}$$

$$\bar{\gamma}_2 = k_1\sqrt{\kappa} \quad . \tag{4.8b}$$

For most practical values of κ, i.e., $|\kappa| \geq 10$, the approximation in (4.8b) is excellent inside the circle $\alpha^2 + \beta^2 \leq k_1^2$. Fortunately, as demonstrated in Figure 14, the decaying exponential in (4.7) can easily overcome the errors introduced by (4.8b) in the region $\alpha^2 + \beta^2 \geq k_1^2$ thereby making this a valid approximation throughout the $\alpha\beta$-plane for a wide range of κ and z_2 parameters, namely,

$$\tilde{\bar{\Pi}}_0 \simeq f(\gamma_1, \bar{\gamma}_2) \exp(-jk_1 z_2) \tag{4.9}$$

where the bar on top represents the approximate quantities. It should be noted that Kuo and Mei [12, Eq. 8] have recently verified and used the aforementioned approximation for simplifying the space domain expressions,

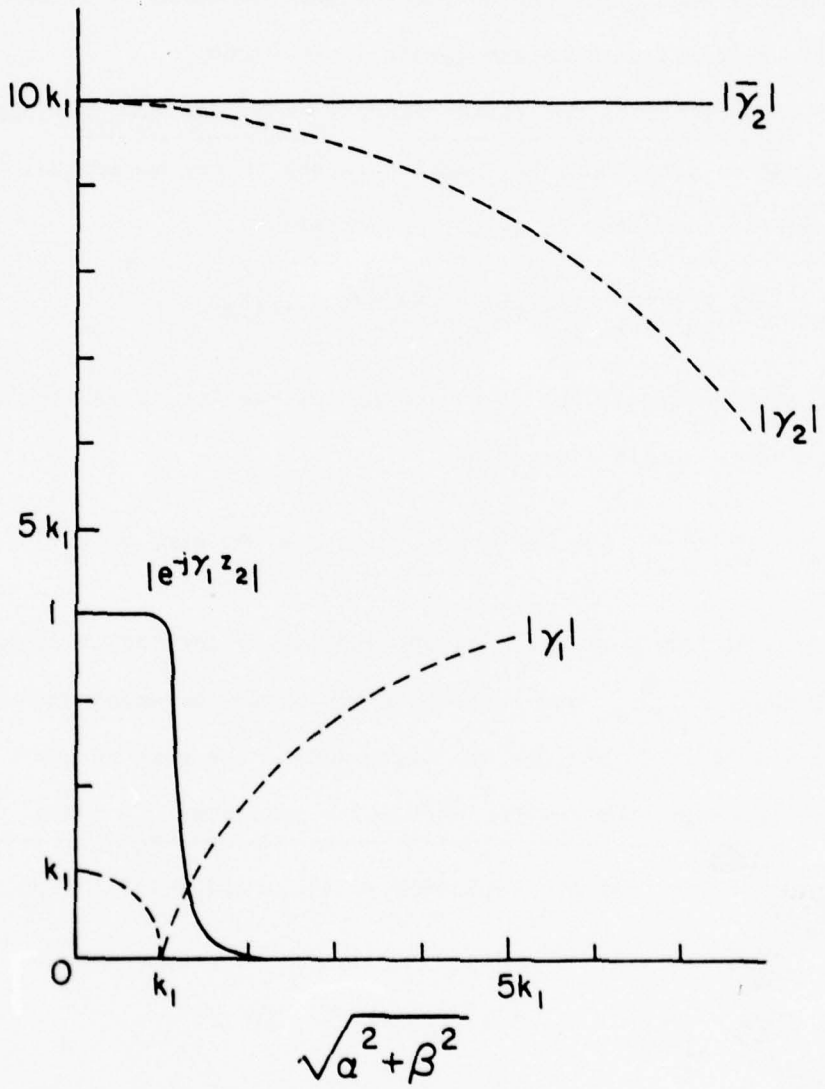

Figure 14. The plot of the functions $|\bar{\gamma}_2|$, $|\gamma_2|$, $|\gamma_1|$, and $|e^{-j\gamma_1 z_2}|$ versus $\sqrt{\alpha^2 + \beta^2}$. Note that for $|\kappa|$ large enough, the following approximation holds: $\gamma_2 e^{-j\gamma_1 z_2} \approx \bar{\gamma}_2 e^{-j\gamma_1 z_2}$.

while Chang et al. [6] have employed an equivalent approximation for representing the vector potential in the vertical current element problem in terms of an incomplete Hankel function. The approximate transform domain vector potential quantities can now be treated individually in order to obtain their respective transform domain expressions.

4.2.1 Approximation for the horizontal component ($_0\bar{\Pi}_{h1x}$). Applying the approximation introduced in Equation (4.8b) to the horizontal correction vector potential component in (4.1), one obtains

$$_0\tilde{\bar{\Pi}}_{h1x} = I_{h0} \frac{1}{jk_1^2(1 - \kappa)} (\gamma_1 - k_1\sqrt{\kappa}) \exp(-j\gamma_1 z_2) \quad , \tag{4.10}$$

and direct application of the (4.6) identities results in the following closed-form space domain expression:

$$_0\bar{\Pi}_{h1x} = \frac{-2I_{h0}}{k_1^2(1 - \kappa)} \left[jk_1\sqrt{\kappa} \frac{\partial}{\partial z} g(x, y, z_2) + \frac{\partial^2}{\partial z^2} g(x, y, z_2) \right] \quad . \tag{4.11}$$

Note that the various partials of g are explicitly derived in Appendix III. The useful range of $_0\bar{\Pi}_{h1x}$ and the comparison of its accuracy and efficiency with other available techniques are discussed in the next section.

4.2.2 Approximation for the vertical components ($_0\bar{\Pi}_{h1z}$ and $_0\bar{\Pi}_{v1z}$). Again the variable γ_2 can be eliminated in (4.2) and (4.3) by applying the approximation in (4.8b), that is,

$$_0\tilde{\bar{\Pi}}_{h1z} = I_{h0} \frac{j\alpha}{k_1^2\kappa} \left[1 - j(\kappa + 1) \frac{c}{j(\gamma_1 + c)} \right] \exp(-j\gamma_1 z_2) \tag{4.12}$$

$$_0\tilde{\bar{\Pi}}_{v1z} = I_{v0} \frac{1}{j(\gamma_1 + c)} \exp(-j\gamma_1 z_2) \quad , \tag{4.13}$$

where the constant c is defined as

$$c = k_1/\sqrt{\kappa} \quad . \tag{4.14}$$

Application of the identities in Equation (4.6) results in the following space domain forms:

$$0\bar{\bar{\Pi}}_{h1z} = \frac{I_{h0}}{k_1^2 \kappa} \left[-2 \frac{\partial^2}{\partial x \partial z} g(x, y, z_2) - jc(\kappa + 1) \frac{\partial}{\partial x} S(x, y, z_2)\right] \quad (4.15)$$

$$0\bar{\bar{\Pi}}_{v1z} = I_{v0} S(x, y, z_2) \quad . \quad (4.16)$$

Unfortunately, the function S, whose transform domain expression is defined as

$$\tilde{S}(\alpha, \beta, z_2) = 0\tilde{\bar{\Pi}}_{v1z}/I_{v0} = \frac{1}{j(\gamma_1 + c)} \exp(-j\gamma_1 z_2) \quad , \quad (4.17)$$

cannot be expressed in a simple closed form. However, by using the (4.6) identities, it can be shown that S satisfies the following first-order inhomogeneous linear differential equation:

$$\frac{\partial}{\partial z} [S(\rho, z_2) \exp(-jcz_2)] = 2 \exp(-jcz_2) \frac{\partial}{\partial z} g(\rho, z_2) \quad , \quad (4.18)$$

where, for convenience, the functional dependences of S and g have been reduced from (x, y, z_2) to (ρ, z_2). By integrating (4.18) with respect to z_2, and after some algebraic manipulations, the following expression is derived for S:

$$S(\rho, z_2) = [S(\rho, z_2') - 2g(\rho, z_2')]\exp[jc(z_2 - z_2')] + 2g(\rho, z_2)$$

$$+ 2jc \exp(jcz_2) \int_{z_2'}^{z_2} g(\rho, z) \exp(-jcz)\, dz \quad . \quad (4.19)$$

The secondary height z_2' is an arbitrary starting point needed for obtaining a unique solution to the (4.18) differential equation. Since no simple starting point can be found at which $S(\rho, z_2')$ is known, it is assumed that z_2' is large enough so that the RCM approximation in Equation (3.27) is

applicable (see Figure 15), that is,

$$S(\rho, z_2') = \frac{2\kappa \cos \theta_2'}{\kappa \cos \theta_2' + \sqrt{\kappa - \sin^2 \theta_2'}} g(\rho, z_2') \tag{4.20}$$

where angle θ_2' is defined in Figure 15. A similar procedure can be used for computing $\frac{\partial}{\partial x} S$, required for ${}_0\bar{\bar{\Pi}}_{h1z}$ in Equation (4.15), by simply differentiating (4.19) with respect to x:

$$\frac{\partial}{\partial x} S(\rho, z_2) = [\frac{\partial}{\partial x} S(\rho, z_2') - 2 \frac{\partial}{\partial x} g(\rho, z_2')] \exp [jc(z_2 - z_2')] + 2 \frac{\partial}{\partial x} g(\rho, z_2)$$

$$+ 2jc \exp (jcz_2) \int_{z_2'}^{z_2} \frac{\partial}{\partial x} g(\rho, z) \exp (-jcz) \, dz \quad , \tag{4.21}$$

and by using the asymptotic expression in (3.29), the following initial value at point z_2' is obtained:

$$\frac{\partial}{\partial x} S(\rho, z_2') = \frac{2j}{c(\kappa + 1)} \left[\frac{\partial^2}{\partial x \partial z} g(\rho, z_2') + k_1^2 \kappa \cos \phi_2 \sin \theta_2' \cos \theta_2' \right.$$

$$\left. \cdot \frac{\cos \theta_2' - \sqrt{\kappa - \sin^2 \theta_2'}}{\kappa \cos \theta_2' + \sqrt{\kappa - \sin^2 \theta_2'}} g(\rho, z_2') \right] \quad . \tag{4.22}$$

In summary, the procedure for computing the vertical vector potential components at the point (ρ, z_2), as demonstrated in Figure 15, is to start from a higher observation point (ρ, z_2'), at which the RCM expressions are valid, and simply use Equation (4.19) or (4.21) to integrate down to (ρ, z_2). This procedure effectively computes a correction term for the RCM approximations of the vertical vector potential components in the region where RCM alone breaks down. The useful range and the accuracy of this procedure are discussed in the following section.

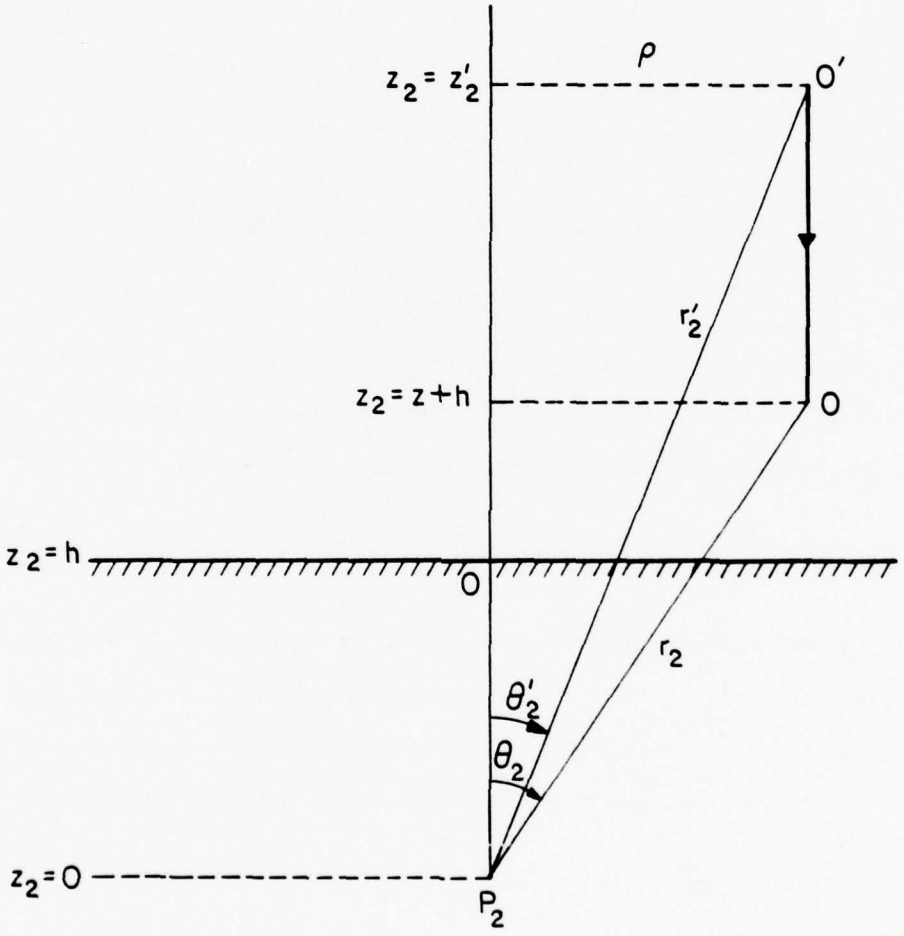

Figure 15. The geometry for computing the vertical vector potential components. r'_2 is chosen to be large enough so that the RCM expressions are valid at 0'. Therefore, the vector potential values along the interval 0'0 are obtained by using the initial initial value at 0' and integrating down along the z-axis.

4.3 Error Estimation for the Approximate Expressions

In the previous section, only the approximation in (4.8) was made to derive the horizontal vector potential component in Equation (4.11). The approximated term T in this vector potential component, for convenience, can be expressed in the following forms:

$$\tilde{T} = \gamma_2 \exp(-j\gamma_1 z_2) \tag{4.23a}$$

$$\tilde{\bar{T}} = \bar{\gamma}_2 \exp(-j\gamma_1 z_2) \tag{4.23b}$$

$$\bar{T} = -2k_1\sqrt{\kappa}\,\frac{\partial}{\partial z}\, g(\rho, z_2) \quad . \tag{4.23c}$$

The error introduced by (4.23b) in the transform domain is simply

$$\Delta\tilde{T} = \tilde{T} - \tilde{\bar{T}} = (\gamma_2 - \bar{\gamma}_2) \exp(-j\gamma_1 z_2) \quad , \tag{4.24}$$

and again referring to the Taylor's series expansion for γ_2 in (4.8a), which is convergent for $\alpha^2 + \beta^2 < k_1^2|\kappa|$, one can assume $\Delta\tilde{T}$ to be proportional to the second term of the expansion, namely,

$$\Delta\tilde{T} \simeq \frac{-(\alpha^2 + \beta^2)}{2k_1\sqrt{\kappa}} \exp(-j\gamma_1 z_2) \quad . \tag{4.25}$$

At the same time, a constraint is needed for z_2 in order to enforce the exponential term in (4.25) to decay sufficiently, i.e., to 1%, when $\alpha^2 + \beta^2 = k_1^2|\kappa|$. This important condition, which allows one to use (4.25) for error analysis, can be expressed in the following simple form:

$$k_1 z_2 > \frac{5}{\sqrt{|\kappa|} - 1} \quad . \tag{4.26}$$

By substituting $\alpha^2 + \beta^2$ from (4.4a) into Equation (4.25), one can obtain ΔT directly via the (4.6) identities, namely,

$$\Delta T = \frac{k_1}{\sqrt{\kappa}}\,\frac{\partial}{\partial z}\, g(\rho, z_2) + \frac{1}{k_1\sqrt{\kappa}}\,\frac{\partial^3}{\partial z^3}\, g(\rho, z_2) \quad . \tag{4.27}$$

The space domain expressions in (4.23c) and (4.27) can be used to define R_T, the relative error in the magnitude of $\bar{T}$, as

$$R_T = \left|\frac{\Delta T}{\bar{T}}\right| \leq \frac{1}{2|\kappa|} + \frac{1}{2k_1^2|\kappa|} \left|\frac{\frac{\partial^3}{\partial z^3} g(\rho, z_2)}{\frac{\partial}{\partial z} g(\rho, z_2)}\right| \quad ; \tag{4.28}$$

and by using the explicit expansions provided in Appendix III, the above relation can be further reduced to

$$R_T < \frac{1}{2|\kappa|} + \frac{1}{2|\kappa|} \left\{ |5\cos^2\theta_2 - 3| \left[\frac{1}{(k_1 r_2)^2} \left(2 + \frac{1}{\sqrt{1 + (k_1 r_2)^2}}\right) + \frac{1}{k_1 r_2} \right] + \cos^2\theta_2 \right\} . \tag{4.29}$$

Equation (4.29) is a useful upper bound for the error existing in the computed magnitude of ${}_0\bar{\Pi}_{h1x}$. The first term in the aforementioned equation sets a limit on the minimum required $|\kappa|$ value; for example, the error condition $R_T < 10\%$ requires $|\kappa| > 10$, while $R_T < 5\%$ will require $|\kappa| > 20$. Figures 16 and 17 demonstrate the valid regions in the (r_2, θ_2) plane as a function of $|\kappa|$ for two useful error conditions, namely, $R_T = 5\%$ and 10%, respectively. Table 4.1 is included to numerically verify the conditions (4.26) and (4.29) by comparing the approximate horizontal vector potential values in (4.11) with the corresponding exact SDP integration results of Chapter 3. As clearly demonstrated in this table, the actual computed errors in the magnitude are consistently below the R_T values obtained from Equation (4.29), for the various (κ, r_2, θ_2) combinations tested.

Unfortunately, because of the complicated nature of the approximate transform expressions (4.12) - (4.13), one cannot derive a simple error condition for the vertical potential components, as was derived for the horizontal case (Equation (4.29)). However, because of the similar nature

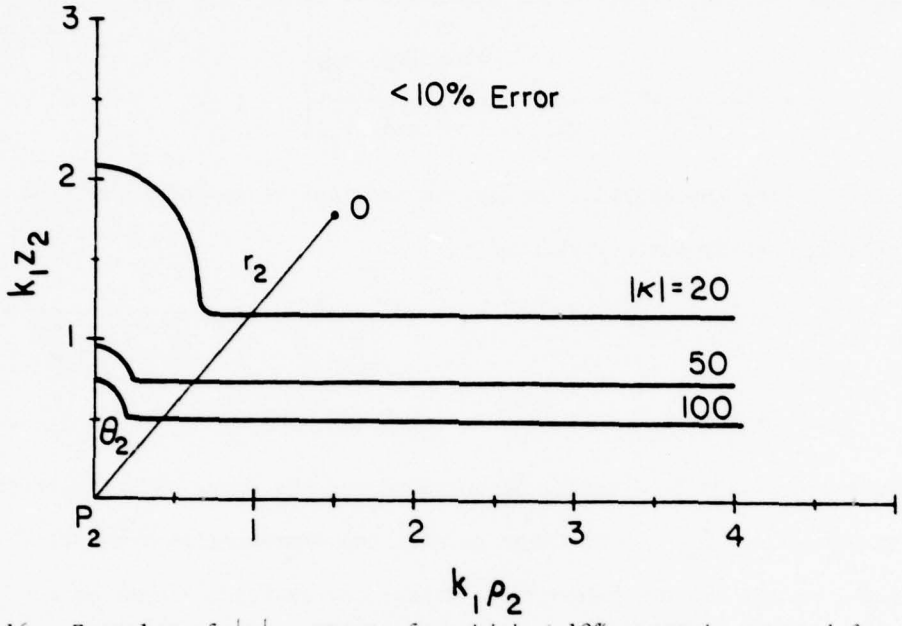

Figure 16. Examples of $|\kappa|$ contours for which < 10% error is ensured for observation points on or above it.

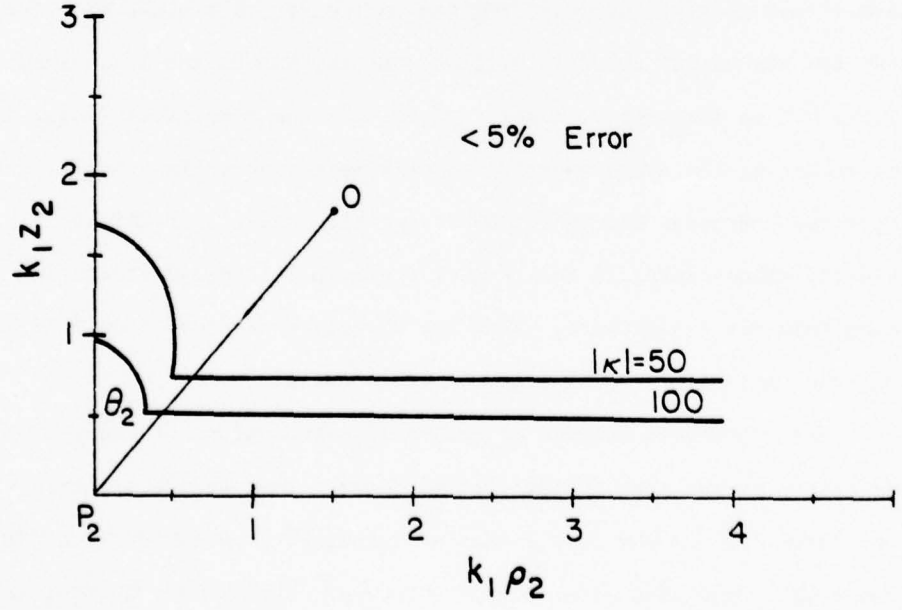

Figure 17. Examples of $|\kappa|$ contours for which < 5% error is ensured for observation points on or above it.

of the approximation for all three of the correction vector potential components, one can assume that conditions (4.26) and (4.29) also apply to the ${}_0\bar{\bar{\Pi}}_{h1z}$ and ${}_0\bar{\bar{\Pi}}_{v1z}$ expressions shown in Equations (4.15) - (4.16). This assumption is verified by the results in Tables 4.2 and 4.3 in which the vertical-correction-vector potential components are computed by using $k_1 r_2' = 10$ as a starting point. Even though these RCM initial values, in general, contain about 5% error, the net errors in all of the cases are well below the predicted ones (Equation (4.29)). Table 4.4 is also included to demonstrate the stability of the final vertical vector potential value as a function of starting point z_2'. Note that when $k_1 r_2' > 10$, the error in the final results stays within acceptable levels of the exact values primarily because the RCM approximation used to compute the starting point becomes reasonably accurate in this region.

Studying the results of this section, one can conclude that the proposed approximate formulas, i.e., (4.11), (4.15) and (4.16), can be employed in most practical antenna problems as long as $|\kappa| > 10$ and condition (4.26) is satisfied.

4.4 Advantages of the Approximate Expressions

The major advantage of the approximate technique introduced in the chapter is, of course, the computation of the vector potentials. For example, on the Cyber-175 computer, the computation time for computing the three vector potential expressions is $\simeq$ 1 msec for the RCM technique, $\simeq$ 5 msec for the approximate technique presented in this chapter, and finally $\simeq$ 50-100 msec for the SDP integration technique discussed in Chapter 3. Note that even though the approximate technique is slightly more time-consuming than the RCM method, it can be applied to a much

Table 4.1 Comparison of the RCM, exact, and the approximate evaluations of $_0\Pi_{v1z}$. For this example, f = 30 MHz, $\theta_2 = 45^o$, $\phi_2 = 0^o$, and $I_{v0} = 1$.

	k_1r_2	k_1z_2	Min. k_1z_2 Eq. (4.26)	RCM value $\times 10^2$	Exact integration $\times 10^2$	Approximate technique $\times 10^2$	% error Eq. (4.29)	% error actual
ε_g=5, σ=.001, $\lvert\kappa\rvert$=5.04	.1	.07	2.49	62.1-j7.49	79.6-j11.2	96.3-j17.2	1551.	16.0
	1.	.71	2.49	3.28-j5.33	3.22-j6.52	2.94-j7.13	33.3	8.7
	2.	1.41	2.49	-1.36-j2.82	-1.84-j2.95	-1.96-j2.88	20.4	4.0
	6.	4.24	2.49	1.01+j.272	1.06+j2.00	1.03-j2.09	16.0	2.9
	10.	7.07	2.49	-.518+j.351	-.507+j.383	-.518+j.351	15.5	5.5
ε_g=10, σ=.01, $\lvert\kappa\rvert$=11.7	.1	.07	1.53	70.5-j12.4	90.8-j15.8	96.6-j15.7	67.0	5.9
	1.	.71	1.53	3.41-j6.30	3.47-j7.76	3.42-j7.86	14.4	1.2
	2.	1.41	1.53	-1.73-j3.14	-2.23-j3.34	-2.28-j3.30	8.8	1.7
	6.	4.24	1.53	1.17+j.247	1.23+j.184	1.19+j.179	6.9	2.8
	10.	7.07	1.53	-.570+j.433	-.562+j.465	-.570+j.433	6.7	4.6
ε_g=40, σ=1, $\lvert\kappa\rvert$=601	.1	.07	.204	95.0-j13.2	99.5-j11.0	99.6-j11.0	13.0	.05
	1.	.71	.204	4.87-j8.26	5.09-j8.52	5.09-j8.52	.28	.06
	2.	1.41	.204	-2.16-j4.28	-2.22-j4.39	-2.22-j4.40	.17	.10
	6.	4.24	.204	1.55+j.388	1.57+j.386	1.57+j.386	.13	.35
	10.	7.07	.204	-.784+j.552	-.788+j.560	-.784+j.552	.13	.95

Table 4.2 Comparison of the RCM, exact, and the approximate evaluations of ${}_0\Pi_{h1x}$. For this example, f = 30 MHz, $\theta_2 = 45^o$, $\phi_2 = 0^o$, and $I_{h0} = 0$.

	k_1r_2	k_1z_2	Min. k_1z_2 Eq. (4.26)	RCM value $\times 10^2$	Exact integration $\times 10^2$	Approximate technique $\times 10^2$	% error Eq. (4.29)	% error actual
$\varepsilon_{cc}=5, \sigma=.001, \lvert\kappa\rvert=5.04$	.1	.07	2.49	24.9-j1.25	48.4-j7.82	1251.-j209.	1551.	96.1
	1.	.71	2.49	1.45-j2.03	1.11-j3.62	-.892+j1.51	33.3	29.4
	2.	1.41	2.49	-.462-j1.16	-.996-j1.18	-1.15-j1.16	20.4	9.7
	6.	4.24	2.49	.393+j1.36	.420+j.078	.452+j.084	16.0	7.1
	10.	7.07	2.49	-.216+j.125	-.205+j.146	-.222+j.156	15.5	7.3
$\varepsilon_{cc}=10, \sigma=.01, \lvert\kappa\rvert=11.7$	.1	.07	1.53	17.4+j.023	45.6-j9.38	452.6+j42.2	670.	90.3
	1.	.71	1.53	1.26-j1.22	.712-j2.55	.510-j2.72	14.4	9.4
	2.	1.41	1.53	-.171-j.859	-.576-j.847	-.592-j.858	8.8	1.9
	6.	4.24	1.53	.254+j.144	.278+j.105	.284+j.110	6.9	2.6
	10.	7.07	1.53	-.165+j.059	-.159+j.075	-.164+j.074	6.7	2.7
$\varepsilon_{cc}=40, \sigma=1, \lvert\kappa\rvert=601$	.1	.07	.204	-2.24-j1.52	-14.5+j5.41	-21.5-j3.74	13.0	9.8
	1.	.71	.204	.272-j.074	.206-j.342	.205-j.343	.28	.09
	2.	1.41	.204	.042-j1.35	-.024-j1.56	-.024-j1.56	.17	.03
	6.	4.24	.204	.025+j.040	.031+j.036	.031+j.036	.13	.03
	10.	7.07	.204	-.028-j.004	-.028-j.002	-.028-j.002	.13	.04

Table 4.3 Comparison of the RCM, exact, and the approximate evaluations of ${}_0\Pi_{hlz}$. For this example, f = 30 MHz, $\theta_2 = 45^o$, $\phi_2 = 0^o$, and $I_{v0} = 0$.

	k_1r_2	k_1z_2	Min. k_1z_2 Eq. (4.26)	RCM value $\times 10^2$	Exact integration $\times 10^2$	Approximate technique $\times 10^2$	% error Eq. (4.29)	% error actual
ε_s=5, σ=.001, K=5.04	.1	.07	2.49	-12.5+j1.25	-14.3+j1.19	-2984.+j23.0	1551.	99.5
	1.	.71	2.49	-.677+j1.05	-.892+j1.51	-1.94+j4.14	33.3	61.9
	2.	1.41	2.49	.260+j.570	.463+j.699	.683+j.915	20.4	27.0
	6.	4.24	2.49	-2.01-j.058	-.225-j.027	-.238-j.032	16.0	5.6
	10.	7.07	2.49	.105-j.068	.100-j.082	.105-j.068	15.5	12.1
ε_s=10, σ=.01, K=11.7	.1	.07	1.53	-11.6-j.126	-18.2+j2.63	-1170.-j448.5	670.	98.7
	1.	.71	1.53	-.753+j.903	-.676+j1.65	-1.16+j2.24	14.4	30.3
	2.	1.41	1.53	.182+j.552	.445+j.611	.456+j.680	8.8	8.6
	6.	4.24	1.53	-.179-j.074	-.202-j.043	-.199-j.049	8.8	3.2
	10.	7.07	1.53	.104-j.052	.997-j.066	.104-j.052	6.7	12.8
ε_s=50, σ=1, K=901	.1	.07	.204	-2.24-j1.52	-14.5+j5.41	-21.5-j3.74	13.0	9.8
	1.	.71	.204	-.258+j.082	-.204+j.328	-.205+j.328	.28	.33
	2.	1.41	.204	-.035+j1.31	.026+j1.53	.026+j1.53	.17	.42
	6.	4.24	.204	-.025-j.037	.032-j.034	-.032-j.032	.13	4.1
	10.	7.07	.204	.027+j.003	.027+j.0005	.027+j.003	.13	10.4

Table 4.4 Demonstration of the stability of the approximate technique as a function of secondary height z_2'. In this example, f = 18 MHz, $r_2/\lambda = 0.6$, and $\theta_2 = 45^\circ$.

z_2/λ	z_2'/λ	Approximate ${}_0\Pi_{h1z} \times 10^3$
.42	.50	1.82-j.953
.42	.75	1.76-j1.39
.42	1.00	1.57-j1.31
.42	1.25	1.64-j1.22
.42	1.50	1.68-j1.29
.42	1.75	1.63-j1.30
.42	2.00	1.62-j1.25

At $z_2/\lambda = .42$ RCM ${}_0\Pi_{h1z} \times 10^3 = 1.64-j.773$

At $z_2/\lambda = .42$ Exact ${}_0\Pi_{h1z} \times 10^3$ 1.58-j1.29

wider range of parameters making it suitable for most practical antenna problems.

Another advantage of this technique is that the horizontal vector potential component $_0\bar{\Pi}_{h1x}$ is expressed in a simple closed form (Equation 4.11), while Kuo and Mei [12] have obtained yet another infinite integral form by applying virtually the same approximation as the one in Equation (4.8b) to the Sommerfeld integrals. Also the finite integrations needed for the vertical vector potential approximations, viz., Equations (4.19) and (4.21), will never have a singularity in their integration interval thus making the integrands well-behaved. In addition, these integrands are independent of z_2', thereby making it possible to compute the vertical vector potential values along the vertical interval $z_2'z_2$ by a single integration, i.e., by using the newly computed value of the vector potential as an initial value for computing the next point on the interval. This procedure, when needed, can appreciably improve the overall efficiency of the technique.

Finally, since the evaluation of the E- and the H-fields is of major importance, the approximate technique presented in this chapter also provides a computationally efficient formulation for computing the various field components. This can be simply demonstrated by observing the matrix Equations (2.9) and (2.10). The various mixed partial derivatives of Π_x and Π_z, needed for the field computations, can be easily expressed in terms of the various mixed partial derivatives of $g(\rho, z_2)$, which in turn are expressed in a computationally efficient closed form in Appendix III.

The following chapter demonstrates the ability of these approximate expressions to efficiently analyze several antenna structures radiating over a lossy half-space.

5. WIRE ANTENNAS RADIATING OVER A LOSSY HALF-SPACE

The approximate field solution to the current element problem radiating over a lossy half-space, developed in the previous chapter, in conjunction with the method of moments [17] can be employed to analyze a wide variety of thin-wire antenna problems radiating over a lossy half-space. Initially, in this chapter, a general integral equation is derived containing the unknown antenna current. The method of moments is then used to reduce the integral equation into a numerically manageable matrix form, and finally, a digital computer program is developed for computing the antenna currents, impedance, and far-field patterns, given a specified antenna geometry. A number of simple antenna structures are considered and their behaviours are numerically predicted and presented in the final sections.

5.1 Antenna Integral Equation

Figure 18 depicts the geometry of an arbitrary wire antenna over a lossy half-space, with (r_a,θ_a,ϕ_a) defining a point on the antenna-axis. For simplicity, it is assumed that the antenna is entirely in the xz-plane ($\phi_a = 0$), since the field computation due to currents in the y-direction can easily be handled by a digital computer program by simply rotating the xy-plane by 90^o about the z-axis. Assuming that the antenna is excited by the field $\vec{E}^{exc}(\vec{r}_a)$, and having a loading function $\Lambda(\vec{r}_a)$ ohms/meter, one can write a general integral equation enforcing the total E-field along the antenna equal to that induced by the possible loading function, that is,

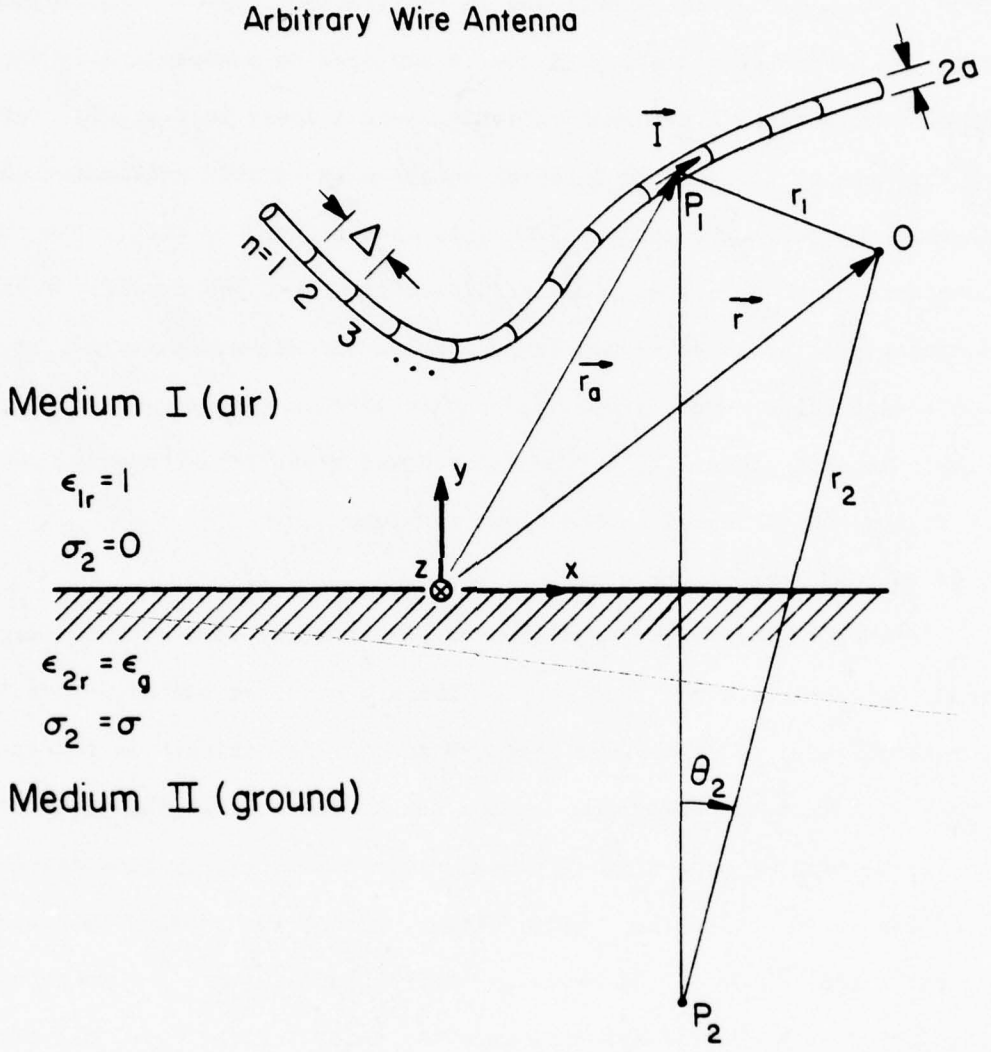

Figure 18. The geometry of an arbitrarily shaped wire antenna located over a lossy half-space.

$$\hat{I}(\vec{r}_a) \cdot \vec{E}^{exc}(\vec{r}_a) + \hat{I}(\vec{r}_a) \cdot \int_{antenna} \left[\vec{G}_v(\vec{r}_a, \vec{r}'_a)\hat{z} \cdot \vec{I}(\vec{r}'_a) + \vec{G}_h(\vec{r}_a, \vec{r}'_a)\hat{x} \cdot \vec{I}(\vec{r}'_a) \right] dr'_a$$

$$= \Lambda(\vec{r}_a)\vec{I}(\vec{r}_a) \quad , \tag{5.1}$$

where $\hat{I}(\vec{r}_a)$ is a unit vector along the antenna direction and the kernels $\vec{G}_v(\vec{r}_a, \vec{r}'_a)$ and $\vec{G}_h(\vec{r}_a, \vec{r}'_a)$ are the E-fields induced at point $\vec{r}_a$ due to a one-ampere electric current element located at $\vec{r}'_a$ and oriented in the z- and the x-directions, respectively. The matrix Equation (2.9), which formulates the electric-field components in terms of the vector potentials, is used to write:

$$\vec{E} = \vec{D}_x \Pi_x + \vec{D}_z \Pi_z \quad , \tag{5.2}$$

where the vector operators $\vec{D}_x$ and $\vec{D}_z$ are defined as:

$$\vec{D}_x = \hat{x}\left(k_1^2 + \frac{\partial^2}{\partial x^2}\right) + \hat{y}\left(\frac{\partial^2}{\partial x \partial y}\right) + \hat{z}\left(\frac{\partial^2}{\partial x \partial z}\right) \tag{5.3a}$$

$$\vec{D}_z = \hat{x}\left(\frac{\partial^2}{\partial x \partial z}\right) + \hat{y}\left(\frac{\partial^2}{\partial y \partial z}\right) + \hat{z}\left(k_1^2 + \frac{\partial^2}{\partial z^2}\right) \quad . \tag{5.3b}$$

By using the general formula in (5.2), one can directly write the two kernels, $\vec{G}_v$ and $\vec{G}_h$, in terms of the incident, perfect reflection, and the correction vector potential components (see Equations (2.20), (2.30), and (2.32)), namely,

$$\vec{G}_v(\vec{r}_a, \vec{r}'_a) = \vec{G}^i_v(\vec{r}_a, \vec{r}'_a) + \vec{G}^r_v(\vec{r}_a, \vec{r}'_a) + {}_0\vec{G}_v(\vec{r}_a, \vec{r}'_a), \tag{5.4}$$

where

$$\vec{G}^i_v(\vec{r}_a, \vec{r}'_a) = (j\omega\varepsilon_0)^{-1}\vec{D}_z g(\vec{r}_a - \vec{r}'_a) \tag{5.5a}$$

$$\vec{G}^r_v(\vec{r}_a, \vec{r}'_a) = (j\omega\varepsilon_0)^{-1}\vec{D}_z g(\vec{r}_a - \vec{r}'_a - 2h\hat{z}) \tag{5.5b}$$

$${}_0\vec{G}_v(\vec{r}_a, \vec{r}'_a) = \vec{D}_z \, {}_0\Pi_{v1z}(\vec{r}_a - \vec{r}'_a - 2h\hat{z}) \Big|_{I_v = 1} \quad , \tag{5.5c}$$

and

$$\vec{G}_h(\vec{r}_a,\vec{r}_a') = \vec{G}_h^i(\vec{r}_a,\vec{r}_a') + \vec{G}_h^r(\vec{r}_a,\vec{r}_a') + {}_0\vec{G}_h(\vec{r}_a,\vec{r}_a') \quad , \tag{5.6}$$

where

$$\vec{G}_h^i(\vec{r}_a,\vec{r}_a') = (j\omega\varepsilon_0)^{-1}\vec{D}_x g(\vec{r}_a - \vec{r}_a') \tag{5.7a}$$

$$\vec{G}_h^r(\vec{r}_a,\vec{r}_a') = (j\omega\varepsilon_0)^{-1}\vec{D}_x g(\vec{r}_a - \vec{r}_a' - 2h\hat{z}) \tag{5.7b}$$

$${}_0\vec{G}_h(\vec{r}_a,\vec{r}_a') = \left[\vec{D}_x\, {}_0\Pi_{h1x}(\vec{r}_a - \vec{r}_a' - 2h\hat{z}) + \vec{D}_z\, {}_0\Pi_{h1z}(\vec{r}_a - \vec{r}_a' - 2h\hat{z})\right]_{I_h = 1} \quad . \tag{5.7c}$$

Note that in the above equations, $h = r_a' \cos(\theta_a')$ is the height of the current source above the half-plane interface and g is the free-space Green's function defined in (4.5b).

The correction vector potential formulation of Chapter 4, namely, Equations (4.11), (4.15), and (4.16), along with the expansions presented in Appendix III, enable one to compute the scattered components of the two kernels, viz., $\vec{G}_v^r, {}_0\vec{G}_v, \vec{G}_h^r$, and ${}_0\vec{G}_h$, without difficulty. However, because of the singular nature of g, the free-space solution of the kernels, $\vec{G}_v^i$ and $\vec{G}_h^i$, should not be computed directly. Instead, as has been successfully reported [11], [14], [18], and [19], the thin-wire approximation is used to shift the observation point r_a to the antenna surface, and in order to further smooth out the singularities, the finite difference scheme is employed to perform the D_x and D_z operations defined in (5.3).

5.2 Method of Moments

As developed by Harrington [17], the method of moments is a convenient approximation for transforming the antenna integral equation into a numerically manageable matrix form. In this work, pulse-basis and delta-matching functions

are chosen since they eliminate the need for integrating the kernels $\vec{G}_v$ and $\vec{G}_h$. The number of unknown patches on the antenna N should be large enough so that the patch length Δ is at most 1/6 of the wavelength. The approximated current along the antenna is therefore represented as:

$$\vec{I} = \sum_{n=1}^{N} I_n \hat{I}_n \quad , \tag{5.8}$$

for which I_n is an unknown constant value over the n^{th} patch and zero outside of it, also $\hat{I}_n$ is a known unit vector tangent to the antenna at the center of the n^{th} patch (see Figure 18). Substituting (5.8) into (5.1) and letting subscripts n = 1,2,3,$\cdots$ denote "evaluation at the center of the n^{th} patch," and letting $[\vec{I}]$ and $[\bar{E}^{exc}]$ be column vectors containing the current and the tangential excitation field values at successive patches, one finally arrives at

$$[\bar{E}^{exc}] = -[Z^{imp}][\bar{I}] + [\Lambda][\bar{I}] \quad , \tag{5.9}$$

where $[\Lambda]$ is a diagonal matrix with elements $\Lambda_1, \Lambda_2, \cdots, \Lambda_n$; and $[Z^{imp}]$ is an $n \times n$ square matrix with its i^{th} row and j^{th} column element defined as:

$$Z_{ij}^{imp} = \Delta \hat{I}(\vec{r}_{ai}) \cdot [\hat{z} \cdot \hat{I}(\vec{r}_{aj}) \vec{G}_v(\vec{r}_{ai}, \vec{r}_{aj}) + \hat{x} \cdot \hat{I}(\vec{r}_{aj}) \vec{G}_h(\vec{r}_{ai}, \vec{r}_{aj})] \quad . \tag{5.10}$$

Note that i and j also refer to patch numbers, and Δ is the patch length. The matrix Equation (5.9) can be solved for the unknown currents $[\bar{I}]$, and by replacing the excitation E-field in terms of the excitation voltage $[\bar{V}]$, one arrives at

$$[\bar{I}] = [Y^{ant}][\bar{V}] \tag{5.11a}$$

$$[Y^{ant}] = \Delta^{-1}\{-[Z^{imp}] + [\Lambda]\}^{-1} \quad . \tag{5.11b}$$

Once $[Y^{ant}]$ is constructed for a given structure, the antenna currents can

be directly computed for a given voltage source excitation. As was discussed in the previous section, the thin-wire approximation and the finite-difference scheme are employed for evaluating the free-space solution components of the kernels, viz., $\vec{G}_v^i$ and $\vec{G}_h^i$. A power series, derived by Harrington [20], is used for the thin-wire approximation computations, and based on the conclusions made in [11], [14], [18], and [19], the finite difference parameter δ is chosen to be equal to $\Delta/2$, e.g.,

$$\left.\frac{\partial^2 f}{\partial x^2}\right|_{x_0} \simeq \frac{f(x_0 + \delta) + f(x_0 - \delta) - 2f(x_0)}{\delta^2} \quad ; \quad \delta = \Delta/2 \quad . \tag{5.12}$$

The free-space solution obtained by using the above approach has been thoroughly tested and, as an example, the generated impedance curves shown in Figures 19 and 20 agree well with the ones reported by Jordan et al. [21].

5.3 Far-Field Radiation Pattern

The RCM expressions, shown in Equations (3.27) - (3.29), are the logical choices for representing the correction vector potential components in the far-field region ($k_1 r >> 10$). Working in the spherical coordinate system (r,θ,ϕ), and neglecting all terms containing r^{-2}, r^{-3}, $\cdots$, one can easily show

$$\nabla\nabla.\vec{\Pi} \cong -k^2 \Pi_r \hat{r} \quad , \tag{5.13}$$

where $\vec{\Pi}$ is the total vector potential. The total electric field $\vec{E}$, from Equation (2.8), can therefore be shown to have no $\hat{r}$-component, namely,

$$\vec{E}(r,\theta,\phi) = (k^2 + \nabla\nabla.)\vec{\Pi} = k^2[(\cos\theta\cos\phi\,\Pi_x - \sin\theta\,\Pi_z)\hat{\theta} - \sin\phi\,\Pi_x\hat{\phi}] \quad . \tag{5.14}$$

As expected, the above far-field expression represents two plane waves

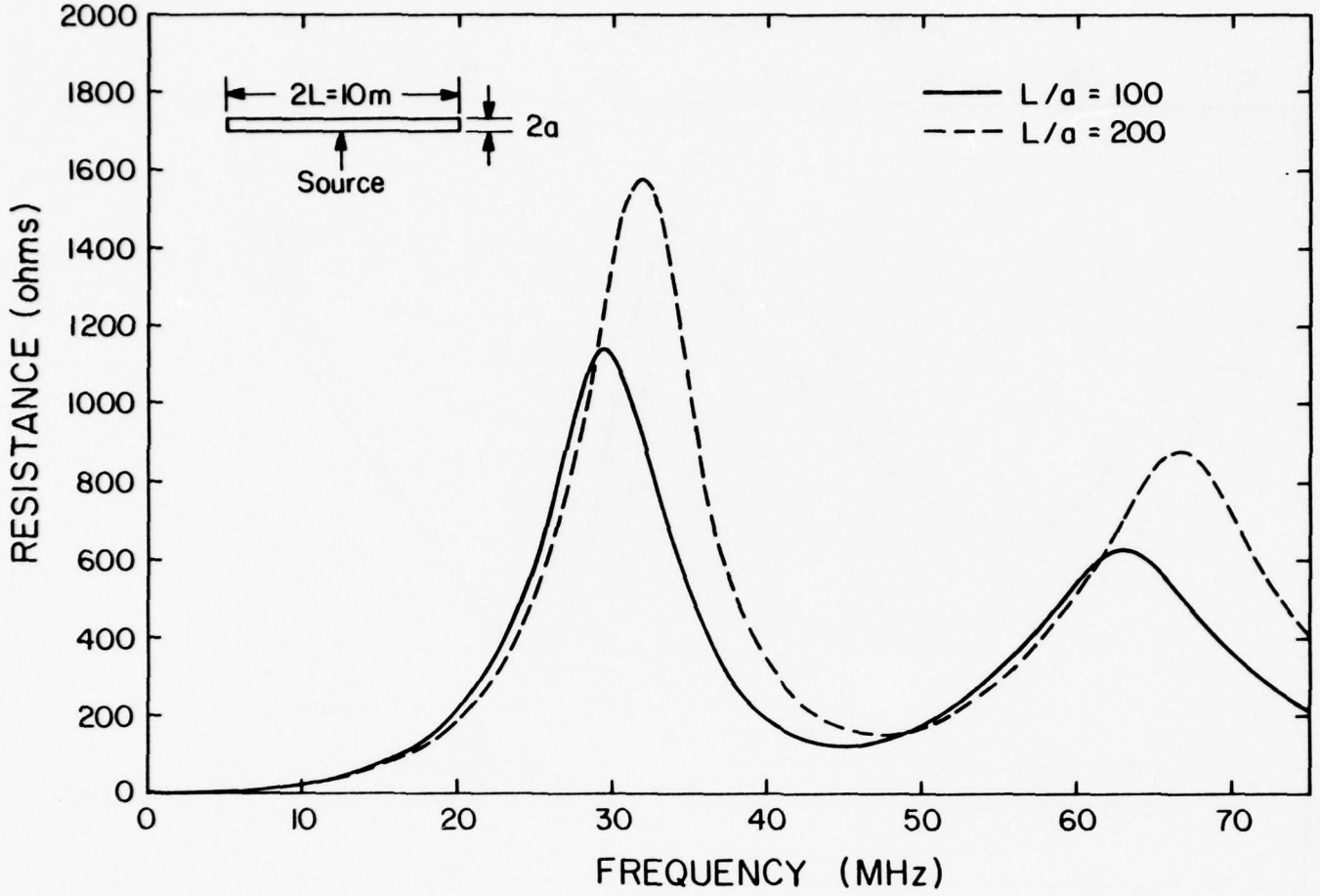

Figure 19. Input resistance of an unloaded dipole antenna (2L = 10m) radiating in free space.

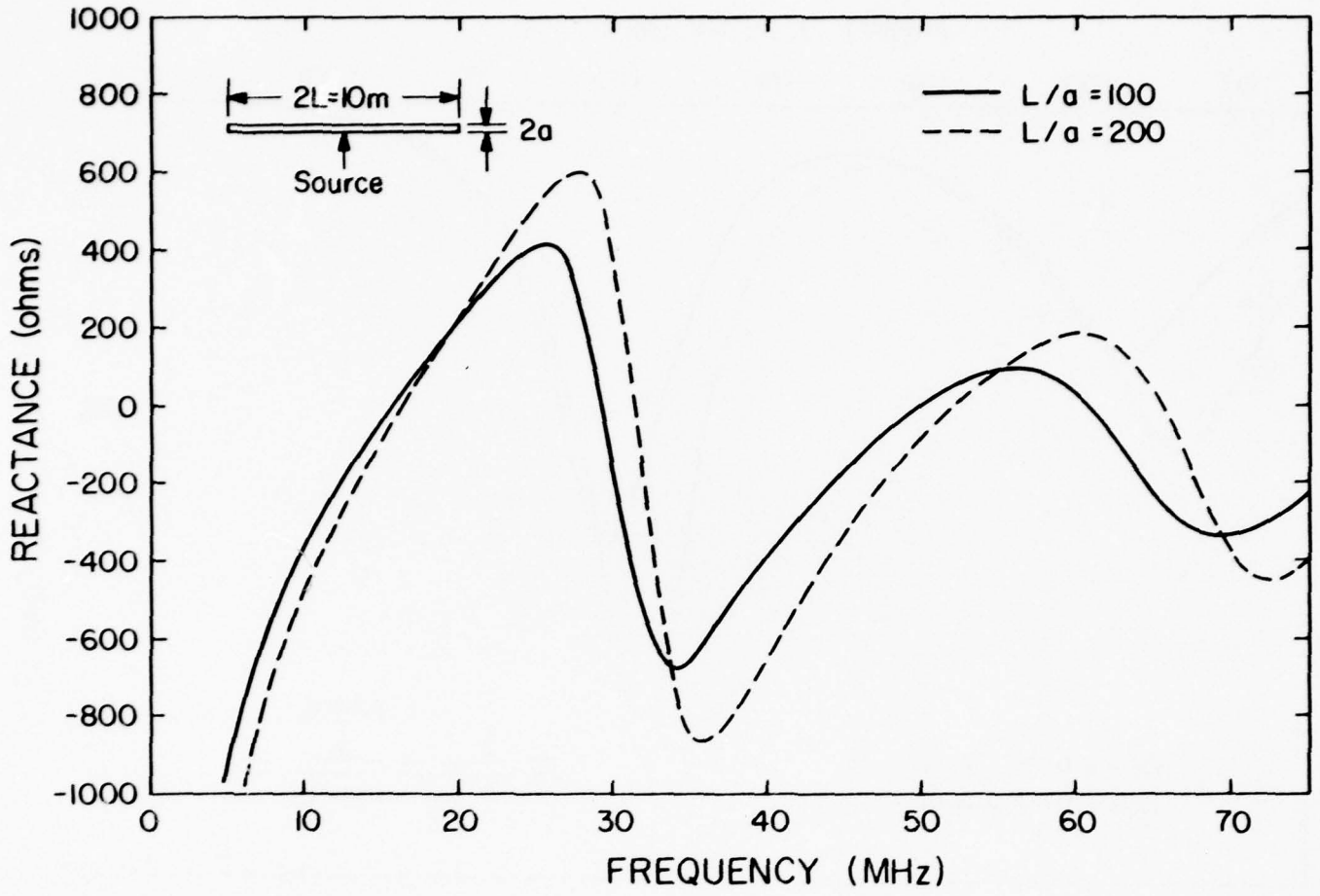

Figure 20. Input reactance of an unloaded dipole antenna (2L = 10m) radiating in free space.

(polarized in the $\hat{\theta}$- and the $\hat{\phi}$- directions) propagating away from the (x,y,z) origin defined in Figure 18. In summary, the far-electric-field radiation pattern due to a current element with no $\hat{y}$-component can be readily computed by initially evaluating the total vector potential components via the RCM approximation and then using Equation (5.14) to obtain the E-field values at the desired observation points.

The far-field pattern for a given antenna structure is simply obtained by applying the superposition theorem to the individual radiation patterns of the antenna current segments defined in the method of moments approximation. Radiation pattern examples are included for the various antenna structures analyzed in the following sections.

5.4 Horizontal Antenna over Lossy Half-Space

The general developments of Sections 5.1 - 5.3 are applied to the horizontal antenna shown in Figure 21. Fortunately, because of the symmetries present in this geometry, the $[Z^{imp}]$ matrix in Equation (5.9) takes the following form (Toeplitz matrix):

$$[Z^{imp}] = \begin{bmatrix} a_1 & a_2 & a_3 & \cdot & \cdot & \cdot & a_n \\ a_2 & a_1 & a_2 & \cdot & \cdot & \cdot & a_{n-1} \\ a_3 & a_2 & a_1 & \cdot & \cdot & \cdot & a_{n-2} \\ \cdot & \cdot & \cdot & \cdot & \cdot & \cdot & \cdot \\ \cdot & \cdot & \cdot & \cdot & \cdot & \cdot & \cdot \\ \cdot & \cdot & \cdot & \cdot & \cdot & \cdot & \cdot \\ a_n & a_{n-1} & a_{n-2} & \cdot & \cdot & \cdot & a_1 \end{bmatrix} . \qquad (5.15)$$

Therefore, one needs to compute only one row of this matrix and use the aforementioned symmetry to complete it. The main program, HORIZ (see Appendix IV),

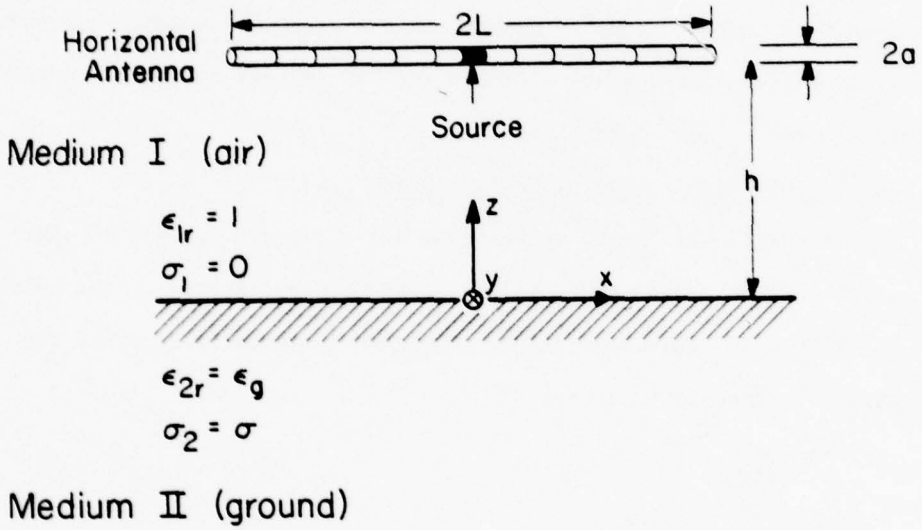

Figure 21. Center-fed horizontal dipole over a lossy half-space.

is developed to analyze the horizontal antenna of Figure 21. Using this program, Figures 22 and 23 are generated to show the impedance variations of a 2L = 10 meters center-fed horizontal antenna located h = 3 meters above various lossy grounds. Radiation pattern of this antenna at 15 MHz is also shown in Figures 24 and 25.

5.5 Vertical Antenna over Lossy Half-Space

The vertical dipole shown in Figure 26 is the next geometry considered. Unfortunately, as was the case for the horizontal antenna, the total $[Z^{imp}]$ matrix is not in a Toeplitz form. However, main program VERT (in Appendix IV) is designed to take maximum advantage of the available symmetry. As an example, Figure 27 is included to show the radiation pattern of a 2L = 10 meters, h = 8 meters, center-fed vertical dipole at resonance (f = 15 MHz) located over various lossy grounds.

5.6 Inverted Vee-Dipole

As a complicated example, the inverted Vee-dipole of Figure 28 is considered. Again, as in the two previous sections, symmetry is used in the main program VEEDIP (Appendix IV) in constructing the $[Z^{imp}]$ matrix. The program is tested for an inverted Vee-dipole structure having L = 7.5 meters, h = 10 meters, and $\Psi = 90^{o}$; Figures 29 and 30 demonstrate the radiation pattern of this structure at 10 MHz and for various lossy grounds.

In all three of these examples, care has been taken not to violate the conditions $|\kappa| > 10$ and Equation (4.26) to ensure the accuracy of the results. Also, since the $[Z^{imp}]$ matrix for these examples turns out to be symmetric, a special inversion routine (XINVZ in Appendix IV) is employed to save an appreciable amount of computer time.

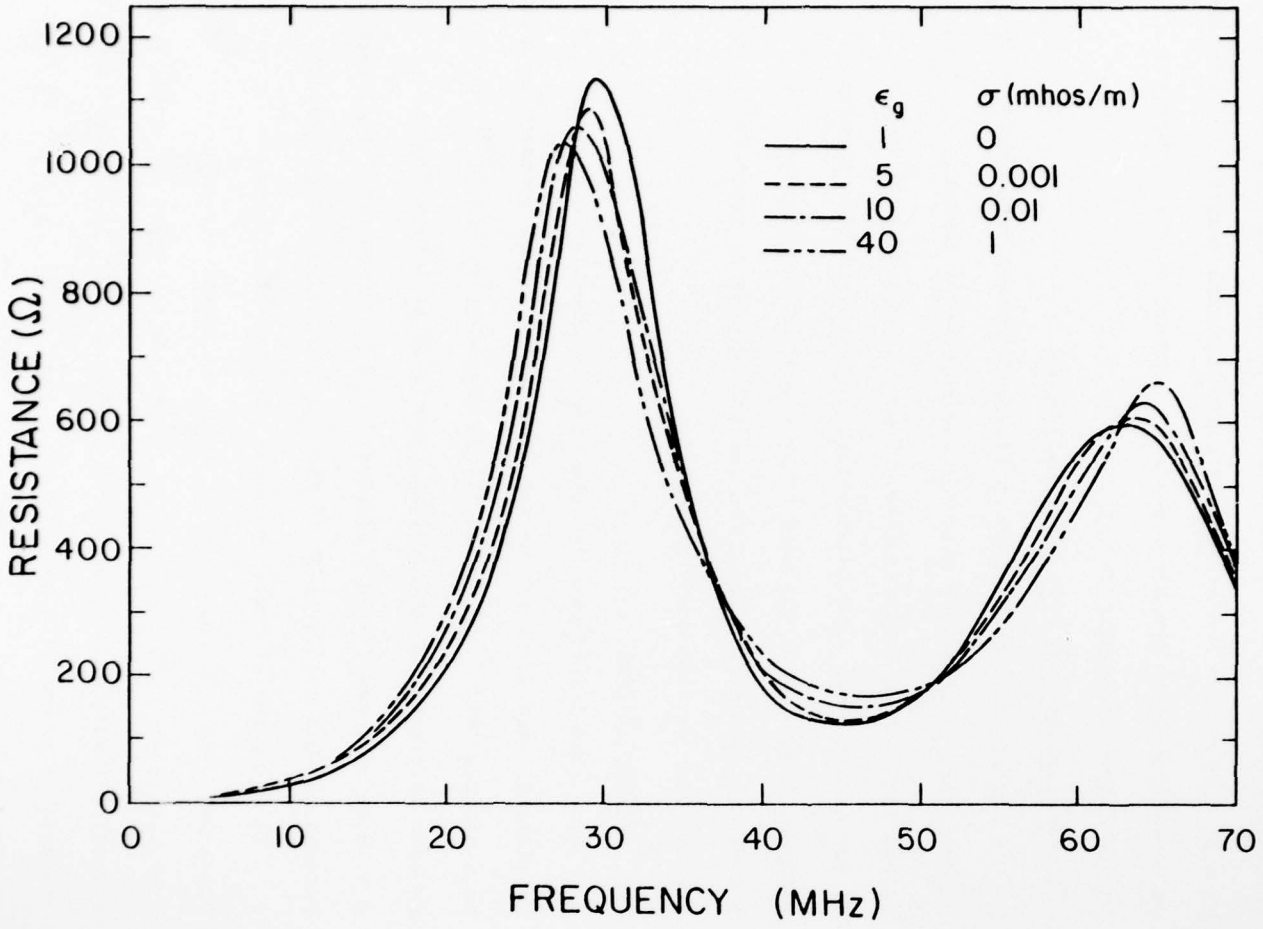

Figure 22. Input resistance of a center-fed horizontal dipole antenna as a function of frequency and the ground parameters. Note that 2L = 10m, 2a = 0.1m, and h = 3m.

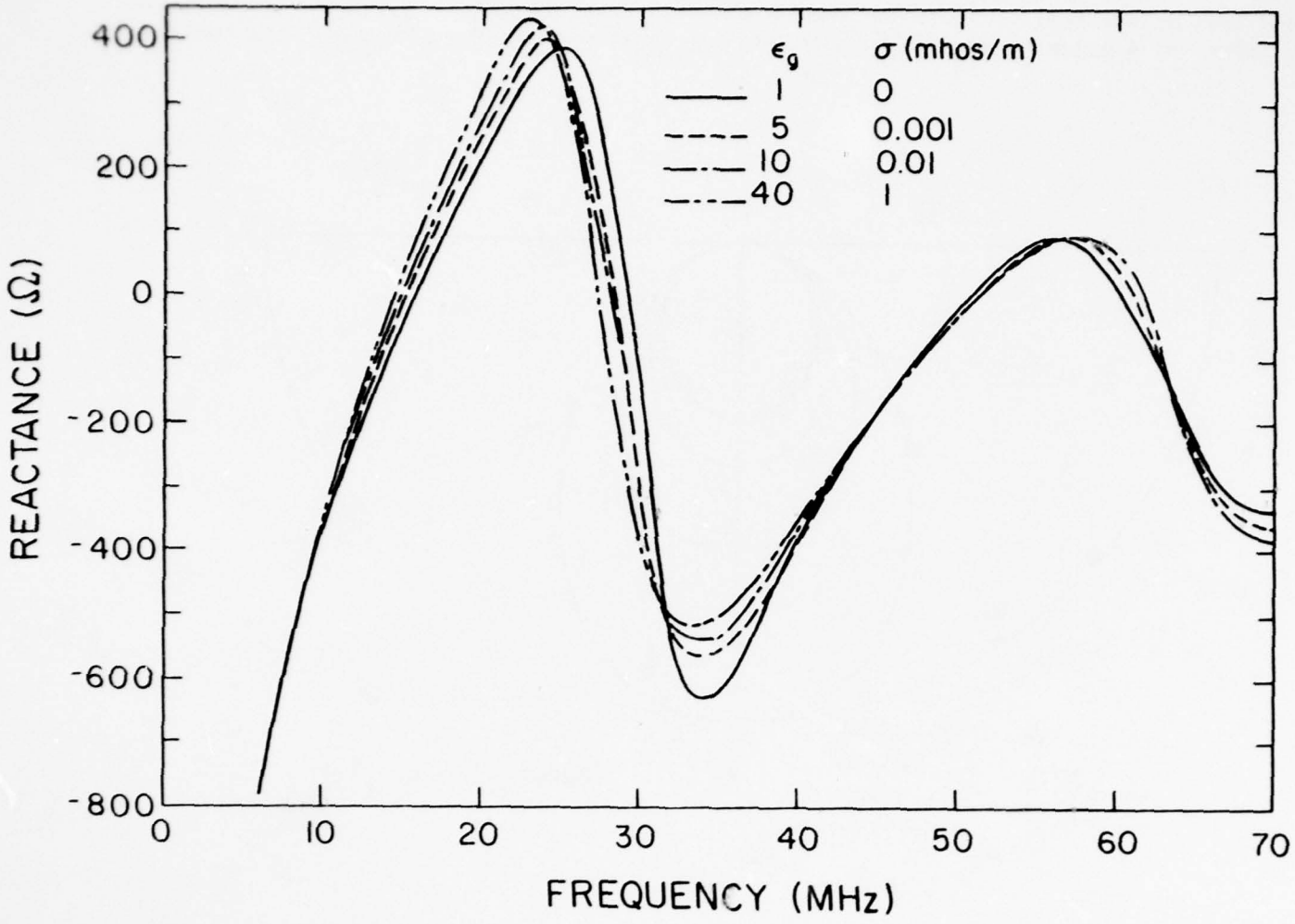

Figure 23. Input reactance of the antenna defined in Figure 22.

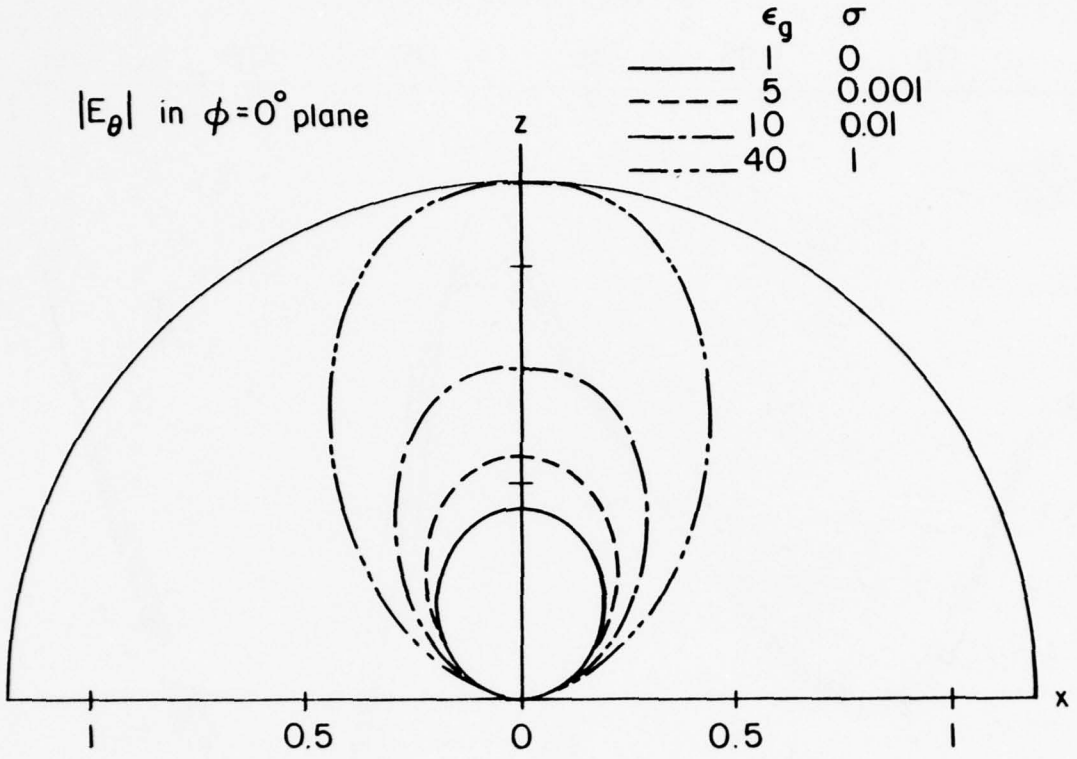

Figure 24. Far-field radiation pattern for the horizontal antenna defined in Figure 22 at 15 MHz. Note that the patterns are computed at $k_1 r = 500$, and in this plane, $|E_\phi|$ is negligible.

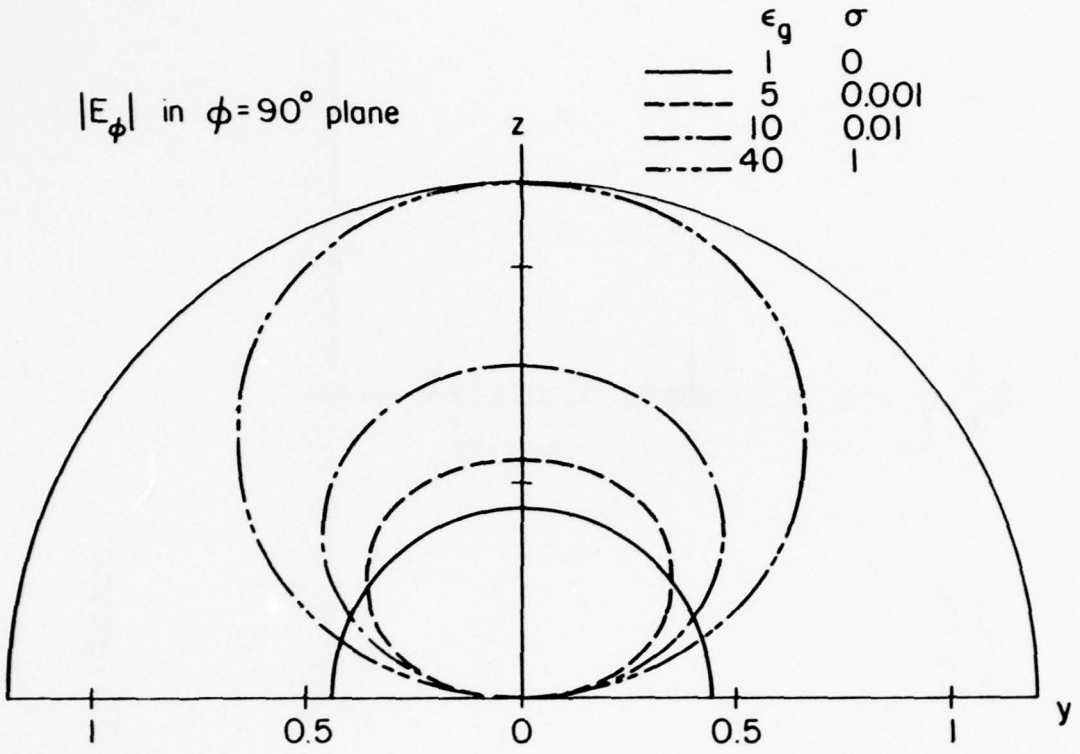

Figure 25. Far-field radiation pattern for the horizontal antenna defined in Figure 22 at 15 MHz. Note that the patterns are computed at $k_1 r = 500$, and in this plane, $|E_\theta|$ is negligible.

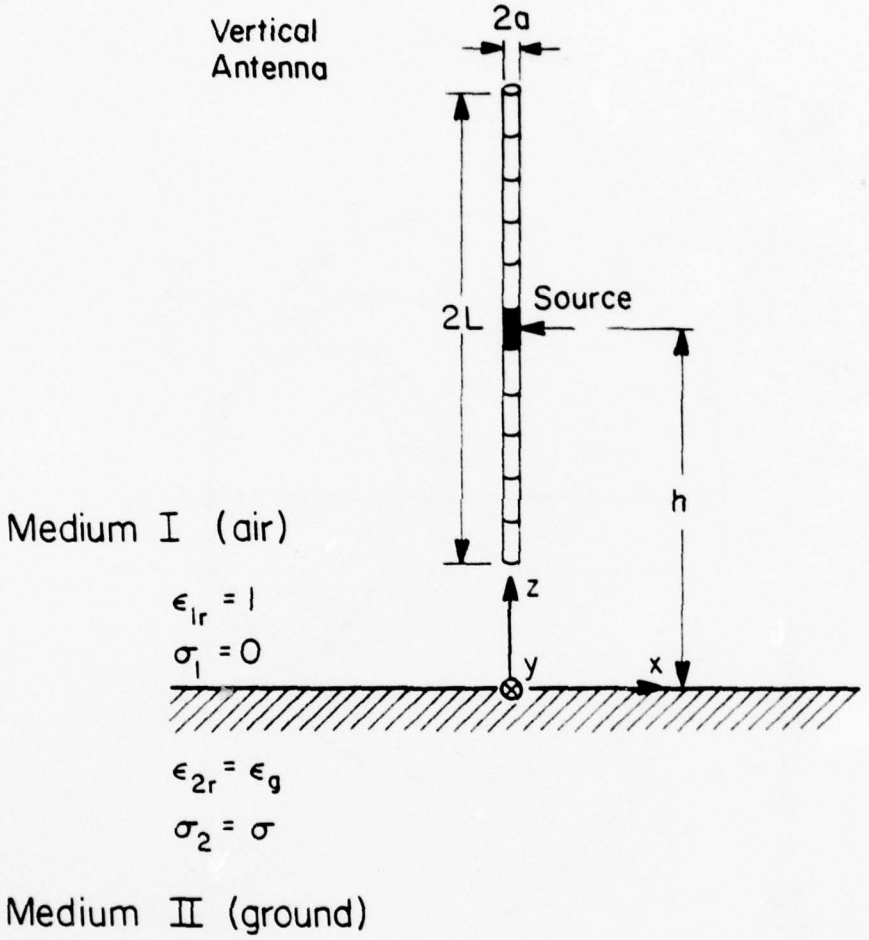

Figure 26. Center-fed vertical dipole over a lossy half-space.

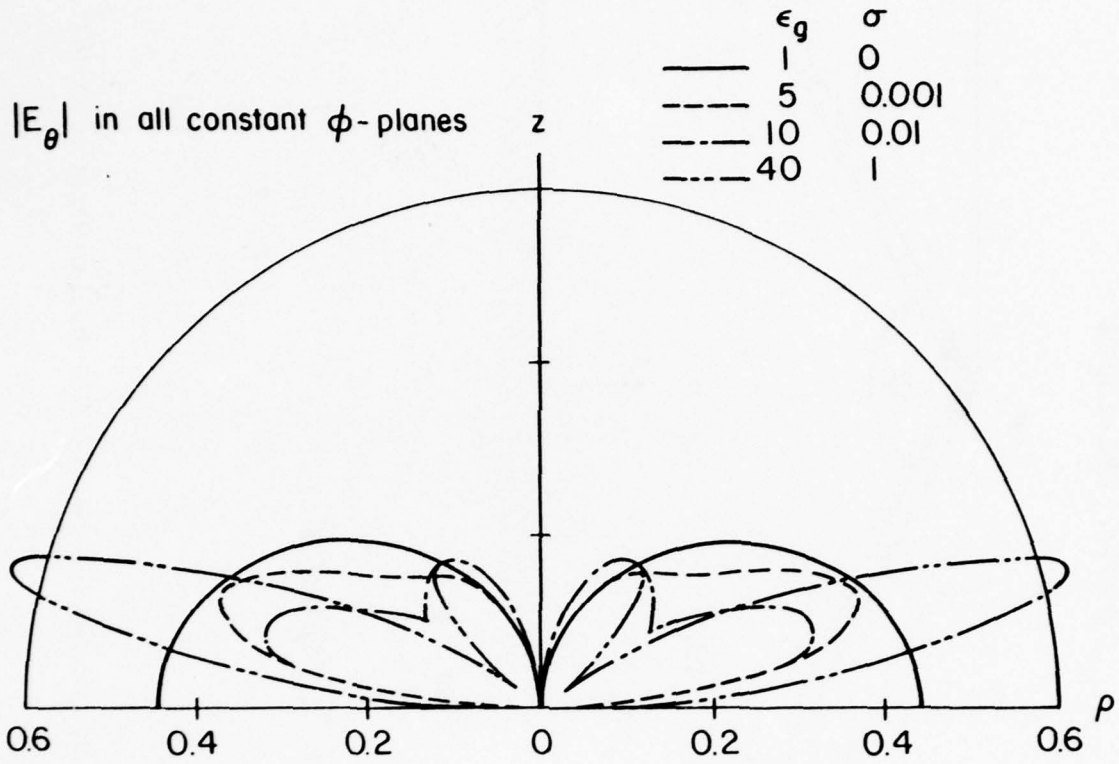

Figure 27. The far-field radiation pattern for a center-fed vertical dipole (2L = 10m, h = 8m, and 2a = 0.1m) at 15 MHz. Note that the patterns are computed at $k_1 r = 500$, and in this example, $|E_\phi|$ is negligible.

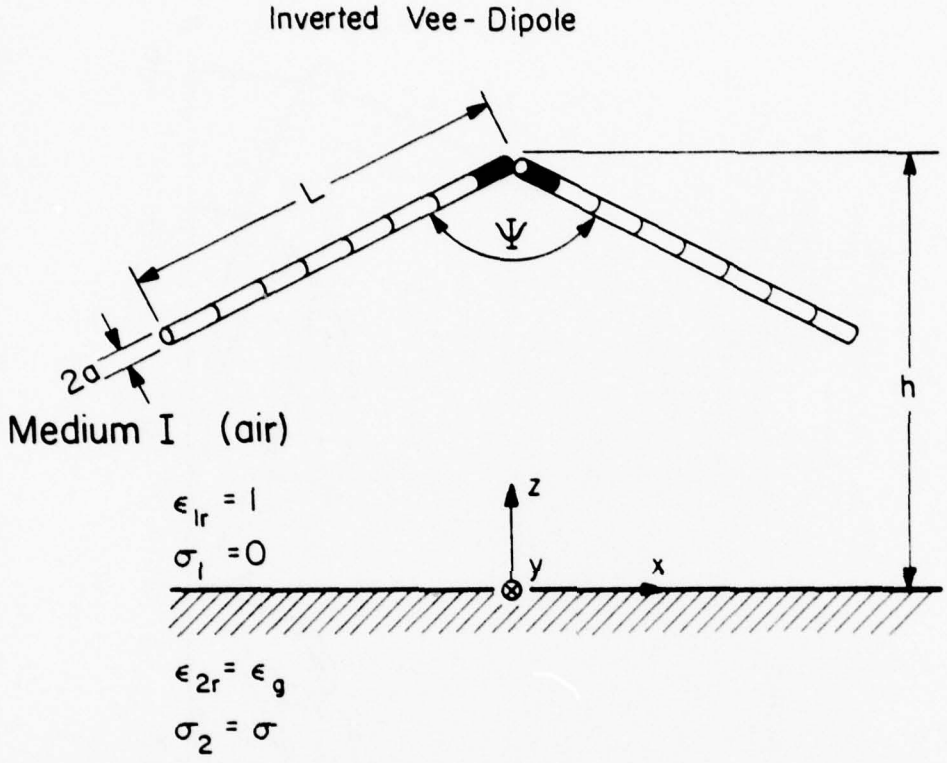

Figure 28. Center-fed inverted Vee-dipole over a lossy half-space.

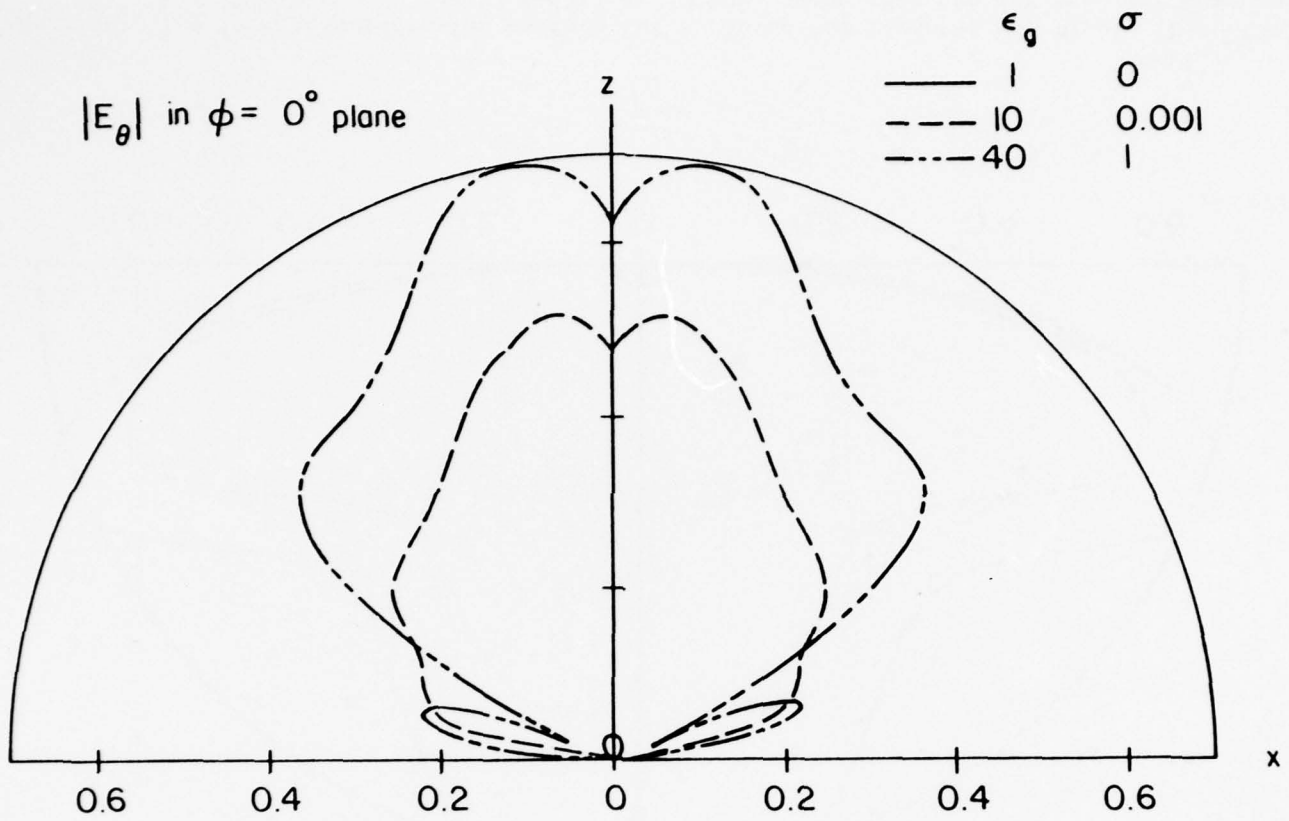

Figure 29. The far-field radiation pattern for a center-fed inverted Vee-dipole (L = 7.5m, h = 10m, $\Psi = 90^\circ$, and 2a = 0.1m) at 10 MHz. Note that the patterns are computed at $k_1 r = 500$, and in this plane, $|E_\phi|$ is negligible.

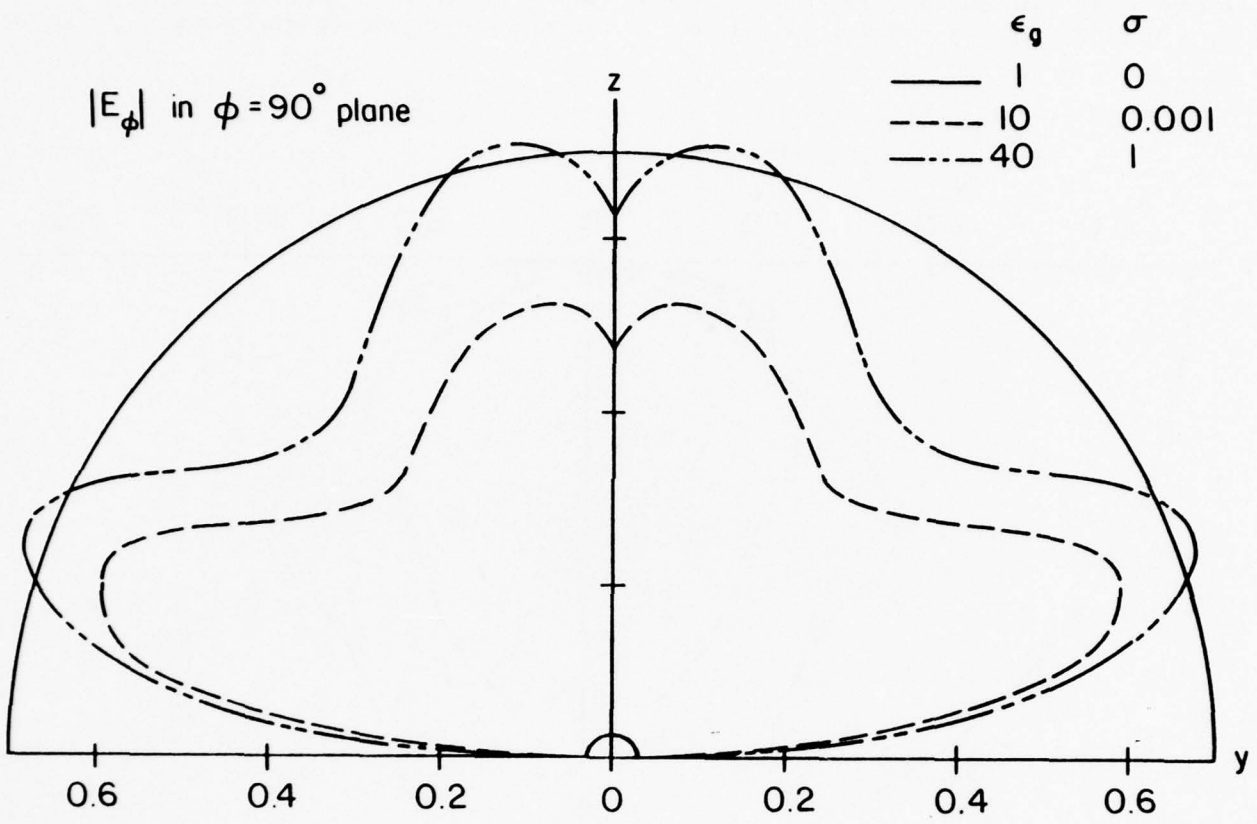

Figure 30. The far-field radiation pattern for a center-fed inverted Vee-dipole (L = 7.5m, h = 10m, $\psi = 90^\circ$, and 2a = 0.1m) at 10 MHz. Note that the patterns are computed at $k_1 r = 500$, and in this plane, $|E_\theta|$ is negligible.

6. CONCLUSIONS

Based on the steepest descent path (SDP) integration technique, an efficient numerical integration procedure is developed in Chapter 3 for computing the Sommerfeld infinite integrals present in the vector potential expressions of a current element radiating over a lossy half-space. Even though this procedure is about an order of magnitude faster than the latest reported Sommerfeld integration techniques, the computation time for a typical antenna problem can still become prohibitive. The reflection coefficient method (RCM) approximations, which are simply the first term in the asymptotic expansion of the Sommerfeld integrals, offer a simple closed-form solution valid only at the high end of the frequency spectrum and which cannot be employed in many practical situations. Also, the addition of the second term in the aforementioned asymptotic expansion to the RCM approximations is ruled out, since the resulting vertical vector potential components diverge from their respective exact integration values.

Chapter 4 presents a novel approach in which the transform domain representation of the vector potentials is approximated such that the resulting space-domain expressions do not require any kind of infinite integration. This approach has the merit of being computationally over an order of magnitude faster than the SDP technique of Chapter 3, while being accurate over a wide range of parameters of practical interest and, in addition, offers a simple and numerically manageable procedure for obtaining the near E- and H-field components.

The general computer program, listed in Appendix IV, is developed by employing the approximate formulas of Chapter 4 and is used to solve several

antenna geometries. With minor modifications, this program can be adapted to analyze most three-dimensional thin-wire antenna structures over a lossy half-space.

APPENDIX I

EVALUATION OF $_0\Pi_{h1x}$, $_0\Pi_{h1z}$, AND $_0\Pi_{v1z}$ AT $\theta_2 = 0$

In this appendix, the behavior of Equations (2.47) - (2.49) is studied at $\theta_2 = 0$. In their present forms, these integrals are not defined at $\rho_2 = 0$, although it is clear that their equivalent forms in (2.42) - (2.44) are bounded. Equation (2.47) can be expressed here for convenience as

$$_0\Pi_{v1z} = \frac{I_{v0}}{4\pi j} \int_{-\infty}^{\infty} \frac{\kappa\lambda}{\kappa\sqrt{k_1^2 - \lambda^2} + \sqrt{\kappa k_1^2 - \lambda^2}} H_0^{(2)}(\rho_2\lambda) e^{-jz_2\sqrt{k_1^2-\lambda^2}} d\lambda \quad (I.1)$$

where $\rho_2 = r_2 \sin\theta_2$. The Hankel function in (I.1) is not bounded at $\theta_2 = 0$. To circumvent this difficulty, one replaces $H_0^{(2)}$ with its expansion from [22]

$$H_0^{(2)}(\rho_2\lambda) = J_0(\rho_2\lambda) - j\left[\frac{2}{\pi} \operatorname{Ln} \frac{\gamma\rho_2\lambda}{2} J_0(\rho_2\lambda) + \frac{2}{\pi} \sum_{m=1}^{\infty} \frac{(-1)^{m+1}}{(m!)^2} \left(\frac{\rho_2\lambda}{2}\right)^{2m} \phi(m)\right] \quad (I.2)$$

where γ is Euler's constant and $\phi(m)$ represents the harmonic series, i.e.,

$$\phi(m) = 1 + 1/2 + 1/3 + \ldots + 1/m \quad . \quad (I.3)$$

Note that both J_0 and the summation terms in (I.2) are even functions of λ, hence, their contributions to the integral (I.1) are zero. Substituting (I.2) into (I.1), one finally arrives at

$$_0\Pi_{v1z} = \frac{I_{v0}}{4\pi j} \int_{-\infty}^{\infty} \frac{\kappa\lambda}{\kappa\sqrt{k_1^2 - \lambda^2} + \sqrt{\kappa k_1^2 - \lambda^2}} \frac{-2j}{\pi} J_0(r_2 \sin\theta_2 \lambda)$$

$$\cdot \operatorname{Ln}(r_2\lambda)\, e^{-jz_2\sqrt{k_1^2-\lambda^2}} d\lambda \quad , \quad (I.4)$$

which is obviously bounded at $\theta_2 = 0$. Introducing the change of variable $\lambda = k_1 \sin \xi$ into (I.4) and setting $\theta_2 = 0$, one finds

$$ {}_0\Pi_{v1z} = \frac{I_{v0} k_1}{4\pi j} \int_{\Gamma} \frac{\kappa \sin \xi \cos \xi}{\kappa \cos \xi + \sqrt{\kappa - \sin^2 \xi}} \frac{-2j}{\pi} \mathrm{Ln}(k_1 r_2 \sin \xi) \quad e^{-jk_1 r_2 \cos \xi} \, d\xi \; ; $$

$$ \theta_2 = 0 \qquad \text{(I.5)} $$

where path Γ is shown in Figure 2. In a similar fashion, one may obtain equivalent expressions for the remaining vector potential components at $\theta_2 = 0$, namely,

$$ {}_0\Pi_{h1x} = \frac{I_{v0} k_1}{4\pi j} \int_{\Gamma} \frac{\sin \xi \cos \xi}{\cos \xi + \sqrt{\kappa - \sin^2 \xi}} \frac{-2j}{\pi} \mathrm{Ln}(k_1 r_2 \sin \xi) \quad e^{-jk_1 r_2 \cos \xi} \, d\xi \; ; $$

$$ \theta_2 = 0 \qquad \text{(I.6)} $$

and

$$ {}_0\Pi_{v1z} = 0 \quad ; \quad \theta_2 = 0 \quad . \qquad \text{(I.7)} $$

APPENDIX II

ASYMPTOTIC EVALUATION

In this appendix, a general formulation is developed for a higher-order asymptotic evaluation of an integral with the following format:

$$u = \frac{1}{4\pi j} \int_{\Gamma} P(\xi)\, e^{-jkr\, \cos(\xi-\theta)}\, d\xi \quad , \tag{II.1}$$

where it is assumed that kr is a large parameter, $-\pi/2 < \theta < \pi/2$, $P(\xi)$ is a slowly varying function and path Γ is shown in Fig. 2. For large values of kr, one is usually interested in determining the asymptotic expression of (II.1); this is done by employing the method of the steepest-descent path integration. At the saddle point $\xi = \theta$, one can deform the integration path Γ to the steepest descent path (SDP) defined by $\mathrm{Re}[\cos(\xi - \theta)] = 1$. Assuming that in this deformation no poles or branch points are encountered, one may express (II.1) as

$$u = \frac{1}{4\pi j} \int_{SDP} P(\xi)\, e^{-jkr\, \cos(\xi-\theta)}\, d\xi \quad . \tag{II.2}$$

Since on the SDP the relation $\mathrm{Re}[\cos(\xi - \theta)] = 1$ holds, one can introduce the change of variable

$$\cos(\xi - \theta_2) = 1 - jt^2 \quad , \tag{II.3}$$

or equivalently,

$$t = \sqrt{2}\, e^{-j\pi/4} \sin\frac{\xi - \theta}{2} \quad , \tag{II.4}$$

in which t is a real variable taking the domain $[-\infty,\infty]$. Substituting (II.4) into (II.2), one arrives at

$$u = \frac{e^{-jkr-j\pi/4}}{2\sqrt{2}\,\pi} \int_{-\infty}^{\infty} Q(t)\, e^{-krt^2}\, dt \qquad \text{(II.5)}$$

where

$$Q(t) = P(\xi)\, \sec \frac{\xi - \theta}{2} \quad , \qquad \text{(II.6a)}$$

in which ξ is replaced with

$$\xi = \pm\left[\frac{\pi}{2} + jLn(t^2 + j + |t|\sqrt{t^2 + 2j})\right] + \theta \quad , \quad t \lesseqgtr 0 \qquad \text{(II.6b)}$$

and Ln is interpreted as being its principal value. The complete asymptotic expansion procedure [23] is now used for the asymptotic evaluation of (II.5). In this procedure, one first expands Q(t) in a Taylor series

$$Q(t) = \sum_{n=0}^{\infty} \frac{Q^{(n)}(0)}{\Gamma(n+1)}\, t^n \qquad \text{(II.7)}$$

where $Q^{(n)}(0) = \dfrac{\partial n}{\partial t^n} Q(t)\Big|_{t=0}$ and Γ is the Gamma function. Then (II.7) is substituted into (II.5) to finally result in

$$u = \frac{e^{-jkr-j\pi/4}}{2\sqrt{2\pi}} \sum_{n=0}^{\infty} \frac{2^{-2n}}{n!}\, (kr)^{-n-1/2}\, Q^{(2n)}(0) \quad . \qquad \text{(II.8)}$$

In constructing the preceding equation, the following identity was used, viz.,

$$\int_{-\infty}^{\infty} t^n e^{-krt^2}\, dt = \begin{cases} (kr)^{-(1+n)/2}\, \Gamma[(1+n)/2] & \text{for n even} \\ 0 & \text{for n odd} \end{cases} \quad . \qquad \text{(II.9)}$$

The task is now to determine $Q^{(2n)}$'s in terms of P. This is achieved by differentiating (II.6a) and arriving at

AD-A068 548 ILLINOIS UNIV AT URBANA-CHAMPAIGN ELECTROMAGNETICS LAB F/G 20/14
ANALYSIS OF ARBITRARILY SHAPED WIRE ANTENNAS RADIATING OVER A L--ETC(U)
MAR 79 P PARHAMI, R MITTRA DAAG29-77-G-0111

UNCLASSIFIED UIEM79-6 ARO-14686.4-EL NL

2 OF 2
AD A068548

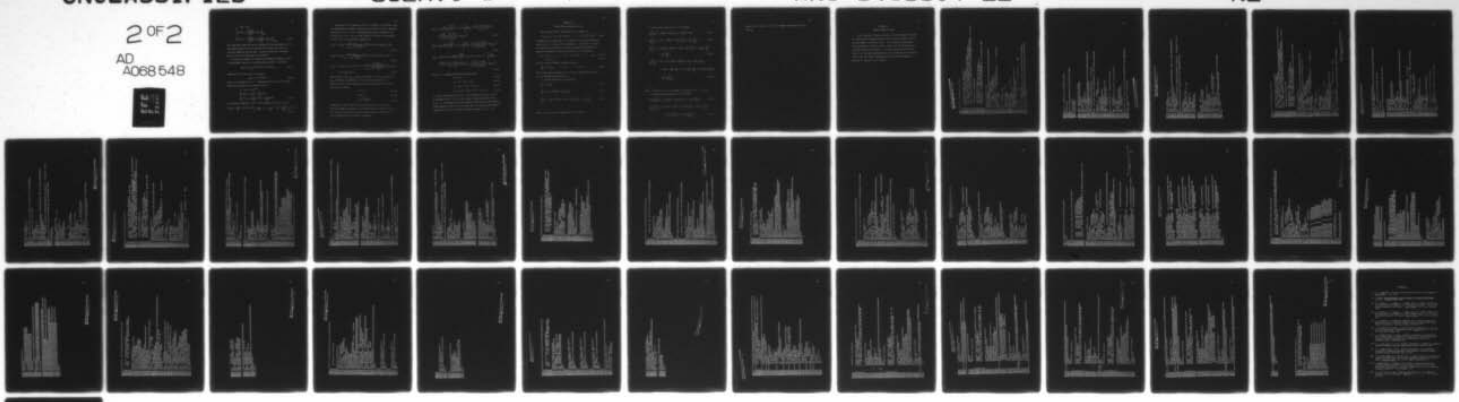

END
DATE FILMED
6-79
DDC

$$\begin{cases} Q(0) = P(\theta) \\ Q^{(2)}(0) = 2j\left[\dfrac{d^2P(\xi)}{d\xi^2} + \dfrac{1}{4}\,P(\xi)\right]_{\xi=\theta} \\ Q^{(4)}(0) = -4\left[\dfrac{d^4P(\xi)}{d\xi^4} + \dfrac{5}{2}\,\dfrac{d^2P(\xi)}{d\xi^2} + \dfrac{9}{16}\,P(\xi)\right]_{\xi=\theta} \end{cases} . \qquad \text{(II.10)}$$

The higher-order terms can also be determined in the same fashion. It is worth emphasizing here that in deriving the preceding equations, the following assumption has been made: neither the poles nor the branch points of $P(\xi)$ are intercepted by the path SDP.

To present an example, the higher-order asymptotic expansion of the following Hankel function of the second kind and order ν is derived:

$$H_\nu^{(2)}(\Omega) = \frac{1}{\pi}\int_\Gamma e^{-j\nu\xi+j\nu\pi/2}\, e^{-j\Omega\cos\xi}\, d\xi \quad . \qquad \text{(II.11)}$$

Comparing (II.11) with (II.1), one obtains

$$P(\xi) = 4j\, e^{-j\nu\xi+j\nu\pi/2} \quad , \qquad \text{(II.12)}$$

where it is assumed that $\Omega >> \nu$. Substituting (II.12) into (II.10) and simplifying the result, one finally arrives at

$$\begin{cases} Q(0) = 4j\, e^{j\nu\pi/2} \\ Q^{(2)}(0) = -8\left[-\nu^2 + \dfrac{1}{4}\right] e^{j\nu\pi/2} \\ Q^{(4)}(0) = -16j\left[\nu^4 - \dfrac{5}{2}\,\nu^2 + \dfrac{9}{16}\right] e^{j\nu\pi/2} \end{cases} . \qquad \text{(II.13)}$$

The asymptotic expansion of $H_\nu^{(2)}$ is then determined using (II.8) to be

$$H_\nu^{(2)}(\Omega) = \sqrt{\frac{2}{\pi\Omega}}\, e^{-j(\Omega-\nu\pi/2-\pi/4)}\left[1 + \frac{j}{2\Omega}\left(\frac{1}{4} - \nu^2\right) - \frac{1}{8\Omega^2}\left(\nu^4 - \frac{5}{2}\nu^2 + \frac{9}{16}\right)\right] + O(\Omega^{-7/2}). \qquad \text{(II.14)}$$

The purpose of this appendix has been to formulate the necessary steps for determining the asymptotic expansion of the vector potential components expressed in (2.47) - (2.49). Rearranging these three expressions into the form of Eq. (II.1), one can easily define a P function corresponding to each of the vector potential components as

$$P_{vlz}(\xi) = I_{v0}k_1\kappa \frac{\sin\xi\cos\xi}{\kappa\cos\xi + \sqrt{\kappa - \sin^2\xi}} H_0^{(2)}(k_1\rho_2 \sin\xi) \exp(jk_1\rho_2 \sin\xi) \tag{II.15}$$

$$P_{hlx}(\xi) = I_{h0}k_1 \frac{\sin\xi\cos\xi}{\cos\xi + \sqrt{\kappa - \sin^2\xi}} H_0^{(2)}(k_1\rho_2 \sin\xi) \exp(jk_1\rho_2 \sin\xi) \tag{II.16}$$

$$P_{hlz}(\xi) = -jI_{h0}k_1 \cos\phi_2 \sin^2\xi \cos\xi \frac{\cos\xi - \sqrt{\kappa - \sin^2\xi}}{\kappa\cos\xi + \sqrt{\kappa - \sin^2\xi}} H_1^{(2)}(k_1\rho_2 \sin\xi)$$
$$\cdot \exp(jk_1\rho_2 \sin\xi) \tag{II.17}$$

where functions P_{vlz}, P_{hlx}, and P_{hlz} correspond to the ${}_0\Pi_{vlz}$, ${}_0\Pi_{hlx}$, and ${}_0\Pi_{hlz}$ expressions, respectively. Since the final results take a complicated form, the following notations are introduced for the ease of representation, namely,

$$c = \cos\theta_2 \tag{II.18a}$$

$$s = \sin\theta_2 \tag{II.18b}$$

$$q = \sqrt{\kappa - \sin^2\theta_2} \quad . \tag{II.18c}$$

Performing the rather tedious differentiation needed in (II.10) and using the asymptotic expansion for the Hankel functions derived in (II.14), one finally arrives at the following two-term asymptotic expression for the aforementioned vector potential components:

$$0\Pi_{v1z} = I_{v0}\frac{2\kappa c}{\kappa c + q}\frac{e^{-jk_1r_2}}{4\pi r_2} + I_{v0}\, j\kappa c\left[\frac{-2}{\kappa c + q} + \frac{A_1(3c - 2/c) + A_2 + \kappa c}{(\kappa c + q)^2}\right.$$

$$\left. + \frac{2s^2A_1^2}{(\kappa c + q)^3}\right]\frac{e^{-jk_1r_2}}{4\pi k_1 r_2^2} + 0(k_1r_2)^{-3} \qquad \text{(II.19)}$$

$$0\Pi_{h1x} = I_{h0}\frac{2c}{c + q}\frac{e^{-jk_1r_2}}{4\pi r_2} + I_{h0}\, jc\left[\frac{A_3}{c + q} + \frac{A_2 + c}{(c + q)^2}\right]\frac{e^{-jk_1r_2}}{4\pi k_1 r_2^2} + 0(k_1r_2)^{-3}$$

(II.20)

$$0\Pi_{h1z} = I_{h0}2\cos\phi_2\, sc\frac{c - q}{\kappa c + q}\frac{e^{-jk_1r_2}}{4\pi r_2} + I_{h0}\cos\phi_2\, jsc(c - q)\left[\frac{A_4}{\kappa c + q}\right.$$

$$\left. + \frac{A_1(5c - 2/c + 2s^2/q) + A_2 + \kappa c}{(\kappa c + q)^2} + \frac{2s^2A_1^2}{(\kappa c + q)^3}\right]\frac{e^{-jk_1r_2}}{4\pi k_1 r_2^2} + 0(k_1r_2)^{-3}$$

(II.21)

where A_1 - A_4 expressions take the following form:

$$A_1 = \kappa q + c \qquad \text{(II.22a)}$$

$$A_2 = (s^4 - 2\kappa s^2 + \kappa)/q^3 \qquad \text{(II.22b)}$$

$$A_3 = 2s^2/q^2 + (3c - 2/c)/q - 2 \qquad \text{(II.22c)}$$

$$A_4 = s^2c/q^3 + s^2/q^2 + 2(3c - 1/c)/q - 6 \quad ; \qquad \text{(II.22d)}$$

s,c, and q were defined in (II.18). It is interesting to point out that in deriving (II.19) - (II.21), one initially encounters singular terms at $\theta_2 = 0$. As expected, after some algebraic manipulations, these singular terms completely cancel out in all three cases, and the two-term asymptotic expressions for the vector potentials remain bounded for $0 \leq \theta_2 < 90$.

APPENDIX III

VARIOUS PARTIAL DERIVATIVES OF g

The free-space Green's function g, which is defined as

$$g = g(x_1, x_2, x_3) = \exp(-jkr)/4\pi r \quad ; \quad r = [x_1^2 + x_2^2 + x_3^2]^{1/2} \tag{III.1}$$

is singular only at the point r = 0, therefore, its partial derivatives exist for all r > 0 and can be represented in a closed form. In order to express these derivatives in an organized manner and suitable for numerical evaluation, the auxiliary function R_i is introduced as

$$R_i = (-1)^i\{1 \times 2 \times 4 \times \ldots \times(2i - 2) + jkr[1 \times 3 \times 5 \times \ldots \times(2i - 3)]\}r^{-2i}; \quad i = 1,2,3,\ldots \tag{III.2}$$

where R_i has the following convenient property

$$\frac{\partial}{\partial x_j} R_i = x_j R_{i+1} \quad ; \quad i = 1,2,\ldots \quad ; \quad j = 1,2,3 \quad . \tag{III.3}$$

The various partial derivatives of g can now be expressed in terms of x_j, R_2, and lower-order partials of g.

a) Partial derivatives of one variable

$$\frac{\partial}{\partial x_j} g = x_j R_1 g \tag{III.4}$$

$$\frac{\partial^2}{\partial x_j^2} g = (R_1 + x_j^2 R_2)g + x_j R_1 \frac{\partial}{\partial x_j} g \tag{III.5}$$

$$\frac{\partial^3}{\partial x_j^3} g = (3x_j R_2 + x_j^3 R_3)g + 2(R_1 + x_j^2 R_2) \frac{\partial}{\partial x_j} g + x_j R_1 \frac{\partial^2}{\partial x_j^2} g \tag{III.6}$$

. . .

. . .

where j = 1,2,3 holds for Equations (III.4) - (III-6).

b) Mixed partial derivatives of two variables

$$\frac{\partial^2}{\partial x_j \partial x_k} g = x_j x_k R_2 g + x_k R_1 \frac{\partial}{\partial x_j} g = x_j x_k (R_1^2 + R_2) g \tag{III.7}$$

$$\frac{\partial^3}{\partial x_j^2 \partial x_k} g = x_k (R_2 + x_j^2 R_3) g + 2 x_j x_k R_2 \frac{\partial}{\partial x_j} g + x_k R_1 \frac{\partial^2}{\partial x_j^2} g \tag{III.8}$$

$$\frac{\partial^4}{\partial x_j^3 \partial x_k} g = x_k (3 x_j R_3 + x_j^3 R_4) g + 3 x_k (R_2 + x_j^2 R_3) \frac{\partial}{\partial x_j} g + 3 x_j x_k R_2 \frac{\partial^2}{\partial x_j^2} g$$
$$+ x_k R_1 \frac{\partial^3}{\partial x_j} g \tag{III.9}$$

$$\frac{\partial^4}{\partial x_j^2 \partial x_k^2} g = [R_2 + (x_j^2 + x_k^2) R_3 + x_j^2 x_k^2 R_4] g + x_k (R_2 + x_j^2 R_3) \frac{\partial}{\partial x_k} g$$
$$+ 2 x_j (R_2 + x_k^2 R_3) \frac{\partial}{\partial x_j} g + (R_1 + x_k^2 R_2) \frac{\partial^2}{\partial x_j^2} g + 2 x_j x_k R_2 \frac{\partial^2}{\partial x_j \partial x_k} g$$
$$+ x_k R_1 \frac{\partial^3}{\partial x_j^2 \partial x_k} g \tag{III.10}$$

. . .

. . .

where $j \neq k$ and $j,k = 1,2,3$ is assumed for Equations (III.7) - (III.10).

c) Mixed partial derivatives of three variables

$$\frac{\partial^3}{\partial x_j \partial x_k \partial x_\ell} g = x_j x_k x_\ell R_3 g + 2 x_k x_\ell R_2 \frac{\partial}{\partial x_j} g + x_\ell R_1 \frac{\partial^2}{\partial x_j \partial x_k} g \tag{III.11}$$

$$\frac{\partial^4}{\partial x_j^2 \partial x_k \partial x_\ell} g = x_k x_\ell (R_3 + x_j^2 R_4) g + 3 x_j x_k x_\ell R_3 \frac{\partial}{\partial x_j} g + 2 x_k x_\ell R_2 \frac{\partial^2}{\partial x_j^2} g$$
$$+ x_j x_\ell R_2 \frac{\partial^2}{\partial x_j \partial x_k} g + x_\ell R_1 \frac{\partial^3}{\partial x_j^2 \partial x_k} g \tag{III.12}$$

. . .

. . .

where $j \neq k \neq \ell$ and $j,k,\ell = 1,2,3$ is assumed for Equations (III.11) - (III.12).

APPENDIX IV

COMPLETE COMPUTER LISTING

In this appendix, a complete listing of a Fortran program is listed for analyzing wire antenna structures over a lossy half-space, based on the developments of Chapters 4 and 5. Also included are subroutines for evaluating the correction vector potential via the SDP integration technique introduced in Chapter 3. To avoid confusion, care has been taken to use the same symbols and names in the program as were introduced in the text, and comment statements have been included frequently to describe the function of each routine.

```
      PROGRAM HORIZ(INPUT,OUTPUT)
C
C
C     CENTER-FED HORIZONTAL WIRE ANTENNA
C     ANTLS   ANTENNA-LENGTH (METERS)
C     RADIUS=   ANTENNA-RADIUS (METERS)
C     HS    ANTENNA-HEIGHT ABOVE THE LOSSY HALF-SPACE
C     EPSR, SIGMAS   GROUND PARAMETERS,  SIGMA IN MMOS/METERS
C      NS    NUMBER OF CURRENT PATCHES (ODD FOR A CENTER-FED ANTENNA)
C     PHIDEG   THE PHI-PLANE IN WHICH PATTERN IS COMPUTED(AS A FUNCTION OF THETA)
C
C       **********INPUT**********
C
C       READ FREQUENCY (MHZ)
C       READ EPSR,SIGMA (DEFINING THE GROUND)
C       IF EPSR<0.    ,    THEN READ A NEW FREQUENCY
C       READ PHIDP (DEGREES) , PATTERN-PLANE
C       IF PHIDP<0.    , PATTERN NOT COMPUTED AND NEW GROUND IS READ
C
C
      IMPLICIT COMPLEX(C,D)
      REAL LOS,LAMS
      COMPLEX KAPPA,ZIN1(21,21),JAN1(21),Z1(21),ZK(21),ZL(21)
      COMMON/PI/    PI,EPSO,CJ
      COMMON/DIMS/    NS,IMS,PHIS
      COMMON/KAPAN/    ANT,KAPPA,CLA
      COMMON/PATTERN/    RV,THV,PHIV
      COMMON/PATCH/    XLOCK,YLOCK,ZLOCK
      PI=4.*ATAN(1.)    ;    EPSO=1.E-9/(36.*PI)    ;    CJ=(0.,1.)
      Z121    CONTINUE
C
      READ(5,9)    FREQ
    9 FORMAT(G14.6)
      IF(FREQ.LT.0.)    STOP
      FREQ=FREQ*1.E6
 1111    CONTINUE
      READ(5,10)    EPSR
      IF(EPSR.LT.0.)    GO TO Z121
      READ(5,10)    SIGMA
      ANT=2.*PI*FREQ/3.E8
      KAPPA=EPSR-CJ*SIGMA/(2.*PI*FREQ*EPSO)
      CLA=1./(CJ*2.*PI*FREQ*EPSO)
C
      ANTL=10.    ;    HS=5.    ;    RADIUS=.05    ;    NS=21
C
      PRINT 22,FREQ,KAPPA
   22 FORMAT(//,"FREQ=",G14.4,5X,"KAPPA=",G12.4,",",G14.6)
      PRINT 33,ANTL,RADIUS,HS
   33 FORMAT(//"ANTL=",G10.5,"ANT-RAD=",G12.6,"ANT-HEIGHT=",
     *G10.5,"   NS=",I4)
```

```
02500C
02600C*****   COMPUTE THE IMPEDANCE MATRIX
02700C
02800 DEL=ANTL/N
02805C
02810C**USE FINITE-DIFFERENCE TECHNIQUE FOR EINC
02815C
02820 DO 100 I=1,N
02830 X=(I-1)*DEL
02840 XR=X+DEL/2.

02850 CALL SI(DEL,RADIUS,X,ZI(I))
02860 CALL SI(DEL,RADIUS,XR,ZR(I))
02870 100   CONTINUE
02880 ZL(1)=ZR(1)
02890 DO 210   I=2,N
02900 210   ZL(I)=ZR(I-1)
02910 DO 120 J=1,N
02920 ZTOT(1,J)=(ZR(J)+ZL(J)-2.*ZI(J))/(DEL/2.)**2+AK1**2*ZI(J)
03020 ZTOT(1,J)=-ZTOT(1,J)*DEL*CI0
03070 120   CONTINUE
03120 IF(EPSR.EQ.1..AND.SIGMA.EQ.0.)   GO TO 200
03130C
03140C***   ADD THE GROUND CONTRIBUTIONS TO THE MATRIX ELEMENTS
03150C
03160 ZZ=2.*H    $   PHI2=0.
03170 C1=(0.,0.)    $   C2=-DEL**2*CI0
03180 DO 110   I=1,N
03190 RHO2=(I-1)*DEL
03200 R2=SQRT(RHO2**2+ZZ**2)
03210 TH2=ACOS(ZZ/R2)
03220 CALL SESAPP(UEX,UEY,UEZ,C1,C2)
03230 ZTOT(1,I)=ZTOT(1,I)+UEX
03240 110   CONTINUE
03250C
03260C***USE SYMMETRY TO COMPLETE THE MATRIX
03270C
03590 200   CONTINUE
03700 850   FORMAT(/,4("(",G10.4," ,",G10.4,")"))
03800 DO 300 I=1,N
03900 DO 300 J=1,N
04000 IF(I.EQ.1)   GO TO 310
04100 ZTOT(I,J)=ZTOT(I-1,J-1)
04200 310   ZTOT(J,I)=ZTOT(I,J)
04300 300   CONTINUE
04350C
04360C***INVERT THE MATRIX AND COMPUTE CURRENTS AND THE IMPEDANCE
04390C
04400 CALL AINVZ(N,21,ZTOT,UDET,IER)
04500 NO2=N/2+1
```

```
046000      DO 406  I=1,N
04/000      JANT(I)=ZTOT(I,NO2)
048000  406   CONTINUE
045400      PRINT049
048800  049   FORMAT(///,"ANTENNA CURRENTS(AMPS), DUE TO 1-VOLT EXCITATION")
049000      PRINT050,(JANT(I),I=1,N)
050000      UZINP=1./JANT(NO2)
050700      PRINT060,UZINP
051700  060   FORMAT(///,"ANTENNA IMPEDANCE(OHMS)= (",G14.6,"  ,",G14.6," )",//)
052700C
053700C***COMPUTE THE E-FIELD PATTERNS IN THE PHI=PHI0P PLANE
054700C
055700      AK1K0=500.
056700      K0=AK1K0/AK1
057700  3131    READ900,PHI0P
058200      IF(PHI0P.LT.0.)    GO TO 1111
059700      PRINT970
060700      PHI0=PHI0P*PI/180.
061700      DO 700  I=1,45
062700      THOP=2.*I
063700      TH0=TH0P*PI/180.
064700      UETH=UEPHI=(0.,0.)

065700C
066700C
067700      DO 750    K=1,N
068700      ZCURR=0    $    YCURR=0.
069700      XCURR=(K-(N+1)/2)*DEL
070700      UIZ=(0.,0.)
071700      UIX=JANT(K)
072700      CALL SEPAT(UIX,UIZ,U1,U2)
073700      UETH=UETH+U1*DEL
074700      UEPHI=UEPHI+U2*DEL
075700  750   CONTINUE
076700      ETH=CABS(UETH)    $    EPHI=CABS(UEPHI)
077700      PRINT975,AK1K0,THOP,PHI0P,ETH,EPHI
078700  700   CONTINUE
079700  970   FORMAT(///)
080700  975   FORMAT(" K1K0=",G8.2," TH0=",G8.2," PHI0=",G8.2,
081700+" MAG-ETH=",G14.6," MAG-EPHI=",G14.6)
082700      GO TO 3131
083700      END
```

```
00100 PROGRAM VERTIC(INPUT,OUTPUT)
00200C
00210C
00220C     CENTER-FED VERTICAL WIRE ANTENNA
00230C     ANTLA    ANTENNA-LENGTH (METERS)
00240C     RADIUS=    ANTENNA-RADIUS (METERS)
00250C     H=    ANTENNA-HEIGHT ABOVE THE LOSSY HALF-SPACE (MEASURED FROM ANTENNA-CENTER)
00260C     EPSR, SIGMA=    GROUND PARAMETERS,  SIGMA IN MHOS/METERS
00270C      N=   NUMBER OF CURRENT PATCHES (ODD FOR A CENTER-FED ANTENNA)
00280C     PHIDP=  THE PHI-PLANE IN WHICH PATTERN IS COMPUTED(AS A FUNCTION OF THETA)
00300C
00305C      **********INPUT**********
00310C
00315C      READ FREQUENCY (MHZ)
00320C      READ EPSR,SIGMA (DEFINING THE GROUND)
00325C      IF EPSR<0.      ,    THEN READ A NEW FREQUENCY
00330C      READ PHIDP (DEGREES) , PATTERN-PLANE
00335C      IF PHIDP<0.     , PATTERN NOT COMPUTED AND NEW GROUND IS READ
00340C
00400C
00500 IMPLICIT COMPLEX(C,U)
00600 REAL COS,CABS
00700 COMPLEX KAPPA,ZIUT(21,21),JANT(21),ZI(21),ZK(21),ZL(21)
00750 COMPLEX ZEXTRA(4)
00775C---ZEXTRA MUST BE DIMENSIONED AT LIST 2*N+1 LONG
00800 COMMON/PI/    PI,EPSN,CJ
00900 COMMON/DOS/    R2,TR2,PHI2
01000 COMMON/PARAM/    ANT,KAPPA,CIN
01100 COMMON/PATTERN/    R0,THR,PHI0
01200 COMMON/PATCH/    XCORR,YCORR,ZCORR
01100 PI=4.*ATAN(1.)    $    EPS0=1.E-9/(36.*PI)    $    CJ=(0.,1.)
01200 2121    CONTINUE
01400C
01600 READ900,FREQ
01615 900    FORMAT(F14.5)
01625C
01650 IF(FREQ.LT.0.)    STOP
01700 FREQ=FREQ*1.E6
01725 1111    CONTINUE
01750 READ900,EPSR
01775 IF(EPSR.LT.0.)    GO TO 2121
01800 READ900,SIGMA
01794 PRINT900,FREQ,EPSR,SIGMA
01800 ANT=2.*PI*FREQ/3.E8
01900 KAPPA=EPSR-CJ*SIGMA/(2.*PI*FREQ*EPS0)
02000 CIN=1./((CJ*2.*PI*FREQ)*EPSR)
02100C
02120 ANTL=10.    $    H=0.    $    RADIUS=.35    $    N=21
02200C
02300 PRINT920,FREQ,KAPPA
02400 920    FORMAT(//,"FREQ=",G14.4,5X,"KAPPA=",G12.4,",",G14.6)
```

```
02440 PRINT 850,ANTL,RADIUS,M,N
02480 850   FORMAT(//"ANT-L=",G10.5,"ANT-RAD=",G12.6,"ANT-HEIGHT=",
02490+G10.5,"   N=",I4)
02500C
02600C*****   COMPUTE THE IMPEDANCE MATRIX
02700C
02800 DEL=ANTL/N
02805C
02810C**USE FINITE-DIFFERENCE TECHNIQUE FOR EINC
02815C

02820 DO 100 I=1,N
02830 X=(I-1)*DEL
02840 XR=X+DEL/2.
02850 CALL SI(DEL,RADIUS,X,ZI(I))
02860 CALL SI(DEL,RADIUS,XR,ZR(I))
02870 100   CONTINUE
02880 ZL(1)=ZR(1)
02890 DO 210   I=2,N
02900 210   ZL(I)=ZR(I-1)
02910 DO 120 J=1,N
02920 ZTOT(1,J)=(ZR(J)+ZL(J)-2.*ZI(J))/(DEL/2.)**2+AK1**2*ZI(J)
03020 ZTOT(1,J)=-ZTOT(1,J)*DEL*C10
03070 120   CONTINUE
03085 DO 150 I=2,N
03100 DO 150 J=1,N
03115 150   ZTOT(I,J)=ZTOT(I-1,J-1)
03120 IF(EPSR.EQ.1..AND.SIGMA.EQ.0.)   GO TO 200
03130C
03140C***   ADD THE GROUND CONTRIBUTIONS TO THE MATRIX ELEMENTS
03150C
03160 RHO2=0.     $   PHI2=0.    $   TH2=0.
03170 C2=(0.,0.)    $   C1=-DEL**2*C10
03180 NPP=2.*N-1
03190 DO 110 I=1,NPP
03200 R2=Z2=2.*M-ANTL+I*DEL
03220 CALL SESAPP(DEX,DEY,DEZ,C1,C2)
03230 ZEXTRA(I)=DEZ
03240 110   CONTINUE
03242 DO 115   I=1,N
03244 DO 115   J=I,N
03246 ZTOT(I,J)=ZTOT(I,J)+ZEXTRA(I+J-1)
03248 115   CONTINUE
03250C
03260C***USE SYMMETRY TO COMPLETE THE MATRIX
03270C
03590 200   CONTINUE
03740 850   FORMAT(/,4("(",G10.4," ,",G10.4,")"))
03800 DO 500 I=2,N
03900 K=I-1
```

```
04000      DO 500 J=1,K
04100      ZIOT(I,J)=ZIOT(J,1)
04200  500 CONTINUE
04330C
04360C***INVERT THE MATRIX AND COMPUTE CURRENTS AND THE IMPEDANCE
04590C
04400      CALL XINVZ(N,21,ZIOT,DUEL,IER)
04500      NO2=N/2+1
04600      DO 400 I=1,N
04700      JANT(I)=ZIOT(I,NO2)
04800  400 CONTINUE
04840      PRINT849
04880  849 FORMAT(///,"ANTENNA CURRENTS(AMPS), DUE TO 1-VOLT EXCITATION")
04900      PRINT850,(JANT(I),I=1,N)
05000      UZIMP=1./JANT(NO2)
05070      PRINT860,UZIMP
05170  860 FORMAT(///,"ANTENNA IMPEDANCE(OHMS)= (",G14.6,"  ,",G14.6," )",//)
05270C
05370C***COMPUTE THE E-FIELD PATTERNS IN THE PHI=PHIOP PLANE
05470C
05570      AK1R0=500.
05670      R0=AK1R0/AK1

05770 3131 READ900,PHIOP
05820      IF(PHIOP.LT.0.)   GO TO 1111
05870      PRINT970
06070      PHI=PHIOP*PI/180.
06170      DO 700 I=1,45
06270      THEP=2.*I
06370      THR=THOP*PI/180.
06470      UETH=UEPHI=(0.,0.)
06570C
06670C
06770      DO 750   K=1,N
06870      XCURR=0.    $   YCURR=0.
06970      ZCURR=H-ANTL/2.+(K-.5)*DEL
07070      UIA=(0.,0.)
07170      UIZ=JANT(K)
07270      CALL SEPAT(UIA,UIZ,U1,U2)
07370      UETH=UETH+U1*DEL
07470      UEPHI=UEPHI+U2*DEL
07570  750 CONTINUE
07670      ETH=CABS(UETH)    $   EPHI=CABS(UEPHI)
07770      PRINT975,AK1R0,THOP,PHIOP,ETH,EPHI
07870  700 CONTINUE
07970  970 FORMAT(///)
08070  975 FORMAT(" K1R0=",G6.2," THO=",G8.2," PHIO=",G8.2,
08170+" MAG-ETH=",G14.6," MAG-EPHI=",G14.6)
08270      GO TO 3131
08370      END
```

```
      PROGRAM VEEDIP(INPUT,OUTPUT)
C
C
C     INVERTED VEE-DIPOLE ANTENNA OVER GROUND
C     ANTLEG=   THE LENGTH OF EACH ANTENNA LEG (METETRS)
C     RADIUS=   ANTENNA-RADIUS (METERS)
C     H=    ANTENNA-HEIGHT ABOVE THE LOSSY HALF-SPACE (MEASURED FROM ANTENNA-CENTER)
C     EPSR, SIGMA=   GROUND PARAMETERS,  SIGMA IN MHOS/METERS
C      N=   NUMBER OF CURRENT PATCHES (EVEN FOR A CENTER-FED ANTENNA)
C     PHIOP=  THE PHI-PLANE IN WHICH PATTERN IS COMPUTED(AS A FUNCTION OF THETA)
C
C      **********INPUT**********
C
C     READ FREQUENCY (MHZ)
C      READ EPSR,SIGMA (DEFINING THE GROUND)
C      IF EPSR<0.      , THEN READ A NEW FREQUENCY
C      READ PHIOP (DEGREES) ,  PATTERN-PLANE
C      IF PHIOP<0.    , PATTERN NOT COMPUTED AND NEW GROUND IS READ
C
C
      IMPLICIT COMPLEX(C,Z)
      REAL COS,CABS
      COMPLEX KAPPA,ZTOT(22,22),JANT(22),ZI(22),ZR(22),ZL(22)
      COMMON/PI/    PI,EPS0,CJ
      COMMON/CONS/    K2,TH2,PHI2
      COMMON/PARAM/    AK1,KAPPA,C10
      COMMON/PATTERN/    K0,THK,PHI0
      COMMON/PATCH/    ALOAK,YCOAK,ZCOAK
      PI=4.*ATAN(1.)    $    EPS0=1.E-9/(36.*PI)    $    CJ=(0.,1.)
 2121    CONTINUE
C
      READ900,FREQ
  900    FORMAT(F14.6)
C
      IF(FREQ.LT.0.)    STOP
      FREQ=FREQ*1.E6
 1111    CONTINUE
      READ900,EPSR
      IF(EPSR.LT.0.)    GO TO 2121
      READ900,SIGMA
      READ900,ANTSI
      PRINT900,FREQ,EPSR,SIGMA
      AK1=6.*PI*FREQ/3.E8
      KAPPA=EPSR-CJ*SIGMA/(2.*PI*FREQ*EPS0)
      C10=1./(CJ*6.*PI*FREQ*EPS0)
C
      ANTLEG=7.5    $    N=10.    $    RADIUS=.05    $    N=22
C
      PRINT820,FREQ,KAPPA
```

```
05100 65    FORMAT(//,"FREQ=",G14.4,5X,"KAPPA=",G12.4,",",G14.6)
05200 PRINT 650,ANTLEG,ANTSI,RADIUS,N
05300 650   FORMAT(//"ANTENNA-LEG=",G10.5,"INVERTED-VEE ANGLE=",G10.5,
05400+"ANT-RADIUS=",G10.5,"ANT-HEIGHT=",G10.5)
05425 PRINT 655,N
05430 655   FORMAT(/"  N= ",I5)
05450 ANTSI=ANTSI*PI/180.
05500C
05600C*****   COMPUTE THE IMPEDANCE MATRIX
05700C
05800 ND2=N/2
05900 DEL=ANTLEG/ND2

06000C
06100C**USE FINITE-DIFFERENCE TECHNIQUE FOR EINC(SYMMETRY IS USED)
06200C
06300 DO 100 I=1,ND2
06400 X=(I-1)*DEL
06500 AK=X+DEL/2.
06600 CALL SI(DEL,RADIUS,X,ZI(I))
06700 CALL SI(DEL,RADIUS,XK,ZK(I))
06800 100   CONTINUE
06900 ZL(1)=ZK(1)
07000 DO 110   I=2,ND2
07100 110   ZL(I)=ZK(I-1)
07200 DO 120 J=1,ND2
07300 ZTOT(1,J)=(ZK(J)+ZL(J)-2.*ZI(J))/(DEL/2.)**2+AK1**2*ZI(J)
07400 ZTOT(1,J)=ZTOT(1+ND2,J+ND2)=-ZTOT(1,J)*DEL*CI0
07500 120   CONTINUE
07600 DO 150 I=2,ND2
07700 DO 150 J=1,ND2
07800 150   ZTOT(I,J)=ZTOT(1+ND2,J+ND2)=ZTOT(I-1,J-1)
07850C
07900C
07915 DO 160 I=1,ND2
07925 K=ND2+1-I
07930 DO 160 J=1,K
07935 X=(ND2-I+.5)*DEL+(J-.5)*DEL*COS(PI-ANTSI)+2.*RADIUS*SIN(PI-ANTSI)
07936 RHO=ABS((J-.5)*DEL*SIN(PI-ANTSI)-2.*RADIUS*COS(PI-ANTSI)+RADIUS)
07935 CALL SI(DEL,RHO,X,DZI)
07940 CALL SI(DEL,RHO,X+DEL/2.,DZIK)
07945 CALL SI(DEL,RHO,X-DEL/2.,DZIKL)
07950 CALL SI(DEL,RHO+DEL/2.,X+DEL/2.,DZIKRK)
07955 CALL SI(DEL,RHO-DEL/2.,X-DEL/2.,DZIKLKL)
07960 CALL SI(DEL,RHO+DEL/2.,X-DEL/2.,DZIKRKL)
07965 CALL SI(DEL,RHO-DEL/2.,X+DEL/2.,DZIKLKR)
07970 DEPAK=(DZIK+DZIKL-2.*DZI)/(DEL/2.)**2+AK1**2*DZI
07975 DEVEK=(DZIKRK+DZIKLKL-DZIKRKL-DZIKLKR)/DEL**2
07980 DET=DEPAK*COS(PI-ANTSI)+DEVEK*SIN(PI-ANTSI)
07985 ZTOT(I,J+ND2)=ZTOT(ND2+1-J,K+1-I)=-DET*DEL*CI0
07990 160   CONTINUE
07995 IF(EPSR.EQ.1..AND.SIGMA.EQ.0.)   GO TO 200
```

```
C
C***   ADD THE GROUND CONTRIBUTIONS TO THE MATRIX ELEMENTS(SYMMETRY IS USED)
C
      DO 210   I=1,NO2
      DO 210   J=1,NO2
      RHO2=ABS(FLOAT(I-J))*DEL*SIN(ANTSI/2.)
      Z2=2.*(H-(NO2-I+.5)*DEL*COS(ANTSI/2.))+ABS(FLOAT(I-J))*DEL*COS(ANTSI/2.)
      PH12=0.
      R2=SQRT(RHO2**2+Z2**2)
      TH2=ATAN(RHO2/Z2)
      C1=-DEL**2*C1M*COS(ANTSI/2.)
      C2=-DEL**2*C1M*SIN(ANTSI/2.)
      CALL SESAPP(UEX,UEY,UEZ,C1,C2)
      UET=UEX*SIN(ANTSI/2.)+UEZ*COS(ANTSI/2.)
      ZTOT(I,J)=ZTOT(I,J)+UET
      ZTOT(N+1-J,N+1-I)=ZTOT(N+1-J,N+1-I)+UET
  210 CONTINUE
      DO 220   I=1,NO2
      DO 220   J=1,NO2
      IF(I.NE.1.AND.J.NE.1)   GO TO 220
      RHO2=(NO2-I+J)*DEL*SIN(ANTSI/2.)
      Z2=2.*H-(NO2-1+J)*DEL*COS(ANTSI/2.)

      PH12=0.
      R2=SQRT(RHO2**2+Z2**2)
      TH2=ATAN(RHO2/Z2)
      CALL SESAPP(UEX,UEY,UEZ,C1,C2)
      UET=UEX*SIN(ANTSI/2.)-UEZ*COS(ANTSI/2.)
      ZTOT(I,J+NO2)=ZTOT(I,J+NO2)+UET
  220 CONTINUE
      DO 250   I=2,NO2
      K=NO2+2
      DO 250   J=K,N
      ZTOT(I,J)=ZTOT(I-1,J-1)
  250 CONTINUE
C
C***USE SYMMETRY TO COMPLETE THE MATRIX
C
  260 CONTINUE
  650 FORMAT(/,4("(",G10.4," ,",G10.4,")"))
      DO 300 I=2,N
      K=I-1
      DO 300 J=1,K
      ZTOT(I,J)=ZTOT(J,I)
  300 CONTINUE
C
C***INVERT THE MATRIX AND COMPUTE CURRENTS AND THE IMPEDANCE
C
      CALL AINVZ(N,22,ZTOT,DET,IER)
      DO 400 I=1,N
      JANT(I)=ZTOT(I,N/2)+ZTOT(I,N/2+1)
```

```
      CONTINUE
      PRINT849
  849 FORMAT(///,"ANTENNA CURRENTS(AMPS), DUE TO 1-VOLT EXCITATION
     + APPLIED TO EACH OF THE TWO CENTER PATCHES")
      PRINT850,(JANT(I),I=1,N)
      ZINP=2./JANT(N/2)
      PRINT860,ZINP
  860 FORMAT(///,"ANTENNA IMPEDANCE(OHMS)= (",G14.6,"  ,",G14.6," )",//)
C
C***COMPUTE THE E-FIELD PATTERNS IN THE PHI=PHINP PLANE
C
      AK1K0=500.
      K0=AK1K0/AK1
 5131 READ900,PHINP
      IF(PHINP.LT.0.)   GO TO 1111
      PRINT970
      PHI0=PHINP*PI/180.
      DO 700 I=1,46
      THNP=2.*(I-1)
      THN=THNP*PI/180.
      UETH=UEPHI=(0.,0.)
C
C
      DO 750   K=1,ND2
      YCURR=0.
      ZCURR=H-(ND2-I+.5)*DEL*COS(ANTSI/2.)
      XCURR=-(ND2-I+.5)*DEL*SIN(ANTSI/2.)
      UIX=JANT(K)*SIN(ANTSI/2.)
      UIZ=JANT(K)*COS(ANTSI/2.)
      CALL SEPAT(UIX,UIZ,U1,U2)
      UETH=UETH+U1*DEL
      UEPHI=UEPHI+U2*DEL
      XCURR=-XCURR

      UIX=JANT(N-K+1)*SIN(ANTSI/2.)
      UIZ=-JANT(N-K+1)*COS(ANTSI/2.)
      CALL SEPAT(UIX,UIZ,U1,U2)
      UETH=UETH+U1*DEL
      UEPHI=UEPHI+U2*DEL
  750 CONTINUE
      ETH=CABS(UETH)      EPHI=CABS(UEPHI)
      PRINT975,AK1K0,THNP,PHINP,ETH,EPHI
  700 CONTINUE
  970 FORMAT(///)
  975 FORMAT(" K1K0=",G8.2," TH0=",G8.2," PHI0=",G8.2,
     +" MAG-ETH=",G14.6," MAG-EPHI=",G14.6)
      GO TO 5131
      END
```

```
00100 SUBROUTINE SEPAT(UIX,UIZ,UETH,UEPHI)
00200C
00300C
00400C    COMPUTE THE FAR-FIELD APPROXIMATION FOR E-THETA AND E-PHI.
00500C    THE OBSERVATION POINT IS LOCATED AT (R0,TH0,PHI0),
00600C    AND THE CURRENT ELEMENT IS LOCATED AT (XCURR,YCURR,ZCURR)
00700C    WITH UIX AMPS IN THE X-DIRECTION AND
00750C         UIZ AMPS IN THE Z-DIRECTION.
00800C
00900C
01000 IMPLICIT COMPLEX (C,U)
01100 REAL COS
01200 COMPLEX KAPPA
01300 COMMON/PI/    PI,EPSN,CJ
01400 COMMON/OBS/   R2,TH2,PHI2
01500 COMMON/PATTERN/   R0,TH0,PHI0
01600 COMMON/PATCH/   XCURR,YCURR,ZCURR
01700 COMMON/PARAM/   AK1,KAPPA,CI0
01800C
01900C
02000 Z2=R0*COS(TH0)+ZCURR
02100 X2=R0*SIN(TH0)*COS(PHI0)-XCURR
02200 Y2=R0*SIN(TH0)*SIN(PHI0)-YCURR
02300 R2=SQRT(X2**2+Y2**2+Z2**2)
02400 TH2=ACOS(Z2/R2)
02440 PHI2=0.
02480 IF(X2.NE.0..OR.Y2.NE.0.)   PHI2=ATAN2(Y2,X2)
02600C
02700C
02800 CALL SRCM1(U1,U2,U3)
02900 R1=SQRT(X2**2+Y2**2+(Z2-2.*ZCURR)**2)
03000 UG1=CEXP(-CJ*AK1*R1)/(4.*PI*R1)
03100 UG2=CEXP(-CJ*AK1*R2)/(4.*PI*R2)
03200 UPIX=UIX*CI0*(UG1-UG2+U2)
03300 UPIZ=UIZ*CI0*(UG1-UG2+U1)+UIX*CI0*U3
03400 UETH=AK1**2*(COS(TH0)*COS(PHI0)*UPIX-SIN(TH0)*UPIZ)
03500 UEPHI=-AK1**2*SIN(PHI0)*UPIX
03600 RETURN
03700 END
```

```
      SUBROUTINE SRCM1(CP0V1Z,CPVM1X,CP0M1Z)
C
C
C       COMPUTING THE 1ST TERM OF THE ASYMPTOTIC EXPANSION
C
C
      IMPLICIT COMPLEX(C,U)
      REAL COS,C
      COMPLEX KAPPA,U
      COMMON/PI/ PI,EPS0,CJ
      COMMON/OBS/ R,TH,PHI
      COMMON/PARAM/ AK1,KAPPA,C10
      CG=CEXP(-CJ*AK1*R)/(4.*PI*R)
      C=COS(TH)
      S=SIN(TH)
      U=CSQRT(KAPPA-S**2)
      CP0V1Z=2.*KAPPA*C/(KAPPA*C+U)*CG
      CP0M1X=2.*C/(C+U)*CG
      CP0M1Z=2.*COS(PHI)*S*C*(C-U)/(KAPPA*C+U)*CG
      RETURN
      END
C
C
C
      SUBROUTINE SRCM2(CP0V1Z,CPVM1X,CP0M1Z)
C
C
C     COMPUTING THE 2ND TERM IN THE ASYMPTOTIC EXPANSION
C
C
      IMPLICIT COMPLEX(C,U)
      REAL COS,C
      COMPLEX KAPPA,U,A1,A2,A3,A4,B1,B2
      COMMON/PI/ PI,EPS0,CJ
      COMMON/OBS/ R,TH,PHI
      COMMON/PARAM/ AK1,KAPPA,C10
      CG2=CEXP(-CJ*AK1*R)/(4.*PI*AK1*R**2)
      C=COS(TH)
      S=SIN(TH)
      U=CSQRT(KAPPA-S**2)
      A1=KAPPA*U+C
      A2=(S**4-2.*KAPPA*S**2+KAPPA)/U**3
      A3=2.*S**2/U**2+(3.*C-2./C)/U-2.
      A4=S**2*C/U**3+S**2/U**2+2.*(3.*C-1./C)/U-6.
      B1=KAPPA*C+U
      B2=C+U
      CPVV1Z=CJ*KAPPA*C*(-2./B1+(A1*(3.*C-2./C)+A2+KAPPA*C)/
     *+B1**2+2.*S**2*A1**2/B1**3)*CG2
      CPVM1X=CJ*C*(A3/B2+(A2+C)/B2**2)*CG2
      CP0M1Z=COS(PHI)*CJ*S*C*(C-U)*CG2
      CPVM1Z=CPVM1Z*(A4/B1+(A1*(5.*C-2./C+2.*S**2/U)+A2+KAPPA*C)/
     *+B1**2+2.*S**2*A1**2/B1**3)
      RETURN
      END
```

```
      SUBROUTINE SI(DELX,P,X,Z)
C
C     INTEGRATION OF THE FREE SPACE GREENS FUNCTION
C     FROM X-DEL/2 TO X+DEL/2 . X IS MEASURED ALONG THE
C     SOURCE AND P IS THE LATERAL DISLACEMENT FROM THE
C     SOURCE POINT.
C
      COMPLEX CMPLX,CEXP,Z,KAPPA
      COMMON/PARAM/   AK,KAPPA,C10
      REAL I1,I2,I3,I4
      PI=3.141592654
      AL=DELX/2.
      R=SQRT(P**2+X**2)
      IF(R.GE.10.*AL) GO TO 100
      S1=SQRT(P**2+(X+AL)**2)
      S2=SQRT(P**2+(X-AL)**2)
      I1=ALOG((X+AL+S1)/(X-AL+S2))
      I2=2.*AL
      I3=.5*(AL+X)*S1+.5*(AL-X)*S2+.5*P**2*I1
      I4=2.*AL*P**2+1./3.*(2.*AL**3+6.*AL*X**2)
      Z=I1-(0.,1.)*AK*(I2-R*I1)-.5*AK**2*(I3-2.*R*I2+R**2*I1)
      Z=Z+(0.,1.)*AK**3/6.*(I4-3.*R*I3+3.*R**2*I2-R**3*I1)
      Z=Z*CEXP(-(0.,1.)*AK*R)/(4.*PI)
      RETURN
  100 CONTINUE
      AUK=AL/R
      XUK=X/R
      A0=1.+1./6.*AUK**2*(-1.+3.*XUK**2)
      A0=A0+1./40.*AUK**4*(3.-30.*XUK**2+35.*XUK**4)
      A1=1./6.*AUK*(-1.+3.*XUK**2)
      A1=A1+1./40.*AUK**3*(3.-30.*XUK**2+35.*XUK**4)
      A2=-1./6.*XUK**2-1./40.*AUK**2*(1.-12.*XUK**2+15.*XUK**4)
      A3=1./60.*AUK*(3.*XUK**2-5.*XUK**4)
      A4=1./120.*XUK**4
      Z=A0+(0.,1.)*AK*AL*A1+(AK*AL)**2*A2
      Z=Z+(0.,1.)*(AK*AL)**3*A3+(AK*AL)**4*A4
      Z=Z*2.*AUK*CEXP(-(0.,1.)*AK*R)/(4.*PI)
      RETURN
      END
```

```
00100      SUBROUTINE SPIAPP(CP0V1Z,CP0M1X,CP0M1Z)
00200C
00300C
00400C     COMPUTE THE VECTOR POTENTIALS VIA THE APPROXIMATE TECHNIQUE
00500C
00600C
00700      IMPLICIT COMPLEX(C,U)
00800      COMPLEX KAPPA
00900      REAL COS
01000      COMMON/PI/    PI,EPS0,CJ
01100      COMMON/OBS/    R2,TH2,PH12
01200      COMMON/PARAM/    AK1,KAPPA,C10
01400      Z2=R2*COS(TH2)    $    RHO2=R2*SIN(TH2)
01500      STOREK=R2    $    STORET=TH2
01600      CALL SDGP1(U6,UGZ,UGZ2,UGXZ,UGX,0,0)
01700      CP0M1X=-2./AK1**2/(1.-KAPPA)*(CJ*AK1*CSQRT(KAPPA)*UGZ+UGZ2)
01800      CONST=AK1/CSQRT(KAPPA)
01900      R2P=15./AK1
02000      IF(R2.GT.R2P)    GO TO 100
02100      Z2P=SQRT(R2P**2-RHO2**2)    $    R2=R2P    $    TH2=ATAN(RHO2/Z2P)
02200      CALL SDGP1(UGP,UGZP,UGZ2P,UGXZP,UGXP,0,0)
02400  999    FORMAT(/6G14.6)
02700      R2=STOREK    $    TH2=STORET
02800      CALL SUS(Z2P,Z2,UGP,U6,UGXZP,CONST,US2,0)
02900      CALL SUS(Z2P,Z2,UGXP,UGX,UGXZP,CONST,US2X,1)
03400      CP0V1Z=US2
03500      CP0M1Z=1./AK1**2/KAPPA*(-2.*UGXZ-CJ*CONST*(1.+KAPPA)*US2X)
03600      RETURN
03700  100    CALL SRCM1(CP0V1Z,U2,CP0M1Z)
03800      RETURN
03900      END
04000C
04100C
04200C
04300      COMPLEX FUNCTION UGAMGV(Z2P)
04400      IMPLICIT COMPLEX (C,U)
04500      COMPLEX KAPPA
04600      REAL COS
04700      COMMON/PI/    PI,EPS0,CJ
04800      COMMON/OBS/    R2,TH2,PH12
04900      COMMON/PARAM/    AK1,KAPPA,C10
05000      STOREK=R2    $    STORET=TH2    $    RHO2=R2*SIN(TH2)
05100      CONST=AK1/CSQRT(KAPPA)
05200      R2=SQRT(Z2P**2+RHO2**2)    $    TH2=ATAN(RHO2/Z2P)
05300      CALL SDGP1(U6,U1,U2,U3,U4,1,0)
05400      UGAMGV=U6*CEXP(-CJ*CONST*Z2P)
05500      R2=STOREK    $    TH2=STORET
05600      RETURN
05700      END
05800C
05900C
06000C
06100      COMPLEX FUNCTION UGAMGM(Z2P)
06200      IMPLICIT COMPLEX (C,U)
```

```
      COMPLEX KAPPA
      REAL LOG
      COMMON/PI/    PI,EPS0,CJ
      COMMON/UBS/    R2,TH2,PHI2
      COMMON/PARAM/    AK1,KAPPA,CI0
      STORER=R2    $    STORET=TH2    $    RHO2=R2*SIN(TH2)
      CONST=AK1/CSQRT(KAPPA)
      Z2P=SQRT(Z2P**2+RHO2**2)    $    TH2=ATAN(RHO2/Z2P)
      CALL SDGPI(U1,U2,U3,U4,UGX,0,1)
      UGARGM=UGX*CEXP(-CJ*CONST*Z2P)
      R2=STORER    $    TH2=STORET
      RETURN
      END
C
C
C
      SUBROUTINE SDGPI(UG,UGZ,UGZZ,UGXZ,UGX,IV,IH)
      IMPLICIT COMPLEX (C,U)
      COMPLEX KAPPA
      REAL LOG
      COMMON/PI/    PI,EPS0,CJ
      COMMON/UBS/    R2,TH2,PHI2
      COMMON/PARAM/    AK1,KAPPA,CI0
      UG=CEXP(-CJ*AK1*R2)/(4.*PI*R2)
      IF(IV.EQ.1)    RETURN
      XC=R2*SIN(TH2)*COS(PHI2)
      UK1=UK(1)
      UGX=XC*UK1*UG
      IF(IH.EQ.1)    RETURN
      ZC=R2*COS(TH2)
      UGZ=ZC*UK1*UG
      UK2=UK(2)
      UGZZ=(UK1+ZC**2*UK2)*UG+ZC*UK1*UGZ
      UGXZ=XC*ZC*UK2*UG+XC*UK1*UGZ
      RETURN
      END
C
C
C
      COMPLEX FUNCTION UK(I)
      IMPLICIT COMPLEX (C,U)
      COMPLEX KAPPA
      COMMON/PI/    PI,EPS0,CJ
      COMMON/UBS/    R2,TH2,PHI2
      COMMON/PARAM/    AK1,KAPPA,CI0
      K1=K2=1
      DO 100 K=1,I
      J1=2*K-2
      IF(J1.GT.1)    K1=K1*J1
      J2=2*K-3
      IF(J2.GT.1)    K2=K2*J2
  100 CONTINUE
```

```
11500 UK=(-1)**I*(K1+CJ*AK1*R2*R2)/R2**(2*I)
11600 RETURN
 1700 END
11800C
11900C
12000C
12100 SUBROUTINE SUS(Z2P,Z2,UGP,UG,UGXZP,CONST,US,IX)
12200C
12300C
12400C    IX=0,    COMPUTES THE S-FUNCTION
12500C    IX=1,    COMPUTES THE DS/DX-FUNCTION
12510C    IX=2,    COMPUTES THE DS/DY-FUNCTION
12520C    IX=3,    COMPUTES THE D2S/DX2-FUNCTION
12530C    IX=4,    COMPUTES THE D2S/DXDY-FUNCTION
12540C    CAUTION:    INPUTS UGP , UG AND UGXZP MUST BE SUPPLIED ACCORDING TO IX
12700C
12800C
12900 IMPLICIT COMPLEX (C,U)
13000 REAL CUS
13100 COMPLEX KAPPA
13200 COMMON/PI/    PI,EPS0,CJ
13300 COMMON/OBS/    R2,TH2,PHI2
13400 COMMON/PARAM/    AK1,KAPPA,C10
13500 EXTERNAL    UGAKGV,UGAKGM
13600 STOKER=R2    $    STORET=TH2    $    STOREP=PHI2
13700 IF(ABS(Z2-Z2P).LT.1.E-12)    GO TO 100
13800 RHO2=R2*SIN(TH2)
13900 R2=SQRT(Z2P**2+RHO2**2)    $    TH2=ATAN(RHO2/Z2P)
14000 100    CALL SKCM1(U1,U2,U3)
14100 R2=STORER    $    TH2=STORET
14150 IF(IX.GE.2)    GO TO 500
14200 USP=U1
14300 IF(IX.EQ.1)    USP=CJ/CONST/(1.+KAPPA)*(2.*UGXZP+AK1**2*KAPPA*U3)
14400 USINT=(0.,0.)
14500 IF(ABS(Z2-Z2P).LT.1.E-12)    GO TO 200
14600 IF(IX.EQ.0)    CALL DUG12(Z2P,Z2,UGAKGV,USINT)
14700 IF(IX.EQ.1)    CALL DUG12(Z2P,Z2,UGAKGM,USINT)
14800 200    US=(USP-2.*UGP)*CEXP(CJ*CONST*(Z2-Z2P))+2.*UG+2.*CJ*
14900+CONST*CEXP(CJ*CONST*Z2)*USINT
15000 RETURN
15100 500    CONTINUE
15200 DEL=.05*2.*PI/AK1
15300 A2=R2*SIN(TH2)*COS(PHI2)    $    Y2=R2*SIN(TH2)*SIN(PHI2)
15350 USINT=(0.,0.)
15400C
15500 IF(IX.NE.2)    GO TO 510
15600 RHO2D=SQRT(A2**2+(Y2+DEL)**2)
15700 R2=SQRT(RHO2D**2+Z2P**2)    $    TH2=ATAN(RHO2D/Z2P)
15800 PHI2=ATAN2(Y2+DEL,A2)
15900 CALL SKCM1(U1DY,U2,U3)
16000 IF(ABS(Z2-Z2P).GT.1.E-12)    CALL DUG12(Z2P,Z2,UGAKGV,USIDY)
16100 RHO2D=SQRT(A2**2+(Y2-DEL)**2)
16200 R2=SQRT(RHO2D**2+Z2P**2)    $    TH2=ATAN(RHO2D/Z2P)
```

```
16300 PHI2=ATAN2(Y2-DEL,X2)
16400 CALL SKCM1(U1DYM,U2,U3)
16500 IF(ABS(Z2-Z2P).GT.1.E-12)   CALL DUG12(Z2P,Z2,UGARGV,USIDYM)
16600 USP=(U1DY-U1DYM)/2./DEL
16700 IF(ABS(Z2-Z2P).GT.1.E-12)   USINT=(USIDY-USIDYM)/2./DEL
16800 R2=STORER    $   TH2=STORET    $   PHI2=STOREP
16900 GO TO 200
17000C
17100 510   IF(IX.NE.3)   GO TO 520
17200 RHO2D=SQRT((X2+DEL)**2+Y2**2)
17300 R2=SQRT(RHO2D**2+Z2P**2)    $   TH2=ATAN(RHO2D/Z2P)
17400 PHI2=ATAN2(Y2+.000001*DEL,X2+DEL)
17500 CALL SKCM1(U1,U2,U3DX)
17600 IF(ABS(Z2-Z2P).GT.1.E-12)   CALL DUG12(Z2P,Z2,UGARGH,USIDX)
17700 RHO2D=SQRT((X2-DEL)**2+Y2**2)
17800 R2=SQRT(RHO2D**2+Z2P**2)    $   TH2=ATAN(RHO2D/Z2P)
17900 PHI2=ATAN2(Y2+.000001*DEL,X2-DEL)
18000 CALL SKCM1(U1,U2,U3DXM)
18100 IF(ABS(Z2-Z2P).GE.1.E-12)   CALL DUG12(Z2P,Z2,UGARGH,USIDXM)
18200 U3=(U3DX-U3DXM)/2./DEL
18300 IF(ABS(Z2-Z2P).GT.1.E-12)   USINT=(USIDX-USIDXM)/2./DEL
18400 USP=CJ/CONST/(1.+KAPPA)*(2.*UGXZP+AK1**2*KAPPA*U3)
18500 R2=STORER    $   TH2=STORET    $   PHI2=STOREP
18600 GO TO 200
18700C
18800 520   IF(IX.NE.4)   RETURN
18900 RHO2D=SQRT(X2**2+(Y2+DEL)**2)
19000 R2=SQRT(RHO2D**2+Z2P**2)    $   TH2=ATAN(RHO2D/Z2P)
19100 PHI2=ATAN2(Y2+DEL,X2)
19200 CALL SKCM1(U1,U2,U3DY)
19300 IF(ABS(Z2-Z2P).GE.1.E-12)   CALL DUG12(Z2P,Z2,UGARGH,USIDY)
19400 RHO2D=SQRT(X2**2+(Y2-DEL)**2)
19500 R2=SQRT(RHO2D**2+Z2P**2)    $   TH2=ATAN(RHO2D/Z2P)
19600 PHI2=ATAN2(Y2-DEL,X2)
19700 CALL SKCM1(U1,U2,U3DYM)
19800 IF(ABS(Z2-Z2P).GT.1.E-12)   CALL DUG12(Z2P,Z2,UGARGH,USIDYM)
19900 U3=(U3DY-U3DYM)/2./DEL
20000 IF(ABS(Z2-Z2P).GE.1.E-12)   USINT=(USIDY-USIDYM)/2./DEL
20100 USP=CJ/CONST/(1.+KAPPA)*(2.*UGXZP+AK1**2*KAPPA*U3)
20200 R2=STORER    $   TH2=STORET    $   PHI2=STOREP
20300 GO TO 200
20400C
20500 END
```

```
00100 SUBROUTINE SESAPP(UEX,UEY,UEZ,C1V,C1M)
00105C
00110C
00115C    COMPUTE THE THREE COMPLEX SCATTERED E-FIELD COMPONENTS IN THE
00120C    (XC,YC,ZC) COORDINATE SYSTEM USING THE APPROXIMATE PROCEDURE
00125C    DEVELOPED IN CHAPTER 4.
00130C
00135C
00200 IMPLICIT COMPLEX(C,U)
00300 COMPLEX KAPPA,UDG(17),UDGP(17)
00400 REAL LOS
00500 COMMON/PI/    PI,EPS0,CJ
00600 COMMON/UDS/    R2,TH2,RH12
00700 COMMON/PARAM/    AK1,KAPPA,C10
00900 ZZ=R2*COS(TH2)    $    RHO2=R2*SIN(TH2)
01000 STORER=R2    $    STORET=TH2
01100 CONST=AK1/CSQRT(KAPPA)
01200 CALL SDGES(UDG)
01300 R2P=15./AK1
01400 IF(R2.GT.R2P)    GO TO 100
01500 ZZP=SQRT(R2P**2-RHO2**2)
01550 R2=R2P    $    TH2=ATAN(RHO2/ZZP)
01600 CALL SDGES(UDGP)
01700 GO TO 110
01800 100    ZZP=ZZ
01900 DO 105 I=1,17
02000 105    UDGP(I)=UDG(I)
02100 110    CONTINUE
02300 R2=STORER    $    TH2=STORET
02310C
02320 UG=UDG(1)    $    UGP=UDGP(1)
02330 UGX=UDG(2)    $    UGXP=UDGP(2)
02340 UGY=UDG(3)    $    UGYP=UDGP(3)
02350 UGZ=UDG(4)    $    UGZP=UDGP(4)
02360 UGXZ=UDG(5)    $    UGXZP=UDGP(5)
02370 UGZZ=UDG(6)    $    UGZZP=UDGP(6)
02380 UGXY=UDG(7)    $    UGXYP=UDGP(7)
02390 UGXZ=UDG(8)    $    UGXZP=UDGP(8)
02400 UGYZ=UDG(9)    $    UGYZP=UDGP(9)
02410 UGXZZ=UDG(10)    $    UGXZZP=UDGP(10)
02420 UGXZZ=UDG(11)    $    UGXZZP=UDGP(11)
02430 UGXZZZ=UDG(12)    $    UGXZZZP=UDGP(12)
02440 UGXZ3=UDG(13)    $    UGXZ3P=UDGP(13)
02450 UGXYZ=UDG(14)    $    UGXYZP=UDGP(14)
02460 UGXZYZ=UDG(15)    $    UGXZYZP=UDGP(15)
02470 UGXYZZ=UDG(16)    $    UGXYZZP=UDGP(16)
02480 UGXYZ2=UDG(17)    $    UGXYZ2P=UDGP(17)
02490C
02500    UEX=UEY=UEZ=(0.,0.)
02600 IF(CABS(C1M).LT.1.E-14)    GO TO 500
02700C
02800C
02900 C2=-2./AK1**2/(1.-KAPPA)
03000 C1=C2*CJ*AK1*CSQRT(KAPPA)
```

```
      C0=-1.
      UPIX=C0*UG+C1*UGZ+C2*UGZZ
      UPIXXZ=C0*UGXZ+C1*UGXZZ+C2*UGXZZZ
      UEX=UEX+C1M*(AK1**2*UPIX+UPIXXZ)
      UPIXXY=C0*UGXY+C1*UGXYZ+C2*XYZZ
      UEY=UEY+C1M*UPIXXY
      UPIXXZ=C0*UGXZ+C1*UGXZZ+C2*UGXZ3

      UEZ=UEZ+C1M*UPIXXZ
C
C
C     CONTINUE
      CALL SUS(ZZP,ZZ,UGP,UG,UGXZP,CONST,US,0)
      CALL SUS(ZZP,ZZ,UGXP,UGX,UGXZP,CONST,USX,1)
      CALL SUS(ZZP,ZZ,UGYP,UGY,UGXZP,CONST,USY,2)
      CALL SUS(ZZP,ZZ,UGXZP,UGXZ,UGXZZP,CONST,USXZ,3)
      CALL SUS(ZZP,ZZ,UGXYP,UGXY,UGXYZP,CONST,USXY,4)
      USZ=CJ*CONST*US+2.*UGZ
      USZZ=CJ*CONST*USZ+2.*UGZZ
      USXZ=CJ*CONST*USX+2.*UGXZ
      USXZZ=CJ*CONST*USXZ+2.*UGXZZ
      USYZ=CJ*CONST*USY+2.*UGYZ
      USXZZ=CJ*CONST*USXZ+2.*UGXZZ
      USXYZ=CJ*CONST*USXY+2.*UGXYZ
      C10=C1V
      C11=-C1M*CJ*CONST*(KAPPA+1.)/(AK1**2*KAPPA)
      C12=-C1M*2./(AK1**2*KAPPA)
      C13=-C1V
      UPIZ=C10*US+C11*USX+C12*UGXZ+C13*UG
      UPIZZ=C10*USZ+C11*USXZ+C12*UGXZZ+C13*UGZZ
      UPIZYZ=C10*USYZ+C11*USXYZ+C12*UGXYZZ+C13*UGYZ
      UPIZXZ=C10*USXZ+C11*USXZZ+C12*UGXZZZ+C13*UGXZ
      UEX=UEX+UPIZXZ
      UEY=UEY+UPIZYZ
      UEZ=UEZ+AK1**2*UPIZ+UPIZZZ
      RETURN
      END
C
C
C
      SUBROUTINE SUGES(UDG)
      IMPLICIT COMPLEX(C,U)
      DIMENSION UDG(17)
      REAL COS
      COMPLEX KAPPA
      COMMON/PI/ PI,EPSO,CJ
      COMMON/UBS/ R2,TH2,PHI2
      COMMON/PARAM/ AK1,KAPPA,C1M
      UDG(1)=UG=CEXP(-CJ*AK1*R2)/(4.*PI*R2)
      RHO2=R2*SIN(TH2)    $    Z2=R2*COS(TH2)
      X2=RHO2*COS(PHI2)    $    Y2=RHO2*SIN(PHI2)
      UR1=UR(1)
      UDG(2)=UGX=X2*UR1*UG
      UDG(3)=UGY=Y2*UR1*UG
```

```
11600 UDG(4)=UGZ=Z2*UR1*UG
11700 UR2=UR(2)
11800 UDG(5)=UGX2=(UR1+X2**2*UR2)*UG+X2*UR1*UGX
11900          UGY2=(UR1+Y2**2*UR2)*UG+Y2*UR1*UGY
12000 UDG(6)=UGZ2=(UR1+Z2**2*UR2)*UG+Z2*UR1*UGZ
12100 UDG(7)=UGXY=X2*Y2*UR2*UG+X2*UR1*UGY
12200 UDG(8)=UGXZ=X2*Z2*UR2*UG+X2*UR1*UGZ
12300 UDG(9)=UGYZ=Y2*Z2*UR2*UG+Y2*UR1*UGZ
12400 UR3=UR(3)
12500            UGZ3=(3.*Z2*UR2+Z2**3*UR3)*UG+2.*(UR1+Z2**2*UR2)*UGZ+
12600+Z2*UR1*UGZ2
12700 UDG(10)=UGX2Z=Z2*(UR2+X2**2*UR3)*UG+2.*X2*Z2*UR2*UGX+Z2*UR1*UGX2
12800 UDG(11)=UGXZ2=X2*(UR2+Z2**2*UR3)*UG+2.*X2*Z2*UR2*UGZ+X2*UR1*UGZ2
12900            UGXY2=X2*(UR2+Y2**2*UR3)*UG+2.*X2*Y2*UR2*UGY+X2*UR1*UGY2
13000 UR4=UR(4)
13100 UDG(12)=UGX2Z2=(UR2+(X2**2+Z2**2)*UR3+X2**2*Z2**2*UR4)*UG+
13200+Z2*(UR2+X2**2*UR3)*UGZ+2.*X2*(UR2+Z2**2*UR3)*UGX+(UR1+Z2**2*UR2)*UGX2+
13300+2.*X2*Z2*UR2*UGXZ+Z2*UR1*UGX2Z
13400 UDG(13)=UGXZ3=X2*(3.*Z2*UR3+Z2**3*UR4)*UG+3.*X2*(UR2+Z2**2*UR3)*UGZ+
13500+3.*X2*Z2*UR2*UGZ2+X2*UR1*UGZ3
13600 UDG(14)=UGXYZ=X2*Y2*Z2*UR3*UG+2.*Y2*Z2*UR2*UGX+Z2*UR1*UGXY
13700 UDG(15)=UGX2YZ=Y2*Z2*(UR3+X2**2*UR4)*UG+3.*X2*Y2*Z2*UR3*UGX+
13800+2.*Y2*Z2*UR2*UGX2+X2*Y2*UR2*UGXZ+Y2*UR1*UGX2Z
13900 UDG(16)=UGXY2Z=X2*Z2*(UR3+Y2**2*UR4)*UG+3.*X2*Y2*Z2*UR3*UGY+
14000+2.*X2*Z2*UR2*UGY2+Y2*Z2*UR2*UGXY+Z2*UR1*UGXY2
14100 UDG(17)=UGXYZ2=X2*Y2*(UR3+Z2**2*UR4)*UG+3.*X2*Y2*Z2*UR3*UGZ+
14200+2.*X2*Y2*UR2*UGZ2+Y2*Z2*UR2*UGXZ+Y2*UR1*UGXZ2
14300 RETURN
14400 END
```

```
      SUBROUTINE SOMINT(CP0V1Z,CP0H1X,CP0H1Z,IV,IH)
C
C
C     COMPUTE SOMMERFELD INTEGRALS
C     IV=0,    DO NOT COMPUTE THE VERTICAL INTEGRAL
C     IH=0,    DO NOT COMPUTE THE HORIZONTAL INTEGRALS
C
C
      IMPLICIT COMPLEX(C,U)
      COMPLEX KAPPA,BKV1Z,BKH1X,BKH1Z
      COMMON/PI/  PI,EPS0,CJ
      COMMON/OBS/ R2,TH2,PH12
      COMMON/PARAM/  AK1,KAPPA,CIU
      EXTERNAL V1ZARG,H1XARG,H1ZARG
      CP0V1Z=CP0H1X=CP0H1Z=(0.,0.)
      TMAX=3./SQRT(AK1*R2)
      A=REAL(CSQRT(KAPPA))
      B=AIMAG(CSQRT(KAPPA-1.))
      TH2MIN=ASIN(1./SQRT(A**2+B**2))-ATAN(B/A)
      TH2P=TH2MIN*180./PI
      PRINT 905,TMAX,TH2P
  905 FORMAT(" ","TMAX=",G10.2,"TH2MIN=",G10.2)
      IF(TH2.LT.TH2MIN)     GO TO 100
      BETA=0.    $   DEL=5.    $   IS=1
   10 BETA=BETA+DEL
      UA=CSQRT(KAPPA-BETA**2)
      UB=CSQRT(KAPPA-1.-BETA**2)
      TH2P=ASIN(1./SQRT(REAL(UA)**2+AIMAG(UB)**2))-ATAN(AIMAG(UB)/REAL(UA))
      IF(ABS(TH2-TH2P).LT.1.E-4)    GO TO 20
      IF((TH2-TH2P)*IS.GT.0.)   GO TO 10
      DEL=-DEL/2.    $   IS=-IS
      GO TO 10
   20     BETA1=BETA
      T1=SQRT(-SIN(TH2)*AIMAG(UA)+COS(TH2)*REAL(UB))
      PRINT 910,T1,BETA1
  910 FORMAT(" ","T1=",G10.2,"BETA1=",G10.2)
      IF(T1.GT.TMAX)   GO TO 100
      CALL BKINT(BETA1,BKV1Z,BKH1X,BKH1Z,IV,IH)
      IF(IV.EQ.0)   GO TO 30
      CALL DQG1C(-TMAX,0.,V1ZARG,U1)
      CALL DQG12(0.,T1-.001*T1,V1ZARG,U2)
      CALL DQG12(T1+.001*T1,TMAX,V1ZARG,U3)
      CP0V1Z=U1+U2+U3+BKV1Z
   30 IF(IH.EQ.0)   RETURN
      CALL DQG12(-TMAX,0.,H1XARG,UX1)
      CALL DQG12(-TMAX,0.,H1ZARG,UZ1)
      CALL DQG12(0.,T1-.001*T1,H1XARG,UX2)
      CALL DQG12(0.,T1-.001*T1,H1ZARG,UZ2)
      CALL DQG12(T1+.001*T1,TMAX,H1XARG,UX3)
      CALL DQG12(T1+.001*T1,TMAX,H1ZARG,UZ3)
      CP0H1X=UX1+UX2+UX3+BKH1X
      CP0H1Z=UZ1+UZ2+UZ3+BKH1Z
      RETURN
```

```
05400 100    IF(IV.EQ.0)    GO TO 110
05500 CALL DGG12(-TMAX,0.,V1ZARG,U1)
05600 CALL DGG12(0.,TMAX,V1ZARG,U2)
05700 CPUV1Z=U1+U2
05800 110    IF(IM.EQ.0)    RETURN
05900 CALL DGG12(-TMAX,0.,M1XARG,UX1)
06000 CALL DGG12(-TMAX,0.,M1ZARG,UZ1)
06100 CALL DGG12(0.,TMAX,M1XARG,UX2)

06200 UVZ=KAPPA/(KAPPA**2*COSXI**2-BETA**2)*UK*UM0
06300 10     IF(IMX.EQ.0)    GO TO 20
06400 CALL MNKL0(C1,UM0)
06500 UMX=UK/(KAPPA-1.)*UM0
06600 20     IF(IMZ.EQ.0)    RETURN
06700 CALL MNKL1(C1,UM1)
06800 UMZ=CJ*COS(PHI2)*(KAPPA+1.)/(KAPPA**2*COSXI**2-BETA**2)*SINXI
06900+*COSXI*UK*UM1
07000 RETURN
07100 END
```

```
      SUBROUTINE PIWARG(IVZ,IHX,IHZ,T,UVZ,UHX,UHZ)
C
C
C     SOMMERFELD INTEGRANDS
C
C
      IMPLICIT COMPLEX(C,U)
      REAL COS
      COMPLEX KAPPA,XI,SINXI
      COMMON/PI/    PI,EPS0,CJ
      COMMON/OBS/    R2,TH2,PHI2
      COMMON/PARAM/    AK1,KAPPA,C10
      UVZ=UHX=UHZ=(0.,0.)
      CALL SOPTXI(T,TH2,XI)
      RHO2=R2*SIN(TH2)
      SINXI=CSIN(XI)
      COSXI=CCOS(XI)
      USQ=CSQRT(KAPPA-SINXI**2)
      IF(T.GT.0..AND.AIMAG(USQ).GT.0.)    USQ=-USQ
      C1=AK1*RHO2*SINXI
      UR=AK1/(2.*PI)*CEXP(-CJ*AK1*R2)/CSQRT(T**2+2.*CJ)
      UR=UR*SINXI*COSXI*CEXP(CJ*C1)*EXP(-AK1*R2*T**2)
      IF(IVZ.EQ.0)    GO TO 10
      IF(TH2.LT.1.E-6)    CH0=-2.*CJ/PI*CLOG(AK1*R2*SINXI)
      IF(TH2.GE.1.E-6)    CALL HNKL0(C1,CH0)
      UVZ=KAPPA*UR*CH0/(KAPPA*COSXI+USQ)
10    IF(IHX.EQ.0)    GO TO 20
      IF(TH2.LT.1.E-6)  CH0=-2.*CJ/PI*CLOG(AK1*R2*SINXI)
      IF(TH2.GE.1.E-6)    CALL HNKL0(C1,CH0)
      UHX=UR*CH0/(COSXI+USQ)
20    IF(IHZ.EQ.0)    RETURN
      IF(TH2.LT.1.E-6)    RETURN
      CALL HNKL1(C1,CH1)
      UHZ=-CJ*COS(PHI2)*UR*CH1*SINXI*(COSXI-USQ)/(KAPPA*COSXI+USQ)
      RETURN
      END
C
C
C
      COMPLEX FUNCTION V1ZARG(T)
      IMPLICIT COMPLEX(V)
      CALL PIWARG(1,0,0,T,V1ZARG,V2,V3)
      RETURN
      END
C
C
C
      COMPLEX FUNCTION H1XARG(T)
      IMPLICIT COMPLEX (H)
      CALL PIWARG(0,1,0,T,H1,H1XARG,H3)
      RETURN
      END
```

```
05200C
05300C
05400C
05500 COMPLEX FUNCTION M1ZARG(T)
05600 IMPLICIT COMPLEX(M)
05700 CALL PINARG(0,0,1,T,M1,M2,M1ZARG)
05800 RETURN
05900 END
06000C
06100C
06200C
06300 SUBROUTINE SQRTX1(T,TM2,X1)
06400 COMPLEX CMPLX,X1
06500 SQ1=SQRT(T**4+4.)
06600 ALPHA=(-T**2+SQ1)/2.
06700 BETA=(T**2+SQ1)/2.
06800 Q1=ALOG(ALPHA)
06900 Q2=ALOG(BETA+SQRT(BETA**2-1.))
07000 X1=CMPLX(Q1,Q2)*SIGN(1.,T)+TM2
07100 RETURN
07200 END
```

```
00100 SUBROUTINE BRINT(BETA1,BRV1Z,BRM1X,BRM1Z,IV,IH)
00200C
00300C
00400C    COMPUTE BRANCH CUT CONTRIBUTIONS
00500C    IV=0    ,    DO NOT COMPUTE THE VERTICAL CASE
00600C    IH=0    ,    DO NOT COMPUTE THE HORIZONTAL CASE
00700C
00800C
00900 COMPLEX BRV1Z,BRM1X,BRM1Z
01000 EXTERNAL BARGVZ,BARGHX,BARGHZ
01100 IF(IV.EQ.0)    GO TO 10
01200 CALL DQG12(0.,BETA1,BARGVZ,BRV1Z)
01300 10    IF(IH.EQ.0)    RETURN
01400 CALL DQG12(0.,BETA1,BARGHX,BRM1X)
01500 CALL DQG12(0.,BETA1,BARGHZ,BRM1Z)
01600 RETURN
01700 END
01800C
01900C
02000C
02100 COMPLEX FUNCTION BARGVZ(BETA)
02200 IMPLICIT COMPLEX (B)
02300 REAL BETA
02400 CALL BRARG(1,0,0,BETA,BARGVZ,B2,B3)
02500 RETURN
02600 END
02700C
02800C
02900C
03000 COMPLEX FUNCTION BARGHX(BETA)
03100 IMPLICIT COMPLEX (B)
03200 REAL BETA
03300 CALL BRARG(0,1,0,BETA,B1,BARGHX,B3)
03400 RETURN
03500 END
03600C
03700C
03800C
03900 COMPLEX FUNCTION BARGHZ(BETA)
04000 IMPLICIT COMPLEX (B)
04100 REAL BETA
04200 CALL BRARG(0,0,1,BETA,B1,B2,BARGHZ)
04300 RETURN
04400 END
04500C
04600C
04700C
04800 SUBROUTINE BRARG(IVZ,IHX,IHZ,BETA,UVZ,UHX,UHZ)
04900 IMPLICIT COMPLEX (C,U)
05000 REAL LOS
05100 COMPLEX KAPPA,SINAI
05200 COMMON/PI/    PI,EPS0,CJ
05300 COMMON/OBS/    K2,IH2,PH12
```

```
05400 COMMON/PARAM/    AK1,KAPPA,C10
05500 COSXI=-CJ*CSQRT(KAPPA-1.,-BETA**2)
05600 SINXI=CSQRT(KAPPA-BETA**2)
05700 RMU2=R2*SIN(TH2)     Z2=R2*COS(TH2)
05800 UR=AK1/(2.*PI*CJ)*BETA**2*CEXP(-CJ*AK1*Z2*COSXI)
05900 C1=AK1*RMU2*SINXI
06000 IF(IV2.EQ.0)   GO TO 10
06100 CALL RNKL0(C1,UM0)

06200 CALL DUG12(0.,TMAX,MIZARG,UZ2)
06300 CPHM1X=UX1+UX2
06400 CPHM1Z=UZ1+UZ2
06500 RETURN
06600 END
```

```
001000C-------------------------------------------------------------------
00200C      SUBROUTINE XINVZ(N,NX,A,D,IERR)
003000C-------------------------------------------------------------------
00400C      PARAMETERS HAVE THE FOLLOWING MEANINGS
00500C      A = N BY N REAL, SYMMETRIC MATRIX TO BE INVERTED, ON OUTPUT A
00600C          CONTAINS A INVERSE.
00700C      D = DETERMINANT OF A.
008000C-------------------------------------------------------------------
00900       IMPLICIT COMPLEX(A-H,O-Z)
01000       DIMENSION A(NX,N),GAMMA(150)
01100C-----INITIALIZE DETERMINANT
01200       D=A(1,1)
01300C-----COMPUTE B(1)**(-1)
01400       A(1,1)=1./A(1,1)
01500       DO 70 I=2,N
01600       IM1=I-1
01700       DO 20 K=1,IM1
01800       GAMMA(K)=0.
01900C-----COMPUTE BV*U
02000         DO 10 KK=1,IM1
02100    10     GAMMA(K)=A(K,KK)*A(I,KK)+GAMMA(K)
02200    20     GAMMA(K)=-GAMMA(K)
02300       ALPHA=0.E0
02400C-----COMPUTE ALPHA
02500       DO 30 KK=1,IM1
02600    30     ALPHA=A(I,KK)*GAMMA(KK)+ALPHA
02700       ALPHA=A(I,I)+ALPHA
02800C-----IF ALPHA=0 THEN GO TO ERROR RETURN
02900       IF(CABS(ALPHA).LE.1.0E-15)GO TO 80
03000       Y=1./(ALPHA)
03100       DO 60 K=1,IM1
03200C-----STORE -BV*U/ALPHA
03300       A(I,K)=GAMMA(K)*Y
03400       A(K,1)=A(I,K)
03500       DO 40 KK=1,K
03600C-----STORE BV+BV*U*U**BV
03700    40     A(K,KK)=A(K,KK)+GAMMA(K)*GAMMA(KK)*Y
03800       IF(K.EQ.1)GO TO 60
03900       KM1=K-1
04000       DO 50 KK=1,KM1
04100C-----STORE -(BV*U/ALPHA)'
04200    50     A(KK,K)=A(K,KK)
04300    60     CONTINUE
04400C-----STORE 1./ALPHA
04500       A(I,I)=Y
04600C-----UPDATE DETERMINANT
04700    70     D=ALPHA*D
04800       IERR=1.0
04900       RETURN
05000    80     IERR=1
05100       RETURN
05200       END
```

```
00100          SUBROUTINE HNAL1(Z,H1)
00110C
00120C
00130C         HANKEL FUNCTION, 1ST ORDER,SECOND TYPE
00140C         USAGE: INPUT COMPLEX*16 Z
00150C         USAGE, OUTPUT COMPLEX*16 H1
00160C         TO CALCULATE J0 AND Y0 HNKL USES AN ANALYTIC CONTINUATION
00170C         OF THE POLYNOMIAL FITS IN ABRAMOWITZ AND STEGUN PG 369
00180C
00190C
00200          COMPLEX A1,Z,H1,Y1,J1
00210          REAL PI
00220          PI=3.141592654
00230          AI=(0.E0,1.E0)
00240          IF(CABS(Z).LE.12.)GOTO10
00250          GOTO 20
00260     10   CONTINUE
00270          CALL Y1(Z,Y1,J1)
00280          H1=J1-AI*Y1
00290          GOTO 99
00300     20   H1=CSQRT(2./(PI*Z))*CEXP(-1.*AI*(Z-3.*PI/4.))*(1.+.15./(128.*Z**
00310+         2)-AI*3./(8.*Z))
00320     99   RETURN
00330          END
00340          SUBROUTINE J1(Z,J1)
00350C
00360C
00370C         BESSEL FUNCTION, 1ST ORDER
00380C         USAGE  INPUT  COMPLEX*16 Z
00390C         USAGE   OUTPUT  COMPLEX*16 J1
00400C         ANALYTICAL CONTINUATION INTO THE FIRST QUADRANT OF THE
00410C         POLYNIMIAL FIT IN ABRAMOWITZ AND STEGUN PG 369
00420C
00430C
00440          COMPLEX J1,J1AS,J1AL,Z,Z1,AI
00450          REAL PI,AP,REAL,AIMAG
00460          PI=3.141592654
00470          AI=(0.E0,1.E0)
00480          Z1=CMPLX(ABS(REAL(Z)),ABS(AIMAG(Z)))
00490          AP=ATAN2(AIMAG(Z),REAL(Z))
00500          IF(CABS(Z).LE.5.0)J1=J1AS(Z1)
00510          IF(CABS(Z).GT.5.0)J1=J1AL(Z1)
00520          IF(AP.GT.PI/2..AND.AP.LT.PI)J1=CEXP(AI*PI)*CONJG(J1)
00530          IF(AP.LE.-1.*PI/2..AND.AP.GT.-1.*PI)J1=CEXP(AI*PI)*J1
00540          IF(AP.LT.0..AND.AP.GE.-1.*PI/2.)J1=CONJG(J1)
00550          RETURN
00560          END
00570          COMPLEX FUNCTION J1AS(Z)
00580          COMPLEX Z,W
00590          W=Z/3.
00600          J1AS=Z*(.5-.5624999*W**2+.2109373*W**4-.0595489*W**6+.
00610+.0044519*W**8-.0003161*W**10+.0000110*W**12)
00620          RETURN
00630          END
```

```
00640         COMPLEX FUNCTION J1AL(Z)
00650         COMPLEX Z,W,F1,TM1
00660         W=3./Z
00670         F1=.79788456+.00000156*W+.01659667*W**2+.00017105*W**3-.
00680+.00249511*W**4+.00113653*W**5-.00020033*W**6
00690         TM1=Z-2.35619449+.12499612*W+.00005650*W**2-.00637879*W**3+.
00700+.00074348*W**4+.00079824*W**5-.00029166*W**6

00710         J1AL=F1*CCOS(TM1)/CSQRT(Z)
00720         RETURN
00730         END
00740         SUBROUTINE YI(Z,Y1,J1)
00750C
00760C
00770C        NEUMANN FUNCTION,1ST ORDER, SUBROUTINE J1 IS CALLED
00780C        USAGE   INPUT  COMPLEX*16 Z
00790C        USAGE  OUTPUT COMPLEX*16 Y1
00800C        ANALYTIC CONTINUATION INTI THE FIRST QUADRANT OF THE
00810C        POLYNOMIAL FIT FOUND IN ABRAMOWITZ AND STEGUN PG 369
00820C
00830C
00840         COMPLEX Y1,Y1AS,Y1AL,Z,Z1,A1,J1
00850         REAL PI,AP,REAL,AIMAG
00860         PI=3.141592654
00870         A1=(0.E0,1.E0)
00880         Z1=CMPLX(ABS(REAL(Z)),ABS(AIMAG(Z)))
00890         CALL J1(Z1,J1)
00900         AP=ATAN2(AIMAG(Z),REAL(Z))
00910         IF(CABS(Z).LE.3.0)Y1=Y1AS(Z1,J1)
00920         IF(CABS(Z).GT.3.0)Y1=Y1AL(Z1)
00930         IF(AP.GT.PI/2..AND.AP.LT.PI)Y1=CEXP(A1*PI)*(CONJG(Y1)+2.*A1*
00940+CONJG(J1))
00950         IF(AP.LE.-1.*PI/2..AND.AP.GT.-1.*PI)Y1=CEXP(A1*PI)*(Y1-2.*A1*J1)
00960         IF(AP.LT.0..AND.AP.GE.-1.*PI/2.)Y1=CONJG(Y1)
00970          IF(AP.GT.PI/2..AND.AP.LT.PI)  J1=-CONJG(J1)
00980          IF(AP.LT.-PI/2..AND.AP.GE.-PI)  J1=-J1
00990          IF(AP.LT.0..AND.AP.GE.-PI/2.)  J1=CONJG(J1)
01000         RETURN
01010         END
01020         COMPLEX FUNCTION Y1AS(Z,J1)
01030         COMPLEX Z,J1,W
01040         REAL PI
01050         PI=3.141592654
01060         W=Z/3.
01070         Y1AS=(1./Z)*((2./PI)*Z*CLOG(Z/2.)*J1-.6366198+.2212091*W**2+2.
01080+1.2656208*W**4-1.3164827*W**6+.5123951*W**8-.0400976*W**10+.
01090+.0027873*W**12)
01100         RETURN
01110         END
01120         COMPLEX FUNCTION Y1AL(Z)
01130         COMPLEX Z,W,TM1,F1
01140         W=3./Z
01150         F1=.79788456+.00000156*W+.01659667*W**2+.00017105*W**3-.
01160+.00249511*W**4+.00113653*W**5-.00020033*W**6
```

```
01170         IM1=Z-2.35619449+.1249612*W+.0000565D*W**2-.00637879*W**3+.
01180+0007434B*W**4+.0007924*W**5-.0002916*W**6
01190         YIAL=PI*CSIN(IM1)/CSQRT(Z)
01200         RETURN
01210         END
01220         SUBROUTINE HNKL0(Z,H)
01230C
01240C
01250C        HANKEL FUNCTION 0TH ORDER,2ND TYPE
01260C        USAGE  COMPLEX*16 Z
01270C        USAGE  COMPLEX*16 H
01280C        TO CALCULATE J0 AND Y0 HNKL USES AN ANALYTIC CONTINUATION
01290C        OF THE POLYNOMIAL FITS IN ABRAMOWITZ AND STEGUN PG 369
01300C
01310C
01320         COMPLEX A1,J0,Y0,Z,H
01330         REAL PI
01340         PI=3.141592654
01350         A1=(0.E0,1.E0)
01360         IF(CABS(Z).LE.12.)GOTO10
01370         GOTO 20
01380    10   CONTINUE
01390         CALL Y0(Z,Y0,J0)
01400         H=J0-A1*Y0
01410         GOTO 99
01420    20   H=CSQRT(2./(PI*Z))*CEXP(-1.*AI*(Z-PI/4.))*(1.-9./(2.*(8.*Z)**2)+
01430+A1/(8.*Z))
01440    99   RETURN
01450         END
01460         SUBROUTINE J0(Z,J0)
01470C
01480C
01490C        BESSEL FUNCTION, 0TH ORDER
01500C        USAGE   INPUT   COMPLEX*16 Z
01510C        USAGE    OUTPUT  COMPLEX*16 J0
01520C        ANALYTICAL CONTINUATION INTO THE FIRST QUADRANT OF THE
01530C        POLYNOMIAL FIT FOUND IN ABRAMOWITZ AND STEGUN PG 369
01540C
01550C
01560         COMPLEX J0,J0AS,J0AL,Z,Z1
01570         REAL PI,AP,REAL,AIMAG
01580         PI=3.141592654
01590         Z1=CMPLX(ABS(REAL(Z)),ABS(AIMAG(Z)))
01600         AP=ATAN2(AIMAG(Z),REAL(Z))
01610         IF(CABS(Z).LE.3.0)J0=J0AS(Z1)
01620         IF(CABS(Z).GT.3.0)J0=J0AL(Z1)
01630         IF(AP.GT.PI/2..AND.AP.LT.PI)J0=CONJG(J0)
01640         IF(AP.LT.0..AND.AP.GE.-1.*PI/2.)J0=CONJG(J0)
01650         RETURN
01660         END
01670         COMPLEX FUNCTION J0AS(Z)
01680         COMPLEX Z,W
01690         W=Z/3.
```

```
01700          JOAS=1.-2.249997*W**2+1.265620*W**4-.316386*W**6+.0444479*W**
01710+8-.00399444*W**10+.0002100*W**12
01720          RETURN
01730          END
01740          COMPLEX FUNCTION JOAL(Z)
01750          COMPLEX THO,FO,Z
01760          FO=.79788456-.00000077*(3/Z)-.00552740*(3/Z)**2-.00009512*(3/Z)*
01770**5+.00137237*(3/Z)**4-.00072805*(3/Z)**5+.00014476*(3/Z)**6
01780          THO=Z-.78539816-.04166397*(3/Z)-.00003954*(3/Z)**2+.00262573*(3/
01790+Z)**3-.00054125*(3/Z)**4-.00029333*(3/Z)**5+.00013580*(3/Z)**6
01800          JOAL=FO*CCOS(THO)/CSQRT(Z)
01810          RETURN
01820          END
01830          SUBROUTINE Y0(Z,YO,JO)
01840C
01850C
01860C         NEUMANN FUNCTION,0TH ORDER,SUBROUTINE J0 IS CALLED
01870C         USAGE  INPUT COMPLEX*16 Z
01880C         USAGE  OUTPUT COMPLEX*16 YO
01890C         ANALYTIC CONTINUATION INTO THE FIRST QUADRANT OF THE
01900C         POLYNOMIAL FIT IN ABRAMOWITZ AND STEGUN PG 369
01910C
01920C

01930          COMPLEX YO,YOAS,YOAL,JO,Z,Z1,AI
01940          REAL PI,AP,REAL,AIMAG
01950          PI=3.141592654
01960          AI=(0.E0,1.E0)
01970          Z1=CMPLX(ABS(REAL(Z)),ABS(AIMAG(Z)))
01980          CALL J0(Z1,JO)
01990          AP=ATAN2(AIMAG(Z),REAL(Z))
02000          IF(CABS(Z).LE.3.0)YO=YOAS(Z1,JO)
02010          IF(CABS(Z).GT.3.0)YO=YOAL(Z1)
02020          IF(AP.GT.PI/2..AND.AP.LT.PI)YO=CONJG(YO)+2.*AI*CONJG(JO)
02030          IF(AP.LE.-1.*PI/2..AND.AP.GT.-1.*PI)YO=YO-2.*AI*JO
02040          IF(AP.LT.0..AND.AP.GE.-1.*PI/2.)YO=CONJG(YO)
02050           IF(AP.GT.PI/2..AND.AP.LT.PI)      JO=CONJG(JO)
02060           IF(AP.LT.0..AND.AP.GE.-PI/2.)    JO=CONJG(JO)
02070          RETURN
02080          END
02090          COMPLEX FUNCTION YOAS(Z,JO)
02100          COMPLEX Z,JO
02110          REAL PI
02120          PI=3.141592654
02130          YOAS=(2./PI)*CLOG(Z/2.)*JO+.36746691+.60559366*(Z/3.)**2-.
02140+.74350384*(Z/3)**4+.25300117*(Z/3)**6-.04261214*(Z/3)**8+.
02150+.00427916*(Z/3)**10-.00024846*(Z/3)**12
02160          RETURN
02170          END
02180          COMPLEX FUNCTION YOAL(Z)
02190          COMPLEX Z,THO,FO
02200          FO=.79788456-.00000077*(3/Z)-.00552740*(3/Z)**2-.00009512*(3/Z)*
02210**5+.00137237*(3/Z)**4-.00072805*(3/Z)**5+.00014476*(3/Z)**6
```

```
02220          THU=Z-.10539616-.04166597*(3/Z)-.00003954*(3/Z)**2+.00262575*(3/
02230+Z)**3-.00054125*(3/Z)**4-.00029333*(3/Z)**5+.00013588*(3/Z)**6
02240          FUAL=FU*CSIN(THU)/CSQRT(Z)
02250          RETURN
02260          END
```

```
00100 SUBROUTINE DOG12(XL,XU,FCT,Y)
00110C
00120C    INTEGRATE COMPLEX FUNCTION FCT FROM XL TO XU
00130C    USING 12-POINT GAUSS QUADRATURE FORMULA,
00140C    EXACT FOR POLYNOMIALS UP TO DEGREE 23.
00150C
00160 COMPLEX Y,FCT
00170 EXTERNAL FCT
00180C
00190 A=.5*(XU+XL)
00200 B=XU-XL
00210 C=.49607003171255596E0*B
00220 Y=.25586661932559146E-1*(FCT(A+C)+FCT(A-C))
00230 C=.45205862818523743E0*B
00240 Y=Y+.53469662997659215E-1*(FCT(A+C)+FCT(A-C))
00250 C=.38495133709715234E0*B
00260 Y=Y+.60039164271673111E-1*(FCT(A+C)+FCT(A-C))
00270 C=.29565897714330672E0*B
00280 Y=Y+.10130371336155296E0*(FCT(A+C)+FCT(A-C))
00290 C=.18591574949909010E0*B
00300 Y=Y+.11674626602691774UE0*(FCT(A+C)+FCT(A-C))
00310 C=.82616704255734458E-1*B
00320 Y=B*(Y+.12457352290670139E0*(FCT(A+C)+FCT(A-C)))
00330 RETURN
00340 END
```

REFERENCES

[1] A. N. Sommerfeld, "Uber die ausbrietung der wellen in der telegraphie," Ann. Physik, p. 665, 1909.

[2] A. Banos, Dipole Radiation in the Presence of Conducting Half-Space. New York: Pergamon Press, 1966.

[3] E. K. Miller, A. J. Poggio, G. J. Burke, and E. S. Selden, "Analysis of wire antennas in the presence of a conducting half-space: Part I. The vertical antenna in free space," Can. J. Phys., vol. 50, pp. 879-888, 1972.

[4] E. K. Miller, A. J. Poggio, G. J. Burke, and E. S. Selden, "Analysis of wire antennas in the presence of conducting half-space: Part II. The horizontal antenna in free space," Can. J. Phys., vol. 50, pp. 2614-2627, 1972.

[5] J. D. McCannon, "A comparative numerical study of several methods for analyzing a vertical thin-wire antenna over a lossy half-space," Ph.D. Thesis, University of Illinois, Urbana, Illinois, 1974.

[6] D. C. Chang and R. Fisher, "A unified theory on radiation of a vertical electric dipole above a dissipative earth," Radio Sci., vol. 9, no. 12, pp. 1129-1138, December 1974.

[7] T. K. Sarker and B. J. Strait, "Analysis of arbitrarily oriented thin wire antenna arrays over imperfect ground planes," Syracuse University Scientific Report 9, December 1975; prepared under Contract No. F19628-73-C-0047, AFCRL-TR-75-0641.

[8] D. L. Lager and R. J. Lytle, "Numerical evaluation of Sommerfeld integrals," Lawrence Livermore Laboratory Report UCRL-51688, October 23, 1974.

[9] D. L. Lager and R. J. Lytle, "Fortran subroutines for the numerical evaluation of Sommerfeld integrals under anderem," Lawrence Livermore Laboratory Report UCRL-51821, May 21, 1975.

[10] J. N. Brittingham, E. K. Miller, and J. T. Okada, "Bivariate interpolation approach for efficiently and accurately modelling antennas near a half-space," Electron. Lett., vol. 13, pp. 690-691, November 1977.

[11] Y. Rahmat-Samii, P. Parhami, and R. Mittra, "Transient response of a loaded horizontal antenna over lossy ground with application to EMP simulators," University of Illinois at Urbana-Champaign, Electromagnetics Laboratory Report No. 77-26, December 1977.

[12] W. C. Kuo and K. K. Mei, "Numerical approximation of the Sommerfeld integral for fast convergence," Radio Sci., vol. 13, no. 3, pp. 407-415, May 1978.

[13] J. D. McCannon, "Numerical analysis of a thin-wire antenna near lossy ground," M. S. Thesis, University of Illinois at Urbana-Champaign, Urbana, Illinois, 1972.

[14] Y. Rahmat-Samii, P. Parhami, and R. Mittra, "Loaded horizontal antenna over an imperfect ground," IEEE Trans. Antennas Propagat., vol. AP-26, no. 6, pp. 789-79-, November 1978.

[15] J. VanBladel, Electromagnetic Fields. New York: McGraw-Hill, 1967.

[16] J. A. Kong, Theory of Electromagnetic Waves. New York: Wiley, 1975.

[17] R. F. Harrington, Field Computation by Moment Methods. New York: McMillan, 1968.

[18] R. Mittra and W. L. Ko, "A finite difference approach to the wire junction problem," IEEE Trans. Antennas Propagat., vol. AP-23, pp. 435-438, May 1975.

[19] P. Parhami, Y. Rahmat-Samii, and R. Mittra, "A technique for calculating the radiation and scattering characteristics of antennas mounted on a finite ground plate," IEE Proc., vol. 124, pp. 1009-1016, November 1977.

[20] R. F. Harrington, "Matrix methods for field problems," Proc. IEEE, pp. 136-149, February 1967.

[21] E. C. Jordan and K. G. Balmain, Electromagnetic Waves and Radiating Systems. New Jersey: Prentice-Hall, 1968, pp. 566-567.

[22] M. Abramowitz and I. A. Stegum, Handbook of Mathematical Functions. New York: Dover Publications, Inc., 1970.

[23] L. B. Felsen and N. Marcuvitz, Radiation and Scattering of Waves. New Jersey: Prentice-Hall, 1973.